Combination therapies to enhance the efficacy of PSMA-targeted radioligand therapy in prostate cancer

Inaugural Dissertation
for
the doctoral degree of

Dr. rer. nat.

from the
Faculty of Biology
University of Duisburg-Essen
Germany

Submitted by
Magdalena Staniszewska

Born in Kedzierzyn Kozle
March 2022

The experiments underlying the present work were conducted from June, 2018 until March, 2022 at the Department of Nuclear Medicine, University Hospital Essen and at the Department of Molecular and Medical Pharmacology, David Geffen School of Medicine, University of California, Los Angeles, USA under supervision of Prof. Dr. med. Wolfgang Fendler und Prof. Dr. phil. sci. Katharina Lückerath.

DOI: 10.17185/duepublico/76150
URN: urn:nbn:de:hbz:465-20220705-071731-8

1. Examiner: Prof. Dr. med. Ken Herrmann

2. Examiner: Prof. Dr. phil. nat. George Iliakis

Chair of the Board of Examiners: Prof. Dr. rer. nat. Verena Jendrossek

Date of the oral examination: June 17, 2022

This dissertation is based in part on the previously published articles listed below.

Staniszewska M, Fragoso Costa P, Eiber M, Klose JM, Wosniack J, Reis H, Szarvas T, Hadaschik B, Lückerath K, Herrmann K, Fendler WP, Iking J. Enzalutamide Enhances PSMA Expression of PSMA-Low Prostate Cancer. Int J Mol Sci. 2021 Jul 11;22(14):7431. doi: 10.3390/ijms22147431. PMID: 34299051; PMCID: PMC8304389.

Staniszewska M, Iking J, Lückerath K, Hadaschik B, Herrmann K, Ferdinandus J, Fendler WP. Drug and molecular radiotherapy combinations for metastatic castration resistant prostate cancer. Nucl Med Biol. 2021 May-Jun;96-97:101-111. doi: 10.1016/j.nucmedbio.2021.03.009. Epub 2021 Apr 9. PMID: 33866131.

List of contents

Abbreviations

%IA/g	Percentage injected activity per gram
µg	Microgramm
µL	Microliter
µm	Micrometer
µM	Micromolar
^{177}Lu	^{177}Lutetium
^{18}F	^{18}Fluoride
^{18}O	^{18}Oxygen
^{225}Ac	^{225}Actinium
^{68}Ga	^{68}Gallium
^{68}Ge	^{68}Germanium
^{223}Ra	^{223}Radium
A. dest.	Aqua destillata
ADT	Androgen deprivation therapy
APC	Antigen presenting cells
AR	Androgen receptor
ARB	Androgen receptor blocade
ATM	Ataxia telangiectasia mutated
ATR	Ataxia telangiectasia and Rad3 related
ATRi	ATR inhibitor/inhibition
BiTE	Bispecific T cell engager
Bq	Becquerel
BRCA1/2	Breast cancer 1 and 2
BSA	Bovine serum albumine
BUN	Blood urea nitrogen
CAR T	Chimeric antigen receptor therapy
CDK	Cyclin-dependend kinase
cGAS–STING	Cyclic GMP-AMP Synthase-Stimulator of Interferon Genes
CRPC	Castration-resistant prostate cancer
CT	Computed tomography
CTLA-4	Cytotoxic T lymphocyte antigen-4
DAMPs	Damage-associated molecular patterns
DBD	DNA-binding domain
DCs	Dendritic cells
DDR	DNA damage response
DNA	Deoxyribonucleic acid
DPBS	Dulbecco´s Phosphate Buffered Saline
dsDNA	Double stranded DNA
EDTA	Ethylendiamintetraacetat
FDA	US Food and Drug Administration
FDG	Fluor-2-desoxy-D-glucose
FFPE	Formalin-fixed parafin-embedded
Fig.	Figure
FOLH1	Folate hydrolase 1
FSC	Forward Scatter
g	Gramm

G	Giga
GCP-II	Glutamate carboxypeptidase II
h	Hour
HCT	Hematocrit
HGB	Hemoglobin
HMGB1	High mobility group box 1
HPLC	High performance liquid chromatography
HR	Homologous recombination
ICB	Immune checkpoint blockade
ICD	Immunogenic cell death
IHC	Immunhistochemistry
i.p.	Intraperitoneal
IT	Immunotherapy
i.v.	Intravenous
kDa	Kilodalton
keV	Kiloelectron Volt
L	Liter
LET	Linear energy transfer
M	Mega
mA	Milliampere
mAb	Monoclonal antibody
MAPK	Mitogen-activated protein kinase
MCH	Mean corpuscular hemoglobin
MCHC	Mean corpuscular hemoglobin concentration
mCRPC.	Metastatic castration-resistant prostate cancer
MCV	Mean corpuscular volume
mg	Milligramm
MHC class I	Major histocompatibility complex class I
min.	Minute
MIP	Maximum intensity projection
mL	Milliliter
MMR	Mismatch repair
MMRd	Mismatch repair deficiency
MSI	Microsatellite instability
mTOR	Mechanistic target of rapamycin
NEPC	Neuroendocrine prostate cancer
ng	Nanogramm
NHEJ	Non-homologous end joining
NK	Natural killer
nm	Nanometer
OS	Overall survival
PARP	Poly(ADP-ribose)-Polymerase
PARPi	PARP inhibitor/inhibition
PBS	Phosphate buffered saline
PCa	Prostate cancer
PCR	Polymerase chain reaction
PD-1/PD-L1	Programmed cell death receptor/ligand

PET	Positron emission tomography
PFA	Paraformaldehyde
PI	Propidium iodide
PI3K	Phosphatidylinositol-3-kinase
PIN	Prostatic intraepithelial neoplasia
PLT	Platelet count
PSA	Prostate specific antigen
PSMA	Prostate specific membrane antigen
PTEN	Phosphatase and tensin homolog
PVE	Partial volume effect
RBC	Red blood cell count
RIPA	Radioimmunoprecipitation buffer
ROI	Region of interest
RLT	Radioligand therapy
rPFS	radiographic progression-free survival
RS	Replication stress
RT	Room temperature
s.c.	Subcutaneous
SD	Standard deviation
SDS PAGE	Sodium dodecylsulfate polyacrylamide gel electrophoresis
sec	Second
SOC	Standard of care
SSC	Side Scatter
STR	Short tandem repeats
TAA	Tumor-associated antigens
Tab.	Table
TAE	Tris-Acetat-EDTA-Puffer
TBE	Tris-Borat-EDTA-Puffer
TBS	Tris Buffered Saline
TLC	Thin layer chromatography
TMB	Tumor mutation burden
TP	Total protein
T_{reg}	Regulatory T cells
Tris	Tris(hydroxymethyl)-aminomethan
TTP	Time to Progression
U	Units
UV	Ultraviolet
V	Volt
VOI	Volume of interest
W	Watt
WBC	White blood cell count
x g	x-fold gravitational acceleration

List of figures

List of tables

1. Introduction

1.1 Cancer- a never ending challenge?

Despite more refined knowledge and therapeutical advances, cancer still remains one of the greatest challenges of modern medicine. In 2020, cancer accounted for nearly 10 million deaths becoming the most common cause of death worldwide[1]. The word “cancer” describes a large group of diseases which can originate from any tissue of the body having similar basic characteristics in common, including uncontrolled growth and spread of abnormal cells throughout the body. Cancer development is a multistep process during which cells undergo multiple alterations leading to formation of malignant neoplasms. Genomic instability fosters carcinogenesis by expediting disbalance of cell cycle control, inducing chronic proliferation, bypassing tumor suppressors and apoptosis[2]. Cells lacking proper growth regulation divide in an uncontrolled manner, infiltrating healthy tissue and eventually spreading throughout the body forming metastases. For the development of novel therapies not only the genetic and phenotypic diversity has to be taken into account but also the complex interactions with tumor stroma and the immune system. To maintain survival, tumors create their own microenvironment by inducing angiogenesis in order to sustain nutrient and oxygen supply. Differentiation of stromal cells towards cancer-associated fibroblasts promotes remodeling of extracellular matrix to support tumor growth and spread[3]. Additionally, to ensure fast cell proliferation, neoplasms alter energy metabolism by favoring glycolysis and glutaminolysis. In past decades, technological advances such as next-generation sequencing, single-cell analysis approaches, “-omics”-technologies and imaging modalities delivered tools allowing more detailed characterization of cancer. However, with progressing understanding of the disease the inter- and intratumoral heterogeneity becomes more apparent which changes the perspective of treatment approaches and shifts the focus to targeted therapies and patient-tailored medicine. Moreover, the multifaceted character of cancer and remarkable adaptation skills contribute to the issue of resistance and recurrence complicating the design of efficient therapeutic regimens. Hence, identifying and targeting of more than one cancer vulnerability in form of well- balanced and personalized combinatory approaches is evolving to a cornerstone of oncology.

1.1.1 The Prostate- small organ, great impact

The prostate gland is an approximately 3 centimeters long and 30 grams in weight organ located in the pelvis at the base of the penis and anterior to the rectum, surrounding the posterior part of the urethra. The word “prostate” has its origins in Greek where it means “one who stands before”, referring to its inferior position to the urinary bladder (**Fig.1**). The prostate gland is encapsulated by connective tissue consisting of several smooth muscle fibers which, during ejaculation, contract and press the fluid out into the urethra. The smooth muscles and fibroblasts are composing the prostate stroma whereas the epithelial compartment of the prostate contains distinct cell types including basal cells, secretory luminal cells and intermediate and neuroendocrine populations[4]. Luminal cells produce secretory proteins such as the prostate-specific antigen (PSA) and express androgen receptor (AR). Basal cells are located between the basal membrane and the luminal cells and express high-molecular-weight cytokeratins 5 and 14 and the stem cell transcription factor p63. The function of neuroendocrine cells is less known; however, they are AR-negative and hormone-resistant and can give rise to an aggressive variant of prostate cancer (PCa), the neuroendocrine prostate cancer (NEPC)[5,6]. The human prostate consists histologically of three zones: peripheral, central and transition zones[7]. The majority of benign hyperplasias originate from the transition zone whereas PCa develops in the peripheral zone .

The main functions of the prostate gland are production of seminal fluid that constitutes about 30 % of the semen, closing of the urethra up to the bladder during ejaculation to prevent semen from entering the bladder, and androgen hormone metabolism.

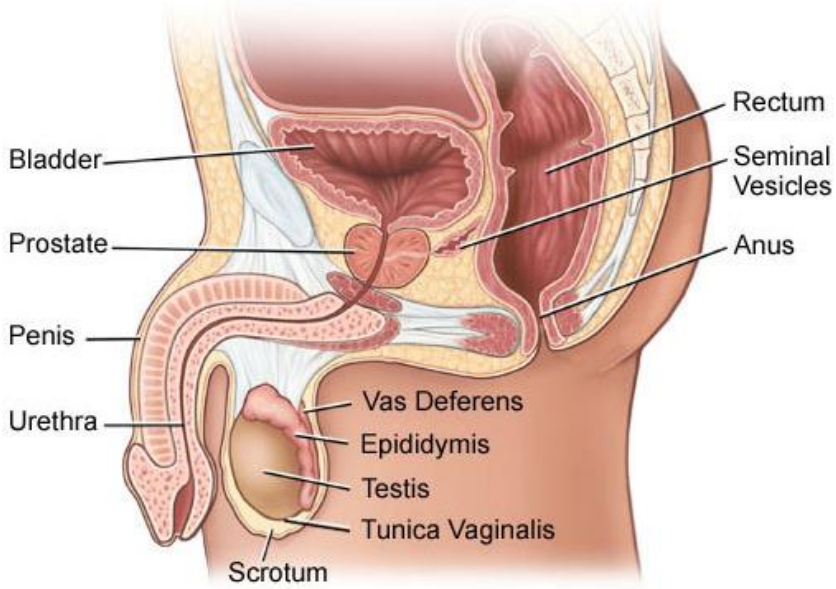

Figure 1 Male reproductive tract.
The prostate gland is located in the pelvis at the base of the penis and anterior to the rectum, surrounding the posterior part of the urethra. Adapted from https://www.uclahealth.org/urology/prostate-cancer/what-is-prostate-cancer

1.1.2 Prostate cancer

PCa is the second most common solid malignancy diagnosed in men with approximately 1.4 million new cases worldwide in 2020[1]. Moreover, it accounted for over 375 thousand deaths becoming the fifth leading cause of cancer death in men. Strongest risk factors for PCa include age, ethnicity and family history[8]. Additionally, infection, obesity and diet have been linked to prostate inflammation and carcinogenesis[9]. In most cases, PCa shows limited aggressiveness and slow growth. At early stages, it rarely exhibits any symptoms. However, with disease progression pain in the lower pelvic area, frequent urination, hematuria and anemia can occur. PCa may also impair sexual functions such as difficulty achieving an erection or painful ejaculation[10]. Standard diagnostic routine of PCa consists of digital rectal examination, PSA blood test and transrectal ultrasound guided biopsy. Histopathological analysis of prostate tissue is performed based on the Gleason score classifying it from 6 to 10 (most to least differentiated)[11]. Invasiveness, lymph node involvement and the presence and degree of metastases are also taken into account[12]. High grade prostatic intraepithelial neoplasia (PIN) is widely accepted as precursor state of PCa[13,14]. Main histological traits of PIN include the appearance of luminal epithelial hyperplasia, reduction in basal cells, enlargement of nuclei and nucleoli, cytoplasmic hyperchromasia, and nuclear atypia along with increased expression of cellular

proliferation markers[5]. Prostate adenocarcinoma exhibits a luminal phenotype and is deficient in basal cells[12], implying that luminal cells correspond to a cell of origin.

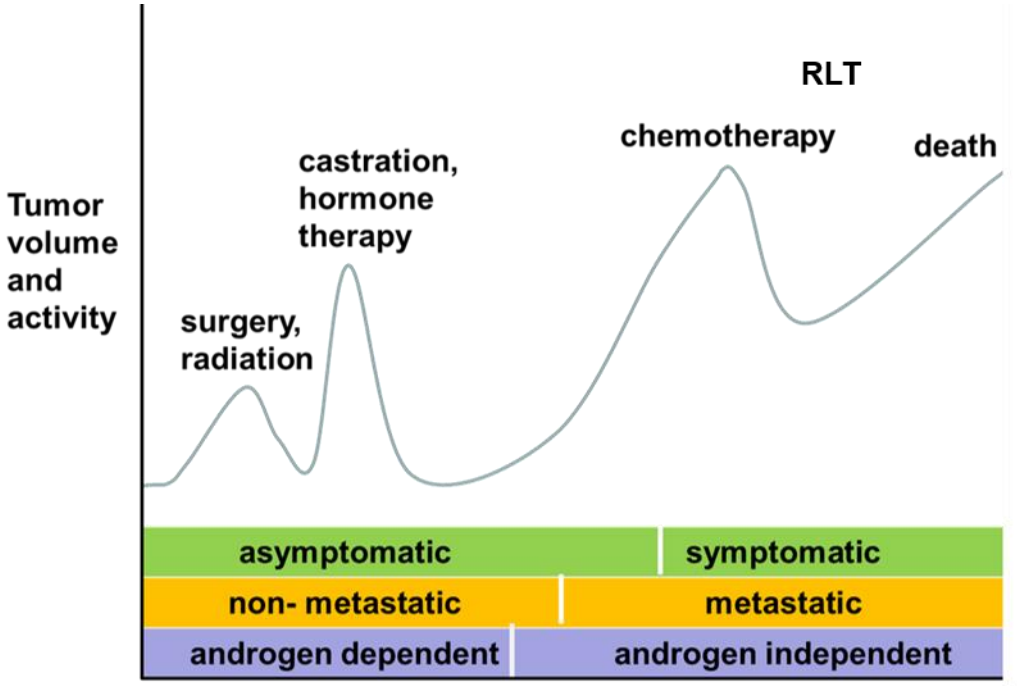

Figure 2 Disease continuum of PCa.
In early stages of PCa, several therapeutic options exist including surgery, castration, and hormone therapy. In later stages, chemotherapy and radioligand therapy (RLT) are available therapeutic modalities, although the disease is incurable. PCa develops from an androgen dependent to an androgen independent state which is characterized by a more aggressive phenotype.

Localized disease is characterized by androgen-dependency and several therapeutic options for primary PCa exist. Thus, with disease progression PCa becomes androgen-independent and symptomatic. The lethal stage of the disease, metastatic castration-resistant PCa (mCRPC) (**Fig. 2**), is characterized by widespread metastases in the body, particularly in the bones[15]. Other common sites of metastases are lung, liver, and pleura. The prognosis of mCRPC patients is very poor with a median survival between 9-13 months[16].

PCa is considered a morphologically and molecularly heterogeneous disease with varying genomic and phenotypic profiles. Primary tumors often harbour multiple independent foci which show high levels of subclonality and different mutation profiles[17,18]. In contrast, analyses of metastatic PCa reveal its monoclonal nature suggesting that metastases might originate from an individual clone and are a result of clonal selection[19]. However, it needs to be evaluated which factors contribute to clonal evolution and selective pressure and especially if this process is fueled by therapeutic

procedures such as androgen deprivation therapy (ADT) and AR blockade (ARB) or chemotherapy. NEPC has been shown to develop primarily as a result of prolonged hormonal therapy but also after docetaxel therapy or even after ARB[20,21]. Compared to other tumor entities such as melanoma and lung cancer, PCa has relatively low tumor mutation burden (TMB)[22]. Genomic abnormalities identified in PCa include aberrations of AR (57 %), ETS genes (30 %), TP53 (43 %) and Phosphatase and Tensin homolog (PTEN) (35 %), with TP53 and AR alterations mostly occurring in mCRPC compared to locally confined PCa. Moreover, aberrations of breast cancer 1 and 2 (BRCA1/2, 15 %), ataxia telangiectasia mutated (ATM) genes (7 %) and ataxia telangiectasia-and rad3-related protein (ATR, 9 %) are more frequent in mCRPC than in primary PCa[23]. On the histological level, the most common type is acinar adenocarcinoma accounting for 93 % of all PCa while other types such as ductal adenocarcinoma, mucinous carcinoma, and signet ring carcinoma are very rare.

1.1.2.1 Androgen signaling axis in PCa

Androgens play an essential role in the development, growth and regulation of physiological functions of the prostate. Androgens are synthesized mainly by the Leydig cells in the testes. This process is regulated through the hypothalamic–pituitary–gonadal axis. Gonadotropin-releasing hormone is released by the hypothalamus which in turn stimulates the secretion of luteinizing hormone by the pituitary gland. Testosterone is then produced by the gonads. After secretion, testosterone circulates in the blood bound to the carrier proteins serum sex hormone-binding globulin or albumin[24,25]. Free testosterone enters the prostate by passive diffusion where it is converted into a more potent form, 5α-dihydrotestosterone which is essential for the growth and physiology of prostate. Androgens mediate their effects via binding to the AR, a member of the nuclear receptor transcription factor superfamily. AR is located in the cytoplasm of prostate stromal cells and is associated with heat-shock proteins. Binding of androgens to AR results in conformational changes, dissociation of chaperone proteins and exposure of the nuclear localization signal which is responsible for import of the androgen/AR complex into the nucleus. In the nucleus, AR dimerises and binds to androgen response elements in the promoter regions of target genes (e.g. PSA, Kallikrein 2), modulating gene transcription[26].

The AR pathway is considered the most important driver of prostate carcinogenesis. Since it was shown that androgen deprivation has a negative impact on PCa growth[27],

ADT/ARB are essential components of disease management and provide long-term remissions even in advanced PCa[28,29]. Unfortunately, PCa becomes resistant to ADT/ARB and progresses to the castration-resistant form (CRPC)[30]. Resistance is mediated by maintenance of AR signaling which is facilitated by AR alterations such as AR splice variants (e.g., AR-V7), hypersensitivity to ligand binding, ligand independent AR activation and intratumoral androgen production[31].

1.1.2.2 Prostate specific membrane antigen

The prostate-specific membrane antigen (PSMA), also known as folate hydrolase 1 (FOLH1) and glutamate carboxypeptidase II (GCP-II), is a type II transmembrane glycoprotein (100–120 kDa) predominantly expressed on prostatic epithelium but also on proximal renal tubules and, to a lower degree, in small intestine, salivary glands and glial cells in the brain[32,33]. The gene encoding PSMA is located on the short arm of chromosome 11[34]. The PSMA protein is composed of a 19 amino acid N-terminal intracellular domain, a 24 amino acid transmembrane domain and a 707 amino acid C-terminal extracellular domain[35]. The extracellular domain of PSMA interacts with ligands (see below) via its catalytic domain and a zinc-containing, substrate-binding site[36]. In normal prostate tissue, PSMA is localized in the cytoplasm and apical site of the epithelium surrounding prostatic ducts. During prostate carcinogenesis, PSMA is translocated from the apical site to the luminal site of prostate ducts. Upon ligand binding, PSMA undergoes clathrin-mediated endocytosis[37]. After internalization, ligands are being released in the cytoplasm while PSMA is recycled[38]. PSMA mainly acts as glutamate-preferring carboxypeptidase but also exhibits enzymatic function as folate hydrolase. Poly-γ-glutamated folate has been identified as PSMA substrate in proximal small intestine[33,39]. In PCa, PSMA has been shown to provide a signal necessary to activate the Akt pathway[40]. Moreover, PSMA is linked to tumor angiogenesis due its expression on neovasculature of solid tumors including renal cell, bladder and colon cancers[33]. However, the exact roles PSMA plays in prostate physiology and pathology are still poorly understood.

PSMA is highly expressed on the majority of prostate cancer cells (100-fold to 1.000-fold compared to expression levels on healthy prostate epithelium, small intestine, renal tubular cells and the salivary glands)[33,41] and its expression correlates with grading and staging of PCa with increased expression levels in advanced and

castration-resistant disease[42,43]. Given this characteristics, PSMA evolved as an attractive target for diagnosis and therapy of PCa.

1.1.2.3 Theranostics in PCa

Theranostics in nuclear medicine is an emerging clinical approach of precision medicine which combines diagnostic imaging and radioligand therapy (RLT) to provide personalized disease management. A theranostic radioligand-pair shares the same target, e.g., a protein overexpressed on target tissue, but is linked to radionuclides with different physical properties (**Fig. 3**). The aim of RLT is to specifically deliver radiation to tumor lesions using high-affinity radioligands targeting overexpressed markers in cancer, and long-lived isotopes with short particle range to spare surrounding tissue. For imaging, short-lived nuclides with long particle range are used such as ^{68}Gallium (^{68}Ga) and ^{18}Fluoride (^{18}F). One of the main imaging modalities in nuclear medicine, positron emission tomography (PET), exploits the beta+ decay of radionuclides; the injected radionuclide binds to the target and enriches in tumors; it emits a positron which interacts with an electron; this collision results in emission of a pair of 511-keV annihilation (gamma) photons, ~180° apart. Those photons are simultaneously detected from many different angles around the patient and images are attenuation-corrected and reconstructed[44], visualizing the distribution of the injected radioligand within the body in a three dimensional resolution. The molecular and functional data obtained by PET are commonly complemented by computed tomography (CT)-derived anatomical information.

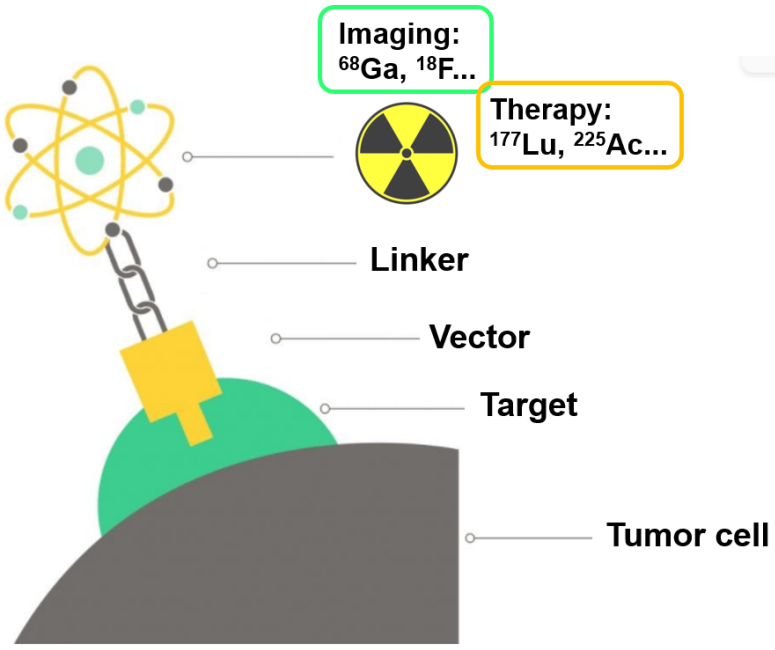

Figure 3 Schematic illustration of a radioligand and the theranostic principle.
The tracer consists of a specific binding entity (vector) which binds to a target on cancer cells, and a linker for labelling with radionuclides. Different radionuclides can be chelated with the linker-vector construct which can be used either for imaging or therapy. Adapted from https://www.genesiscare.com/au/treatment/cancer/theranostics/.

Due to its favorable features described above (1.1.2.2), introduction of PSMA as a target revolutionized theranostics for PCa. The first PSMA-targeting theranostic agent was the radiolabeled antibody 7E11-C5[45]. However, despite promising results in preclinical studies, its clinical application for imaging was impeded because 7E11-C5 binds to the intracellular domain of PSMA binding only dying or dead cells. Further development of monoclonal antibodies (mAbs) targeting the extracellular domain of PSMA resulted in new promising agents such as mAb J591[46]. J591 showed promising therapeutic efficacy in mCRPC patients[47,48]. However, long circulation times and slow penetration characteristics limits the applications of mAb in theranostic approaches. Thus, the breakthrough was made with PSMA-targeting small molecules that mostly are mimetics of its natural ligand, N-acetylaspartylglutamate and can be divided into three groups: phosphorus-based, thiol-based and urea-based structures. So far, urea-based peptidomimetics have been the most successful in clinical applications.

For imaging purposes, ^{68}Ga-PSMA-11 is the most widely used PSMA PET tracer due to its favorable properties such as high receptor affinity and excellent tissue penetration, even in osseous metastases[49,50].

^{177}Lutetium-PSMA-617 (^{177}Lu-PSMA-617) is a beta-emitting peptidomimetic that has been introduced as novel therapy for mCRPC. ^{177}Lu-PSMA-617 shows high and specific affinity for PSMA and favorable physical properties which contribute to prolonged anti-tumor effects, such as a 7- days half-life. Particle range is an important factor in the choice of the appropriate isotope for RLT. Although beta emitters have relatively long particle range (670 µm for ^{177}Lu) compared to alpha emitters (~80 µm) and thus might cause less severe clustered DNA damage, this apparent disadvantage might enable “crossfire effects” that allow destruction of the PSMA-positive radioligand-bound tumor cells as well as of PSMA-negative cells, compensating for heterogeneity in target expression.

Promising results of ^{177}Lu-PSMA-617 in mCRPC patients (**Fig. 4**) have been reported by several trials[41,43,51,52] and ^{177}Lu-PSMA-617 RLT moved closer to regulatory approval. The VISION trial demonstrated that addition of ^{177}Lu-PSMA-617 to standard of care therapy (SOC) led to a 60 % reduction in the risk of death and a 4-month improvement in median overall survival (OS) versus SOC alone. Addition of RLT also led to a 5.3-month improvement in median radiographic progression-free survival (rPFS)[52]. Nearly half of the patients (46 %) experienced PSA drop by 50 % or greater. Similarly, 66 % of mCRPC patients in the TheraP trial exhibited a PSA response ≥50 %, while the remaining 34 % of patients did not show a relevant PSA decline after RLT[53]. Moreover, 59 % of patients in this trial showed at least one mismatch metastasis in combined ^{18}F-2-Fluor-2-desoxy-D-glucose (FDG) and ^{68}Ga-PSMA-11 PET imaging (^{18}F-FDG-positive and ^{68}Ga-PSMA-11-negative). The presence of discordant ^{18}F-FDG-avid lesions without sufficient PSMA expression was associated with poor outcome (median OS from the time of combined PET imaging: 3.3 months vs. 6.1 months; from the start of PSMA-RLT: 9.7 months vs. 15.3 months, respectively). The VISION trial demonstrated that about 10 % of patients will not be eligible for RLT due to insufficient tumoral PSMA expression (based on ^{68}Ga-PSMA-11 PET imaging)[52]. Given that approx. one third of patients will not respond to RLT, there is an urgent need to improve ^{177}Lu-PSMA-617 RLT efficacy. The underlying resistance mechanisms are still poorly understood; however, de-regulation of DNA damage response (DDR) pathways[54] and tumor-immune system interactions[55] are discussed as potential factors conferring treatment resistance.

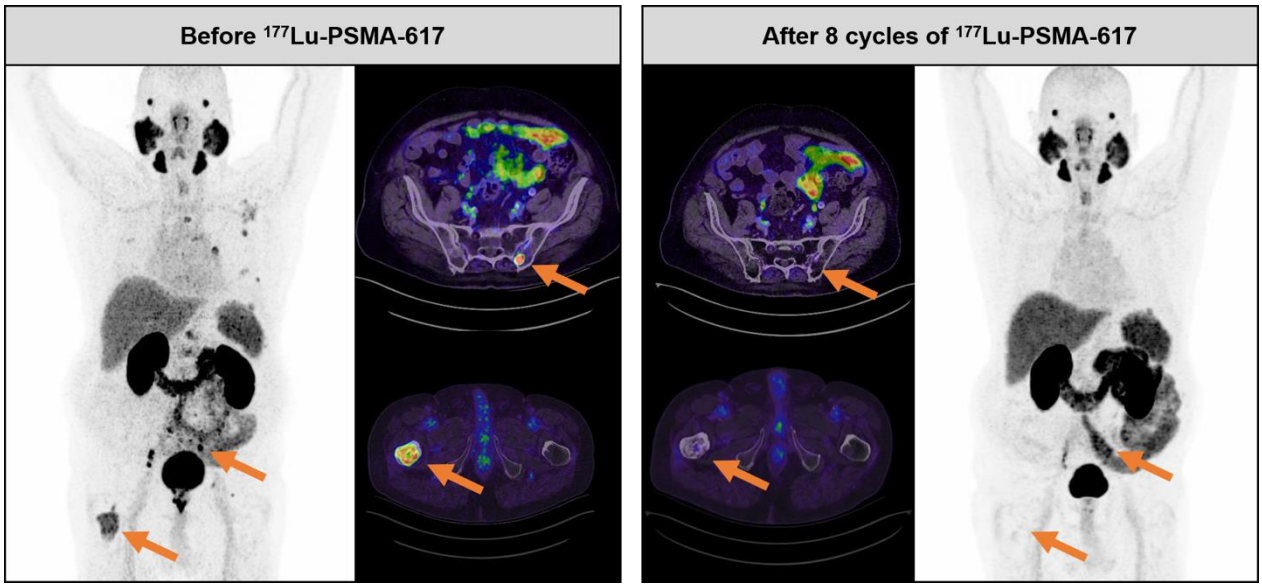

Figure 4 Case example of a mCRPC patient treated with ^{177}Lu-PSMA-617.
The patient was pretreated with novel androgen axis drugs and taxane-based chemotherapy before undergoing ^{177}Lu-PSMA-617 therapy. PSA dropped from 22.1 ng/mL to 0.48 ng/mL after eight cycles of RLT. ^{68}Ga-PSMA-11 PET (right side) revealed complete resolution of osseous metastasis (orange arrows). Data were generated at the University Hospital Essen, Germany[56].

1.1.2.4 DNA damage response in PCa

Genomic instability is one of the hallmarks of cancer[2]. DNA is targeted by various environmental and intrinsic factors and occurrence of spontaneous DNA damage is estimated at ~2 x10^5 lesions per day[57]. Such high rate of damage necessitated the emergence of advanced repair pathways to ensure DNA integrity. Although the majority of damage is repaired quickly and does not pose a high threat to the cell, a rare fraction of lesions are DNA double strand breaks (DSBs), highly toxic events which can be induced by ionizing radiation (IR), such as delivered by RLT[58,59]. When DNA damage occurs, a complex network of intersecting signaling pathways referred to as DNA damage response (DDR) signaling is activated. Depending on the severity of the damage, different pathways might be activated, which in turn determines outcome. The primary three pathways include homologous recombination repair (HR), nonhomologous end joining (NHEJ) and alternative end joining which differ from each other in accuracy of restoring the original DNA sequence. It has been reported that HR provides high-fidelity repair and maintaines the original DNA sequence[60] whereas NHEJ and alternative end joining are more error-prone[61]. Therefore, especially for the repair of DSBs, and to maintain genome integrity, cells rely on an intact HR pathway. Multiple studies indicate that germline mutations in HR-involved genes are associated

with a higher risk of developing PCa[62,63] but those alterations are also reported to enrich during PCa progression[64]. In mCRPC, aberrations in BRCA1/2 (15 %), ATM (7 %) and ATR (9 %) were observed at higher frequencies[23,65] as compared to localized disease. Thus, targeting HR deficiency has become a promising approach for PCa treatment[66] based on the concept of synthetic lethality. Synthetic lethality occurs when deletion of two genes simultaneously results in cell death, whereas the inactivation of only one of these genes has no or little impact on cell viability[67,68]. Especially Poly(ADP-ribose) polymerase (PARP) became an interesting target due to its interaction with BRCA1 and BRCA2. Tumors with mutations in BRCA1/2 genes were shown to be sensitive to PARP inhibition[69]. PARP is one of the main enzymes involved in detection and repair of DNA single strand breaks (SSBs). PARP inhibitors trap PARP1 at the site of SSBs which require BRCA1/2-dependent repair[70]. Unrepaired SSBs lead to collapse of replication forks and, in consequence, to development of DSBs (**Fig. 5**).

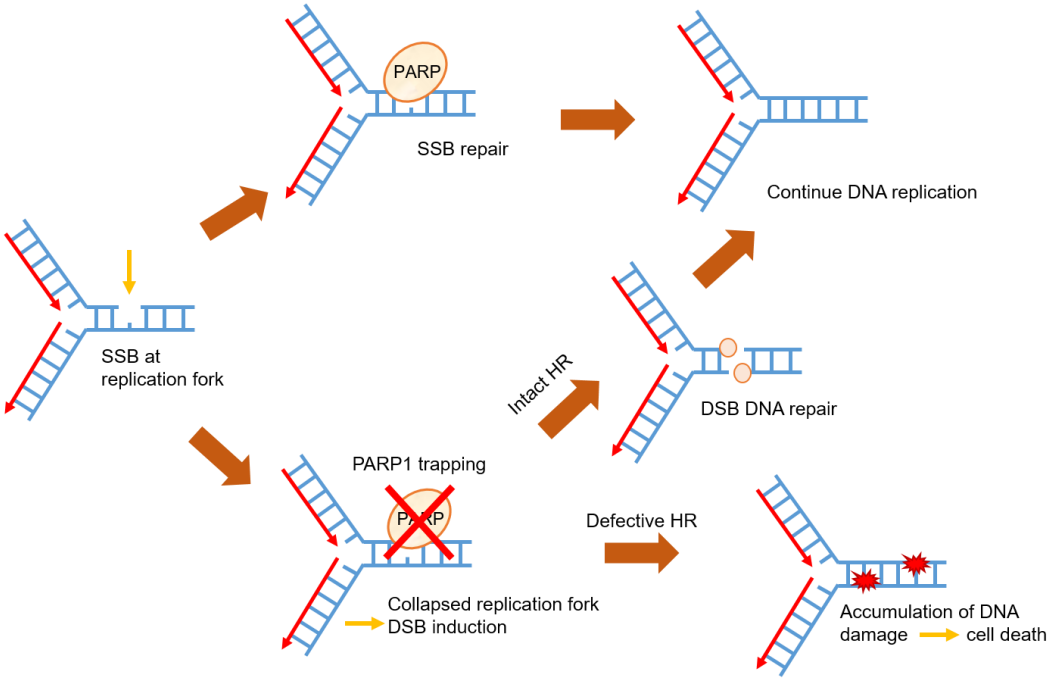

Figure 5 Mechanism of action of PARP1 and its inhibition.
PARP is recruited to SSB site at replication forks and induces HR-dependent DNA repair. PARP inhibition causes PARP to be trapped in the DNA leading to collapse of replication fork and induction of DSBs which can be repaired through intact HR mechanism. In case of defective HR, DSB remain unrepaired leading to accumulation of DNA damage and in consequence to cell death. Figure adapted from Personalized Medicine 2015 Future medicine Ltd.

ATM and ATR play central regulatory functions in DDR and coordinate a complex network of downstream signals (**Fig. 6**). ATM initially promotes HR; however, it is not

essential for HR-mediated repair[71]. In contrast, ATR, controlling later steps of HR, was reported to play an essential role for HR-mediated repair and its inhibition or loss impairs the ability of cells to utilize HR[72]. ATR induces restoration of stalled replication forks and delay of cell cycle progression through activation of the G2/M checkpoint, which arrests cells in the G2 phase to give them time for DNA repair. Thus, ATR inhibition (ATRi) results in premature mitotic entry, chromosome aberrations and apoptosis. Therefore, ATR gained attention in recent years as a potential target to inhibit DDR. Because PARP inhibition (PARPi) increases the reliance on ATR signaling for genome stability, and vice versa, inhibition of ATR might increase reliance on HR for proper replication, the combination of PARPi with ATRi might be a promising combinatory approach to overcome resistances to RLT[73].

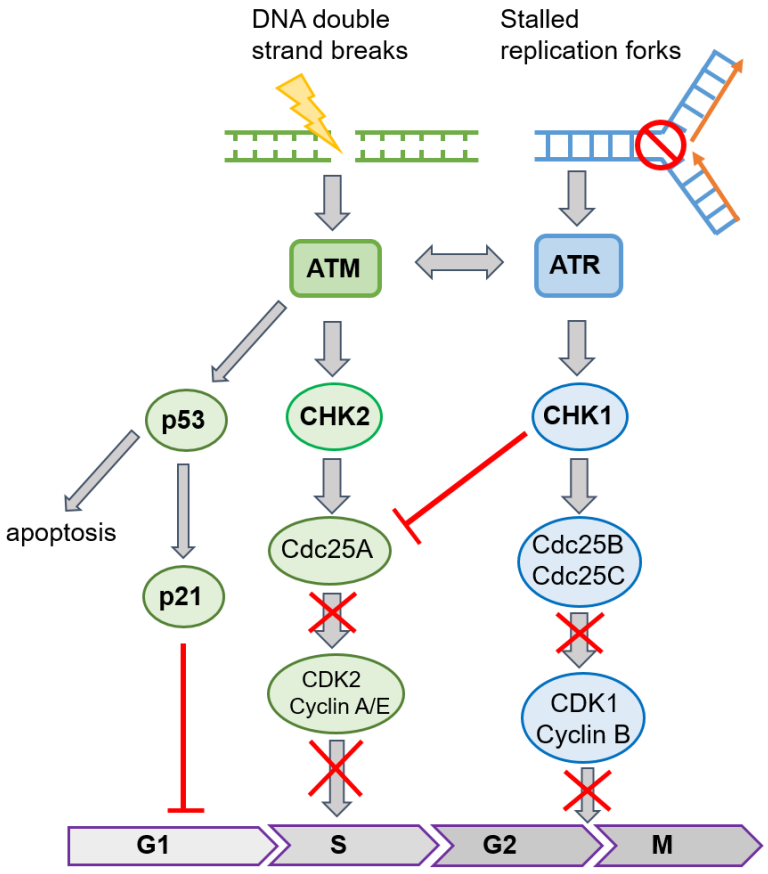

Figure 6 Simplified representation of ATM and ATM pathways.
ATM and ATR pathways are activated by DNA double-strand breaks or by DNA single strand breaks and replication stress, respectively. Cell cycle checkpoints are induced primarily through phosphorylation of p53, CHK2 and CHK1. Activated p53 leads to G1-phase arrest which is mediated through increase of p21 and induces apoptosis. Cdc25 phosphatase control cyclin-dependent kinases (CDKs), which in turn control progression through S-phase and entry into mitosis. Phosphorylation of Cdc25 phosphatases by CHK1 or CHK2 inhibits their activity abolishing CDK–cyclin activation. ATM and ATR overlap in their signaling pathways. Both, CHK1 and CHK2 can phosphorylate Cdc25A and Cdc25C, depending on the source of genotoxic stress. Adapted from Qiu et al., 2018, Molecular Radiobiology[74].

PARP inhibitors have already been introduced into the clinic with olaparib and rucaparib being the two agents approved by the US Food and Drug Administration (FDA) for the treatment of mCRPC patients with deleterious germline or somatic HR gene mutations[66,75]. Other PARP inhibitors, niraparib and talazoparib, are currently under investigation showing good safety and effectivity[76-81]. ATR inhibitors for PCa are still evaluated in clinical trials, e.g., ceralasertib (NCT04564027) and M6620 (NCT03517969). Combined ATRi and PARPi in mCRPC is currently tested in a phase II trial (NCT03787680).

Besides HR, DNA mismatch repair (MMR) fulfills important functions in detection and repair of errors during DNA replication[82]. MMR deficiency (MMRd) can lead to genetic hypermutability often referred to as microsatellite instability (MSI). MSI occurrence correlates with increased mutational load[83] and expression of tumor neoantigens, which might induce immune responses[84]. Loss of function alterations in MMR genes (i.e., MLH1, MSH2, MSH6 and PMS2) have been found in a small subset of patients with advanced PCa (3.1 %)[85]. Reportedly, MMRd-tumors show a higher probability for responses to immune checkpoint blockade (ICB)[86].

1.1.2.5 Immune landscape of PCa

In recent years, immunotherapy (IT) has revolutionized the disease management of a broad range of cancer types[87-89]. Unfortunately, this has not been observed in PCa so far. This may be attributed to the predominantely “immune-excluded” or “immune-desert” immunophenotype of PCa. The immune desert phenotype is characterized by low T-cell infiltration, presence of immunosuppressive cell populations in the tumor microenvironment such as myeloid-derived suppressor cells[90,91] and low major histocompatibility complex (MHC) class I expression[92]. The phenomenon of immune exclusion can be described as limited presence of T cells at the periphery of tumors without intra-tumoral infiltration[93]. Additionally, low TMB, a reduced chemokine gradient and impaired T-cell functionality contribute to poor responsiveness to IT[92]. The application of immunotherapeutics in PCa provided only modest survival benefits. Sipuleucel-T (PROVENGE), the first FDA approved cell-based cancer IT, is based on antigen presenting cells (APCs) which are isolated from patients and primed *ex vivo* with a recombinant fusion protein build of prostate antigen, prostatic acid phosphatase, and granulocyte-macrophage colony-stimulating factor (an immune cell activator). Sipuleucel-T conferred a median OS benefit of 4.1 months but no improvement in PFS

or decline of PSA levels have been reported[94]. Another cancer vaccine, PROSTVAC, failed in a phase III trial having no effect on OS[95]. However, the second-generation human Ad5 (hAd5) IT vaccine targeting tumor-associated antigens (TAA) of PSA, MUC-1, and brachyury met its primary endpoints and showed good tolerability[96]. Another group of therapeutics, ICB, has become a pillar of IT. The programmed cell death receptor 1 (PD-1) / PD-Ligand 1 (PD-L1) and the cytotoxic T lymphocyte antigen-4 (CTLA-4) signaling axes represent mechanisms by which tumors evade the immune system. PD-1 is expressed on activated T, natural killer (NK) and B lymphocytes, macrophages, dendritic cells (DCs) and monocytes[97] and on tumor-specific T cells. PD-1 plays an immunosuppressive role and its expression leads to T cell exhaustion. PD-L1 is usually expressed by macrophages, activated T cells and B cells, DCs and some epithelial cells[98]. It acts as an “adaptive immune evasion mechanism” in cancer cells[99] allowing them to escape anti-tumor responses. Interaction between PD-1 and PD-L1 results in inhibition of downstream signaling and T cell biological functions, including lymphocyte proliferation, cytokine secretion, and cytotoxic T lymphocyte cytotoxicity[100]. While PD-1/ PD-L1 inhibition in PCa results in very limited responses, pembrolizumab, an anti-PD-1 antibody, was approved in 2017 for patients with metastatic, MSI-high or MMRd-solid tumors because of improved outcome in this patient cohort[101]. However, due to the low prevalence of MSI-high/MMRd PCa phenotypes, only a small cohort of patients benefit from treatment with pembrolizumab. CTLA-4, another immune checkpoint, is expressed by both $CD4^+$ and $CD8^+$ T cells and interacts with two ligands expressed on APCs, CD28 and CD80, with higher affinity for CD80[102]. The CTLA-4-CD80 binding inhibits further activation of T cells by indirect suppression of signaling through the co-stimulatory receptor CD28[103]. The anti-CTLA-4 agent ipilimumab was tested in three phase III trials in mCRPC patients and failed to improve OS in two of them[104,105]. However, Fizazi et al. reported two to three times higher OS rates when ipilimumab was combined with radiotherapy arm vs. placebo[106]. Another immunotherapeutic approach includes bispecific antibodies which are used to mediate the interaction between tumor cells and T cells. The bispecific antibody MOR209/ES414 (NCT02262910) and the bispecific T cell engager (BiTE) AMG 160 are currently being tested in CRPC patients in combination with pembrolizumab (NCT03792841).

Both MOR209/ES414 and AMG 160 target PSMA on tumor cells and CD3 on the T cells which induces the proliferation of $CD3^+$ cells and subsequent secretion of cytokines leading to tumor cells death[107,108]. Chimeric antigen receptor therapy (CAR T) is another emerging concept of IT[109]. CARs are engineered receptors on patients own T cells utilizing defined specifity (either antibody-derived antigen-binding motifs or receptor or ligand derived domains[110,111]) to recognize tumor antigens. Once applied, CAR T cells travel to tumor sites where they killtumor cells. The subsequent release of TAA can trigger additional proliferation of CAR T cells but also the recruitment of non-CAR T cells inducing further anti-tumor responses. Next-generation anti-PSMA CAR T cells showed moderate responses in PCa xenograft mouse models[112,113]. Anti-PSMA CAR T cells for PCa are currently extensively investigated in clinical trials[114-116]. Although the field is rapidly evolving, IT as single treatment might not be sufficient to achieve long-term responses in PCa. To fully exploit the potential of IT, combination with other therapeutic agents that enhance PCa immunogenicity might be required.

1.1.2.6 Therapeutic options for advanced PCa- where do we stand?

Despite several new therapeutic options, mCRPC still remains incurable and the survival benefits of therapy regimens are rather poor.

For localized disease, several potentially curable therapies exist including radical prostatectomy, brachytherapy and external beam radiation therapy along with active surveillance for low-risk disease.

Given that the development of PCa is highly dependent on androgen receptor signaling, targeting the androgen receptor signaling axis with ADT and ARB are considered as backbone of disease management. However, those therapies will eventually fail as PCa becomes insensitive to ADT and ARB over time progressing to the lethal stage of PC, the CRPC. Yet, next generation androgen-signaling inhibitors have been approved for CRPC patients who progressed under first-line ADT/ARB including abiraterone acetate and enzalutamide. Enzalutamide was shown to increase median rPFS by 14.6 months, and median OS before chemotherapy, despite cross-over, by 4 months when compared to placebo[28]. Unfortunately, most patients ultimately develop resistance.

Until 2004, chemotherapy provided only palliative benefits for advanced PCa patients. Docetaxel was the first taxane-based chemotherapy which had been approved for

mCRPC, showing life prolonging properties[117,118]. Since then, several other agents with survival advantage have been introduced. In 2010, a third-generation chemotherapeutic cabazitaxel has been approved for mCRPC patients who failed treatment with docetaxel[119]. In the phase III TROPIC trial, patients treated with cabazitaxel demonstrated longer OS and PFS when compared to the control group. For mCRPC patients harboring symptomatic bone metastases ^{223}Radium- dichloride (^{223}Ra-dichloride), a high-energy alpha-emitter, has been approved in 2013. This therapy resulted in delayed symptomatic skeletal events and improved OS (3 months)[120]. Recently, PSMA emerged as important target for RLT. ^{177}Lu-PSMA-617 RLT has been introduced as a novel therapeutic option for mCRPC. In the phase III VISION trial ^{177}Lu-PSMA-617 met both primary endpoints and improved OS and rPFS in patients with PSMA-positive mCRPC. Based on these encouraging results FDA has granted Breakthrough Therapy designation moving ^{177}Lu-PSMA-617 RLT closer to regulatory approval. For patients harboring mutations in DDR genes two PARP inhibitors (olaparib and rucaparib) have been approved. Despite sipuleucel-T and pembrolizumab, exploration of the full potential of IT for PCa is still under investigation.

1.1.2.7 Combinatory approaches to overcome resistance in PCa

Combinatory approaches for cancer treatment open new perspectives and hopes for patients with advanced or recurrent carcinomas. The idea of combination therapies was conceptualized in 1965[121], however, the last years brought forth several trials investigating different combinatory regimens. Combining two or more therapeutic agents which act in synergistic manner might enhance cancer cytotoxicity. Additionally, combination regimens might also be beneficial for overcoming resistances and helping to achieve more durable responses even in metastatic disease.

RLT can be combined with modalities such as inhibition of DDR or immunotherapy. RLT effectively induces DNA damage, especially DSBs which are highly cytotoxic and if unrepaired, cause genome instability consequentially leading to cell death. Therefore, an intact DDR is crucial for effective repair of DNA damage. Abrogation of DDR pathways might prevent the repair of RLT-induced lesions and enhance the efficacy of RLT. An ongoing phase I dose-escalation and dose-expansion study is currently evaluating the safety and tolerability of olaparib in combination with ^{177}Lu-PSMA-617 in mCRPC (NCT03874884).

Moreover, emerging evidence supports RLT as a potent immune adjuvant. Ionizing radiation creates an inflammatory, immunogenic environment by inducing immunogenic cell death (ICD). This results in release of necrotic and apoptotic tumor cells as well as debris designated as tumor-associated antigens. Those antigens are then captured by dendritic cells and presented on MHC class I and MHC class II molecules, together with co-stimulatory signal to T cells[122] resulting in the priming and activation of effector T cell responses against cancer-specific antigens. Cytotoxic $CD8^+$ T cells infiltrate the tumor microenvironment, recognize the cancer cell and induce cell death[123](**Fig. 7**). The combination of ^{177}Lu-PSMA-617 and pembrolizumab in mCRPC patients is currently evaluated in clinical trials (NCT03658447, NCT03805594).

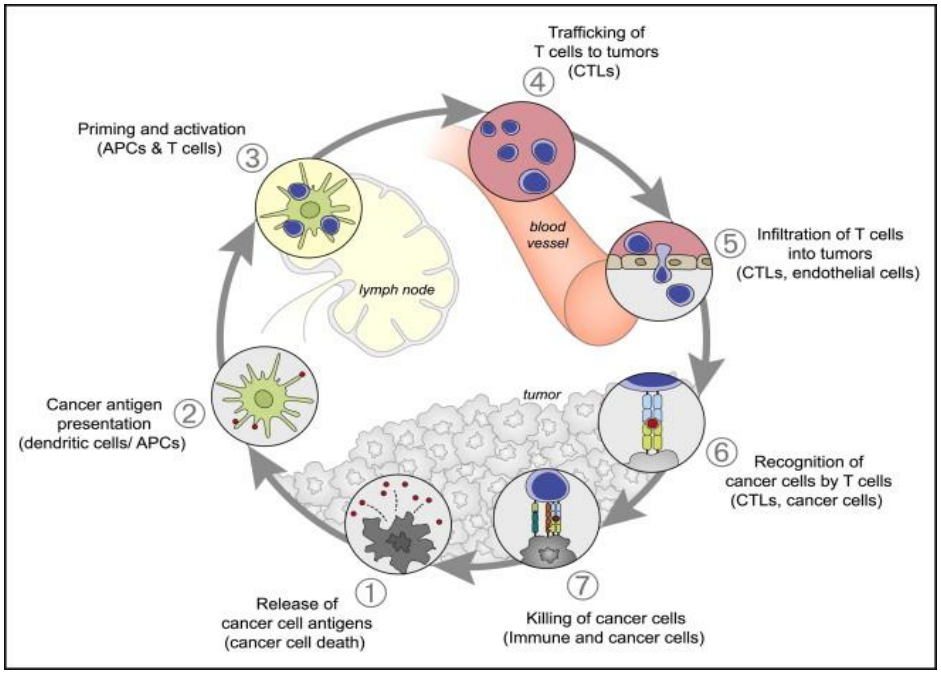

Figure 7 Cancer immunity cycle.
The cancer immunity cycle is a self-propagating regulatory feedback mechanism consisting of seven major steps, initiated by induction of immunogenic cell death and ending with cancer cell death. APCs: antigen presenting cells; CTLs: cytotoxic T lymphocytes[123].

1.2 Aim of the thesis

This thesis aimed to establish rational combination therapies to enhance the efficacy of ^{177}Lu-PSMA RLT in PCa cell and mouse models. ^{177}Lu-PSMA RLT is a novel promising therapeutic option for mCRPC patients targeting PSMA on PCa cells. However, one third of patients will not respond to RLT or develop resistances. To improve the outcome of PCa after RLT, three approaches were investigated: 1. To use ARB as pharmacological tool to enhance PSMA expression and thus, improve therapeutic targeting with PSMA-ligands; 2. To exploit RLT-induced DNA damage by combining ^{177}Lu-PSMA and DDR inhibitors; and 3. To use RLT as an *in situ* vaccines to enhance PCa immunogenicity (combination of ^{177}Lu-PSMA and ICB).

.

2. Materials and Methods

2.1 Materials

2.1.1 Cell culture

Table 1 Cell culture

Product	Company
Dulbecco's phosphate buffered saline without Calcium and Magnesium (PBS) (1x)	Gibco, Thermo Fisher Scientific, Darmstadt, Germany
Fetal bovine serum (FBS), qualified, heat inactivated	Gibco, Thermo Fisher Scientific, Darmstadt, Germany
Roswell Park Memorial Institute1640 Medium	Gibco, Thermo Fisher Scientific, Darmstadt, Germany
Trypsin-EDTA (0.05 %), phenol red	Gibco, Thermo Fisher Scientific, Darmstadt, Germany

2.1.2 Chemicals and drugs

Table 2 Chemicals and drugs

Product	Company
10 x Tris Glycine	National Diagnostics, Atlanta, GA, USA
6 x loading dye (blue)	Thermo Fisher Scientific, Darmstadt, Germany
Agarose Electrophoresis Grade	Invitrogen, Thermo Fisher Scientific, Darmstadt, Germany
Amersham ECL Full-Range Rainbow Molecular Weight Markers Code: RPN800E	Sigma Aldrich, Taufkirchen, Germany
Bovine serum albumine	Sigma Aldrich, Taufkirchen, Germany
Ceralasertib (AZD6738)	AstraZeneca, Cambridge, UK
Crystal violet solution 1 %	Sigma Aldrich, Taufkirchen, Germany
Dimethylsulfoxide (DMSO)	Serva, Heidelberg, Germany
Enzalutamide	Hycultec, Beutelsbach, Germany
Formaldehyde	VWR, Randor, PA, United States
GelRed Nucleic Acid Gel Stain, 10.000 x	Biotium, Fremont, CA, USA
Halt Protease and Phosphatase Inhibitor Cocktail (100 x)	Thermo Fisher Scientific, Darmstadt, Germany
Heparin-Natrium-5000 I.E./0.2 ml	ratiopharm, Ulm, Germany
Interferon-γ	PBL Assay Science, Piscataway, NJ, USA
Isoflurane	AbbVie, Wiesbaden, Germany
Isopropyl alcohol	Sigma Aldrich, Taufkirchen, Germany
Labrasol	Gattefossé, Lyon, France
LaemmLi SDS-Sample Buffer (4 x, Reducing)	Boston BioProducts, Inc., Ashland, MA, USA
Matrigel	Fisher Scientific, Waltham, MA, USA

Methanol	Sigma Aldrich, Taufkirchen, Germany
Non- fat dry milk	Labscientific, Danvers, MA, USA
Olaparib	Selleckchem, Houston, TX, USA
Paraformaldehyde (PFA) 4 %	VWR, Randor, PA, United States
Polyethylene glycol PEG200	Merck, Darmstadt, Germany
Propidium Iodide (PI)	Miltenyi Biotec, Bergisch Gladbach, Germany
Propylene Glycol	Sigma Aldrich, Taufkirchen, Germany
Propylene Glycol	Sigma Aldrich, Taufkirchen, Germany
Quick-load Purple 100 bp DNA Ladder	New England Biolabs, Ipswich, MA, USA
Radioimmunoprecipitation buffer (RIPA)	Boston BioProducts, Inc., Ashland, MA, USA
Ribonuclease A	Thermo Fisher Scientific, Darmstadt, Germany
Sodium citrate	Sigma Aldrich, Taufkirchen, Germany
SuperSignal Femto ECL reagents	Thermo Fisher Scientific, Darmstadt, Germany
SuperSignal Pico ECL reagents	Thermo Fisher Scientific, Darmstadt, Germany
Transcutol	Gattefossé, Lyon, France
Triton-X 100	Sigma Aldrich, Taufkirchen, Germany
Tween 80	Sigma Aldrich, Taufkirchen, Germany

2.1.3 Buffer and solutions

Table 3 Buffer and solutions

Buffer/Solution	**Recipe/Company**
CC1 tris-based buffer	Ventana medical systems, Hoffmann-La Roche, Basel, Switzerland
Hypotonic DNA staining buffer	1 g/l sodium citrate 25 mg Propidium Iodide 5 mg Ribonuclease A 0.3 % Triton X-100 250 mL distilled water
Freeze media	10 % DMSO 20 % FCS 70 % RPMI
UltraPure™ TBE-Puffer, 10 x	Invitrogen, Fisher Scientific, Waltham, MA, USA
0.01 M citrate buffer, pH 6.0	Sigma Aldrich, Taufkirchen, Germany
20 x Bolt MES MOPS Running Buffer	Thermo Fisher Scientific, Waltham, MA, USA
Transfer buffer	200 mL 10 x Tris-Glycine 1400 mL miliQ H_2O 400 mL MeOH
TBS-T	50 mL 20 x TBS 950 mL miliQ H_2O 1 mL Tween-20

Pierce™ 20 x TBS Buffer	Thermo Fisher Scientific, Waltham, MA, USA

2.1.4 Assay kits

Table 4 Assay kits

Product	Company
^{68}Ga-PSMA-11 radiolabeling kit	Eckert & Ziegler Eurotope GmbH, Berlin, Germany
Betazoid DAB Chromogen Kit	Biocare Medical, Pacheco, CA, USA
CellTiter-Glo 107 Luminescent Cell Viability Assay	Promega, Walldorf, Germany
OptiView DAB IHC Detection Kit	Ventana Medical Systems Inc., Tucson, AZ, USA
Pierce™ BCA Protein Assay Kit	Thermo Fisher Scientific, Waltham, MA, USA
Venor®GeM OneStep kit	Minerva Biolabs, Berlin, Germany

2.1.5 Antibodies

Table 5 Antibodies

Product	Host species	Company
Flow cytometry		
Anti-H-2K (clone Y-3)	Mouse	Merck, Billerica, MA, USA
Anti-Mouse IgG, FITC	Goat	Thermo Fisher Scientific, Waltham, MA, USA
anti–mPD-L1-PE antibody (clone 10F.9G2)	Rat	Biolegend, San Diego, CA, USA
PD-1-PE (clone RMP1-14, BE0146)	Syrian Hamster BKH cells transfected with mouse PD-1 cDNA	Bxcell, Lebanon, NH, USA
PSMA-APC (clone: REA408)	Human	Miltenyi Biotec, Bergisch Gladbach, Germany
rat-IgG2a isotype control (clone 2A3, BE0089)	Rat	Bxcell, Lebanon, NH, USA
Western blot		
Anti-rabbit IgG (clone 7074)	Goat	Cell Signaling, Cambridge, UK
p-STAT1 (clone Y701)	Rabbit	Cell Signalling, Cambridge, UK
Vinculin (clone E1EV)	Rabbit	Cell Signalling, Cambridge, UK
Immunhistochemistry		
AR (clone SP107)	Rabbit	Cell Marque, Rocklin, CA, USA
PSMA (clone 3E6)	Mouse	Dako, Glostrup, Denmark

2.1.6 Radiopharmaceuticals

Table 6 Radiopharmaceuticals and peptides

Product	Company
^{177}Lu chloride	ITM-radiopharma, Munich, Germany
^{18}F	In house production
FDG	GE Healthcare Buchler GmbH & Co. KG, Braunschweig, Germany
^{68}Ga	In house production
PSMA-11	ABX, Radeberg, Germany
PSMA-617	ABX, Radeberg, Germany

2.1.7 Supplies

Table 7 Supplies

Product	Company
Bolt 4-12 % Bis Tris Plus Gel	Invitrogen, Fisher Scientific, Waltham, MA, USA
iBlot Transfer stacks, regular PVDF	Thermo Fisher Scientific, Waltham, MA, USA
MiniCollect® RÖHRCHEN 0.25/0.5 mL K3E K3EDTA	Greiner Bio-One, Solingen, Germany
Test stripes Kidney Panel- 3	scil Vet, Viernheim, Germany

2.1.8 Equipment

Table 8 Equipment

Product	Company
^{68}Germanium/^{68}Ga Generator (GalliaPharm)	Eckert & Ziegler Radiopharma, Berlin, Germany
Amersham Imager 600	GE Healthcare, IL, USA
CHEMOSTAR Touch 21.5	Intas Science Imaging Instruments GmbH, Göttingen, Germany
Cyclone 18	IBA RadioPharma Solutions, Louvain-la-Neuve, Belgium
CytoFlex S flow cytometer	Beckman Coulter, Munich, Germany
Eppendorf™Mastercycler™ Nexus Gradient	Sigma Aldrich, Taufkirchen, Germany
Fastlab II modul	GE Healthcare Buchler GmbH & Co. KG, Braunschweig, Germany
Genesys8 PET/CT	Sofie Bioscience, Los Angeles, CA, USA
LSRII flow cytometer	BD Biosciences, Franklin Lakes, NJ, USA
Modular Lab eazy modul	Eckert & Ziegler Radiopharma, Berlin, Germany
Nalgene Mr. Frosty Freezing Container	Thermo Fisher Scientific, Darmstadt, Germany
Olympus BX 50 device	Olympus, Tokio, Japan
scil Vet abc Plus	scil Vet, Viernheim, Germany
SpectraMax luminometer	Molecular Devices, San Jose, CA, USA

SpotChem EZ Vet	scil Vet, Viernheim, Germany
Ventana automated slide staining device	Ventana Medical Systems Inc., Tucson, AZ, USA
X-ray machine RS320	Xstrahl Ltd, Surrey, UK
β-CUBE (PET) and X-CUBE (CT)	MOLECUBES, Gent, Belgium

2.1.9 Software

Table 9 Software

Product	**Company**
FlowJo software	Tri Star Inc., Ashland, OR, USA
PMOD software v. 4.1	PMOD Technologies Ltd., Zürich, Switzerland
GraphPad Prism	GraphPad software Inc., CA, USA
OsiriX version 10.0.2	Pixmeo SARL, Geneva, Switzerland

2.2. Methods

2.2.1 Cell cultivation

Human prostate cancer cell lines 22Rv1, C4-2 and LNCaP and the murine prostate cancer cell line RM1-PGLS were obtained from Dr. Johannes Czernin's group (Department of Molecular and Medical Pharmacology, David Geffen School of Medicine, University of California Los Angeles). In July 2020, 22Rv1, C4-2 and LNCaP underwent polymorphic short tandem repeat loci (STRs) profiling to rule out cross contaminations. Cell line identity was confirmed. The procedure was carried out by the company Microsynth, Balgach, Switzerland. Cells were cultured in RPMI 1604 supplemented with 10 % FCS and maintained at 37°C with 5 % CO_2 in a humidified incubator. Cells were passaged at 80 % confluence. For the passage, cells were rinsed with PBS and trypsinized with 0.05 % Trypsin-EDTA for 4 min at 37°C. Trypsin was diluted with RPMI/10 % FCS and the cell suspension was transferred into a fresh flask containing RPMI/10 % FCS at desired concentration.

2.2.2 Cell thawing and freezing

For thawing, a cryovial was removed from liquid nitrogen storage and immediately placed into a 37°C water bath. Thawed cell suspension was transferred into a tube containing 10 mL PBS and spun down at 450 x g for 5 min. The supernatant was discarded and pellet resuspended in pre-warmed (37°C) RPMI/10 % FCS. The cell suspension was transferred into a cell culture flask and incubated.

For cryoconservation, cells were washed with PBS, trypsinized and spun down at 450 x g for 5 min. Cells were resuspended at a concentration of 2 x 10^6/mL in freezing medium. Cells were frozen at a cooling rate of 1°C/min and transferred to liquid nitrogen for long term storage.

2.2.3 Mycoplasma test

Cells were routinely assessed for mycoplasma contamination using the Venor®GeM OneStep kit. Briefly, at 80 % confluence, 500 µL of cell culture supernatant from the test culture was collected and incubated at 95°C for 10 min. Samples were centrifuged for 15 sec at 16000 x g to pellet any cellular debris. 2 µL of the supernatant were directly used for polymerase chain reaction (PCR).

PCR program:

1 cycle 94°C for 2 min

39 cycles 94°C for 30 sec

55°C for 30 sec

72°C for 30 sec

hold 4 to 8°C

PCR products were mixed with 6x loading dye and analyzed by agarose gel electrophoresis. A 1.5 % (in 1x TBE) agarose gel containing 10 µL GelRed DNA stain was cast. Gel electrophoresis was performed for 30 min at 120 V. Gels were detected by Amersham Imager 600. Detection of mycoplasma band was at 270 bp.

2.2.4 Flow cytometry

2.2.4.1 Flow cytometric analysis of PSMA

Cells were seeded at a density of 1 x 10^5/well (22Rv1), 0.5 x 10^5/well (C4-2) or 0.7 x 10^5/well (LNCaP) in 6-well plates. Medium was changed every other day. On the day of medium change, cells were treated with 1 µM DMSO (vehicle) or 10 µM enzalutamide. Single-cell suspensions were stained with 5 µL anti-human PSMA-APC antibody (clone: REA408) in PBS or incubated with 50 µL PBS only (unstained control) for 15 min at 4°C in the dark. Samples were measured after one, two or three weeks of treatment (each experiment = one sample per condition, n = 3-5) with a CytoFlex S flow cytometer and analyzed using FlowJo software[124]. For the analysis, debris was excluded and single cells were gated. The geometric mean of marker positive cells was normalized to that of unstained samples. The gating strategy is shown in **Fig. 8**.

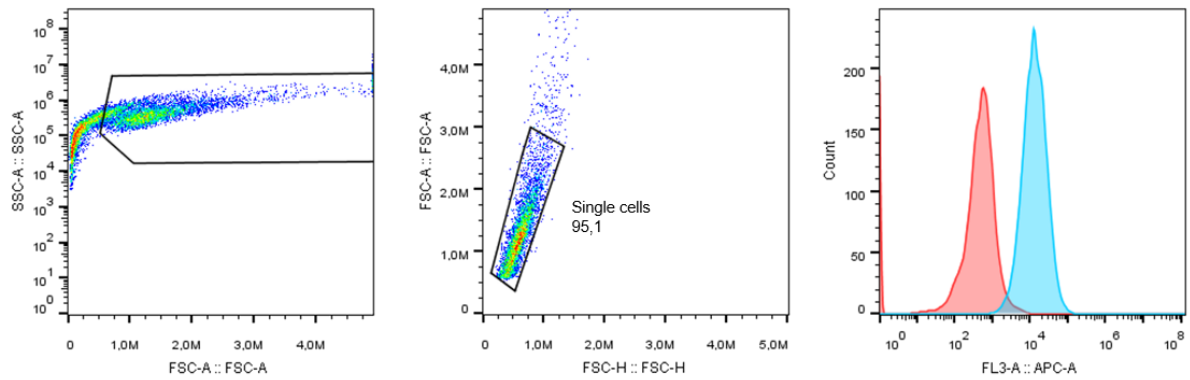

Figure 8 Gating strategy for PSMA staining.
For the analysis, debris was excluded and single cells were gated. PSMA expression was visualized in a histogram. Unstained shown in red, stained in blue.

2.2.4.2 Flow cytometric analysis of PDL-1 and MHC-I

RM1-PGLS cells were irradiated (10 Gy) and analyzed 24 h, 48 h and 72 h post IR. PD-L1 expression was determined using an anti–mPD-L1-PE antibody (1:20, clone 10F.9G2). MHC-I expression was determined using anti-H-2K (1:40, clone Y-3) and anti-mouse IgG, FITC (1:1000) antibodies. Cells were incubated with the primary antibody diluted in PBS/1 % FCS for 30 min at 4°C in the dark. For MHC-I, incubation with the primary antibody was followed by incubation with the secondary antibody diluted in PBS for 15 min at 4°C in the dark. Samples were washed twice with PBS/1 % FCS and resuspended with PBS. Samples were measured on an LSRII flow cytometer and analyzed using FlowJo.

2.2.4.3 Analysis of cell cycle/apoptosis

22Rv1, C4-2 and LNCaP cells were seeded at a density of 1 x 10^5/well in 6-well plates. Cells were treated with ceralasertib (1 µM), olaparib (1 µM) and irradiated with 8 Gy. After 72 h, culture media was collected and samples were trypsinized and spun down at 450 x g for 5 min (together with culture media). Pellets were resuspended in 1 mL hypotonic DNA staining buffer. Samples were incubated at 4°C for 30-60 min protected from light before analysis. Flow cytometry data were acquired on a CytoFlex S flow cytometer and analyzed using FlowJo software. All cells followed by single cells were gated (doublets were excluded). Distribution of DNA content divided in sub-G1, G1, S and G2/M phase was analyzed. Gating strategy and exemplary cell cycle profile are shown in **Fig. 9**.

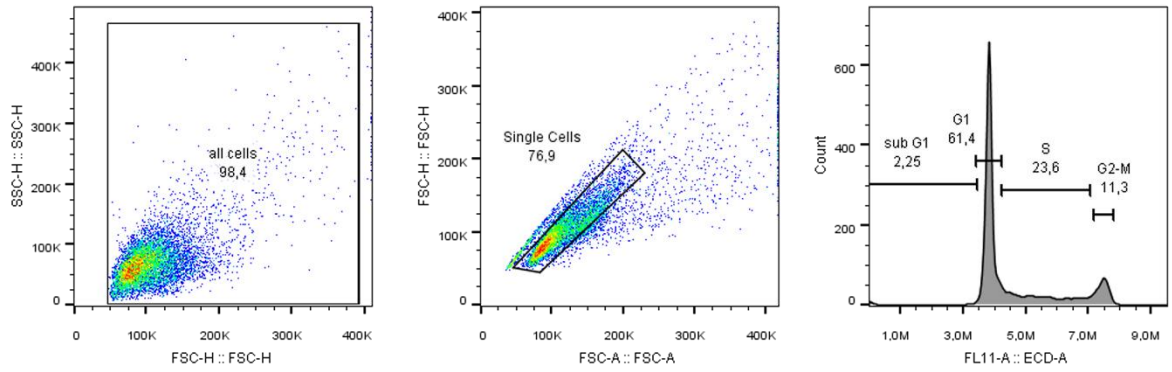

Figure 9 Gating strategy for PI cell cycle profile.
All cells followed by single cells were gated (doublets were excluded). Distribution of DNA content divided in sub-G1, G1, S and G2/M phase was analyzed.

2.2.5 IC50 determination

Cells were plated in 384-well plates (1000 cells/well in 25 µL RPMI). Drugs were serially diluted to desired concentrations (10-0.0045 µM). Diluted drugs (10 µL) were added to each well (4 technical replicates). ATP content was measured after 72 h using CellTiter-Glo reagent according to manufacturer's instructions (Promega, CellTiter-Glo 107 Luminescent Cell Viability Assay) and analyzed using the SpectraMax luminometer. IC50 values, i.e., the concentration required to inhibit proliferation by 50 % compared to DMSO treated cells, were calculated using Prism 6.0 h (Graphpad Software). Experimental CellTiter-Glo values were normalized to DMSO treated cells.

2.2.6 Crystal violet staining to determine cell growth inhibition

Cells were seeded at a density of 1 x 10^5/well in 6-well plates. On the next day, cells were treated with ceralasertib (1 µM), olaparib (1 µM) and irradiated with 2 Gy at 300 kV, 10 mA, dose rate 0.9 Gy/min using an X-ray machine RS320. One week after IR cells were fixed with 4 % PFA (15 min in the dark, RT). Fixed cells were then incubated with 0.05 % Crystal violet solution for 15 min on a rocker at RT, washed with H_2O and air dried overnight. Plates were photographed for visualization.

2.2.7 Immunohistochemistry

Cell pellets consisting of ~1 x 10^6 cells were embedded in paraffin. Formalin-fixed paraffin-embedded (FFPE) blocks were cut into 3 µm sections and dewaxed. Samples were pretreated with CC1 tris-based buffer at 90°C for 32 min for PSMA and 64 min for AR, respectively. All reactions were performed on an Ventana automated slide staining. Samples were stained for PSMA (clone 3E6, 1:50) and androgen receptor (AR; clone SP107, 1:2000) and detected using the OptiView DAB IHC Detection Kit. The percentage of stained cells was semi-quantitatively analyzed on an Olympus BX 50 device by a genitourinary pathologist. For AR immunohistochemistry (IHC), only nuclear immunoreactivity and for PSMA IHC, only cytoplasmic immunoreactivity was evaluated[124].

2.2.8 Immunoblot analysis

RM1-PGLS cells were treated with interferon-γ (10 ng/mL) for 24 h. 22Rv1, C4-2 and LNCaP cells were irradiated with 5 Gy and analyzed 6 h post IR. Cells were trypsinized and spun down at 450 x g for 5 min. Pellets were washed with PBS and resuspended in cold radioimmunoprecipitation (RIPA) buffer supplemented with protease and phosphatase inhibitors. Protein lysates were normalized using Pierce™ BCA Protein

Assay Kit (following manufacturers instructions), diluted using RIPA and 4 x Laemmli loading dye. Sodium dodecyl sulfate polyacrylamide gel electrophoresis (SDS PAGE) was performed on 4 %–12 % Bis-Tris gels at 175 V for 60 min and electro-transferred to PVDF membranes at 110 V for 90 min. After blocking with 5 % nonfat milk in TBS + 0.1 % Tween-20 (TBS-T) for 30 min, membranes were incubated overnight with primary antibodies (p-STAT1, Y701, 1:5000; Vinculin E1EV, 1:10000) in 5 % BSA in TBS-T. Membranes were washed with TBST-T and incubated with HRP-linked secondary antibody prepared at a 1:2500 dilution in 5 % nonfat dry milk in TBS-T. HRP was activated by incubating membranes with a mixture of SuperSignal Pico and SuperSignal Femto ECL reagents (100:1 ratio) for 1 min. Immunoreactivity was detected using the CHEMOSTAR Touch 21.5.

2.2.9 Radiolabeling

2.2.9.1 ^{18}F-FDG

No-carrier-added ^{18}F (2-3 GBq) was produced via the nuclear reaction ^{18}Oxygen (^{18}O)(p,n)^{18}F by bombardment of 2-2.5 mL^{18}O-enriched water for 2-30 min with a 17 MeV proton beam and 15-35 µA current at the Cyclone 18/9 at the Department of Radiopharmacy, Clinic for Nuclear Medicine, University Hospital Essen. ^{18}F-FDG was produced using the Fastlab II modul.

2.2.9.2 ^{68}Ga-PSMA-11

No-carrier-added ^{68}Ga-chloride was produced using ^{68}Germanium (^{68}Ge)/^{68}Ga Generator. ^{68}Ga-PSMA-11 was produced using Modular-Lab eazy modul. Radiochemical purity was determined with radio-High Performance Liquid Chromatography (HPLC) and thin-layer chromatography (TLC; TLC-SG) and exceeded 98 % for ^{68}Ga-PSMA-11.

2.2.9.3 ^{177}Lu-PSMA-617

^{177}Lu-PSMA-617 was produced using Modular-Lab eazy modul. Consumables and reagent were supplied by Eckert & Ziegler Radiopharma, Berlin, Germany.

2.2.10 Animal studies

All animal studies were performed in accordance with the recommendations of the Society for Laboratory Animal Science (GV-SOLAS) and the European Health Law of the Federation of Laboratory Animal Science Associations (FELASA). The protocol was approved by the North Rhine-Westphalia State Agency for Nature, Environment and Consumer Protection (LANUV), Germany (permit number: AZ.81-

02.04.2018.A133). Intact male, 6-10 weeks old NOD/Scid gamma mice (Charles River Laboratories, Sulzfeld, Germany) were housed under pathogen-free conditions. Water and food were provided ad libitum. Mice were included into studies following one week acclimatization. ^{177}Lu-PSMA-617/anti-PD-1 studies were performed in intact male, 6- to 8-weeks-old C57BL/6 mice (Jackson Laboratory, Bar Harbor, ME, USA; permit number: UCLA ARC 2005-090).

2.2.10.1 ARB to enhance PSMA expression *in vivo*

Mice were injected subcutaneously (s.c.) with 2 x 10^6 22Rv1 cells in 50 µL Matrigel/ 50 µL PBS into the shoulder region. Tumor growth was monitored by CT (2.2.10.4). Animals were sacrificed upon reaching any predefined termination criteria, including bad general and social habitus, apathy, ulceration, severe weight loss, tumor size ≥2 cm^3 or other signs of deteriorating condition. Mice bearing 22Rv1 xenografts (n = 9) were treated with 50 µL 10 mg/kg enzalutamide diluted in 68 % PEG-200, 30 % Transcutol, 1 % Labrasol and 1 % Tween-80 5 times a week for 2 weeks by oral gavage. Treatment with enzalutamide was started as soon as the tumors were palpable (approx. day 14–21 post-inoculation). Experimental design is shown in **Fig 10**.

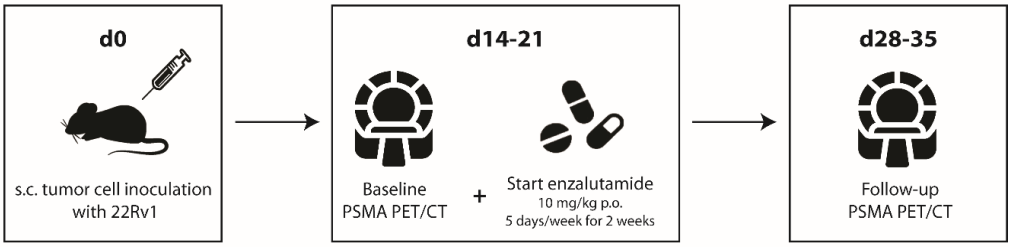

Figure 10 Experimental design of ARB in 22Rv1 xenograft model.

2.2.10.2 Combined ^{177}Lu-PSMA-617 +/- ATRi +/- PARPi to improve the efficacy of RLT

PSMA-low 22Rv1 xenografts were pre-treated with enzalutamide given orally for seven days (10 mg/kg) to enhance PSMA expression before a single intraperitoneal (i.p.)[125]. dose of 30 MBq ^{177}Lu-PSMA-617. Treatment with ceralasertib (50 mg/kg, diluted in 10 % DMSO+ 40 % propylene glycol+ 50 % de-ionized sterile water; according to Astra Zeneca's compound handling instructions), olaparib (50 mg/kg, diluted in 50 % PEG200 + 30 % transcutol+ 20 % labrasol), or ceralasertib (50 mg/kg)+olaparib (50 mg/kg) was initiated one day before RLT and commenced for one week (olaparib once daily, ceralasertib twice daily a 25 mg/kg, given orally). Metabolic response to

RLT was determined by ^{18}F-FDG PET/CT (2.2.10.4). Tumor growth (caliper measurement three times per week using the formula 0.5*(length*width^2), weekly CT), overall survival and toxicity profile (weight control, histopathological analysis of organs and blood post-mortem) were monitored. Experimental design is shown in **Fig. 11.**

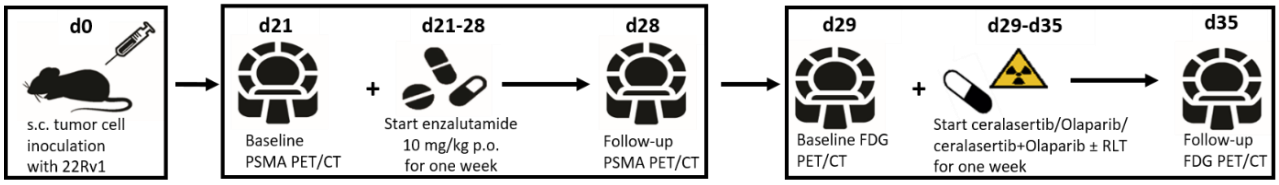

Figure 11 Experimental design for combined ^{177}Lu-PSMA-617/ATRi/PARPi in 22Rv1 xenograft model.

2.2.10.3 Combined ^{177}Lu-PSMA-617/ anti-PD1 to improve the efficacy of RLT

RM1-PGLS cells (0.1 x 10^6 cells in in 50 µL Matrigel/ 50 µL PBS) were s.c. inoculated into the shoulder region of mice. When tumors reached 121 ± 11 mm^3 (day 5), the mice were randomized on the basis of tumor volumes into 4 groups (n =12 mice per group). Anti-PD-1 (clone RMP1-14, BE0146) or the rat-IgG2a isotype control (clone 2A3, BE0089) was given i.p. (10 mg/kg in PBS) at the day of RLT and then every 3-4 days for two weeks (4 treatments in total). The mice were treated with 30 MBq of ^{177}Lu-PSMA617 on day 9. Tumor volumes (CT) and body weights were measured twice weekly until the tumors reached ≥ 2 cm^3 or the mice reached a humane endpoint.

2.2.10.4 PET/CT

As previously described[124], static PET/CT images of 22Rv1 xenografts were acquired 60 min after intraperitoneal injection of approximately 3 MBq ^{68}Ga-PSMA-11 using the β-CUBE (PET) and X-CUBE (CT). C4-2 and LNCaP xenografts were injected with 1.1 MBq ^{68}Ga-PSMA-11 and imaged with Genesys8 PET/CT. Mice were imaged under 1.5 % isoflurane anaesthesia in temperature- controlled beds with continuous monitoring of breathing frequency. Image acquisition time was 15 min (PET) and 3 min (CT). Images were reconstructed using an iterative reconstruction algorithm (ISRA, 30 iterations) with attenuation correction of the corresponding CT image. PET data were reconstructed into a 192 x 192 transverse matrix, producing a 400 µm isometric voxel size. PET images were evaluated by analysis of decay-corrected injected activity per gram of tissue (%IA/g). The x-ray source (CT) was a tungsten anode (peak voltage, 50 kVp; tube current, 350 µA; 0.8 mm aluminum 759 filter). The detector used was a cesium iodide (CsI) flat-panel, building up a screen with 1536 x 864 pixels.

Measurements were carried for individual 120 ms exposures, with angular sampling intervals of 960 exposures per rotation, for a total of 7 rotations and a total exposure time of 6 s. Tumor volume was calculated based on CT data using PMOD. Regions of interest (ROIs) were created in at least three levels and interpolated to one volume of interest (VOI). The entire tumor VOI was copied to the PET dataset to calculate the mean %IA/g. Partial volume effects due to varying tumor sizes were excluded by applying a partial volume correction. A partial volume correction factor profile was fitted to an asymptotic curve with a dependency on the cavity volume measured in a mouse-like phantom. The partial volume correction factor was calculated by dividing the calibrated activity concentration by the mean calibrated activity contained in the PET reconstructed images.

For ^{18}F-FDG PET/CT, mice were deprived of food for 5 h prior to i.p. injection of 3 MBq ^{18}F-FDG. Mice had access to drinking water at all times. Before injection and during the uptake time (1 h), warming was achieved by placing the cage under a red light lamp. PET/CT and data analysis was carried out as described above.

2.2.10.5 Histopathological analysis of organs and blood

Organs (tumor, kidney, liver, heart, lung, stomach, proximal intestine, spleen, salivary glands) were extracted post-mortem and formaline fixed and paraffin-embedded. Blocks were cut into 3 µm sections, dewaxed and re-hydrated and counterstained with hematoxylin and eosin. Organs were analyzed by a genitourinary pathologist for any abnormality compared to untreated tissue. Blood samples were collected post- mortem and analyzed using SpotChem EZ Vet for the kidney panel and scil Vet abc Plus for total blood count.

2.2.11 Statistics

All data were analyzed with GraphPad Prism software (version 9.0.1). Data are presented as mean ± standard deviation (SD). Statistical significance between two unpaired groups was assessed using the one-tailed unpaired t-test with Welch's correction for unequal SD. Statistical significance between two paired groups was assessed using the Wilcoxon matched-pairs signed-rank test. Statistical significance between more than two unpaired groups was assessed using the ordinary one-way ANOVA test with Sidak's multiple comparisons test. Time to progression (TTP) to 0.75 cm^3 tumor volume and survival were analyzed using the log-rank test. P-values below

0.05 were considered statistically significant. Statistically significant data are indicated by asterisks (* $p < 0.05$, ** $p < 0.01$, *** $p < 0.001$, **** $p < 0.0001$).

3. Results

Part 1

3.1 ARB to enhance PSMA expression levels in PSMA-low PCa

RLT was shown to prolong OS in men with mCRPC[52]. Focal PSMA expression is a prerequisite for PSMA-targeted RLT[126,127]. Men with low PSMA expression are not eligible for RLT[128]. Here, we assessed *in vitro* and *in vivo* whether ARB (enzalutamide) can induce PSMA expression in PSMA-low PCa.

3.1.1 PSMA and AR expression in three different PCa cell lines

PSMA expression levels *in vivo* in 22Rv1, C4-2 and LNCaP xenografts were evaluated by PET/CT. ^{68}Ga-PSMA tumor uptake was 1.3 %IA/g for 22Rv1, 13.1 %IA/g for C4-2 and 22.3 %IA/g for LNCaP tumors, respectively (**Fig. 12 A**). *In vitro*, IHC analysis revealed significantly lower expression of PSMA in 22Rv1 cells (mean ± SD: 21.7 % ± 2.9 % PSMA+ cells; $p < 0.0001$ vs. C4-2 and LNCaP; $n = 3$) compared to C4-2 (mean ± SD: 100.0 % ± 0 % PSMA+ cells) and LNCaP (mean ± SD: 96.7 % ± 5.8 % PSMA+ cells) cells (**Fig. 12 B**). AR was highly expressed in all three cell lines (AR+ cells: 22Rv1, mean ± SD: 91.7 % ± 2.9%; C4-2, mean ± SD: 86.7 % ± 15.3 %; LNCaP, mean ± SD: 85.0 % ± 8.7 %) (**Fig. 12 C**).

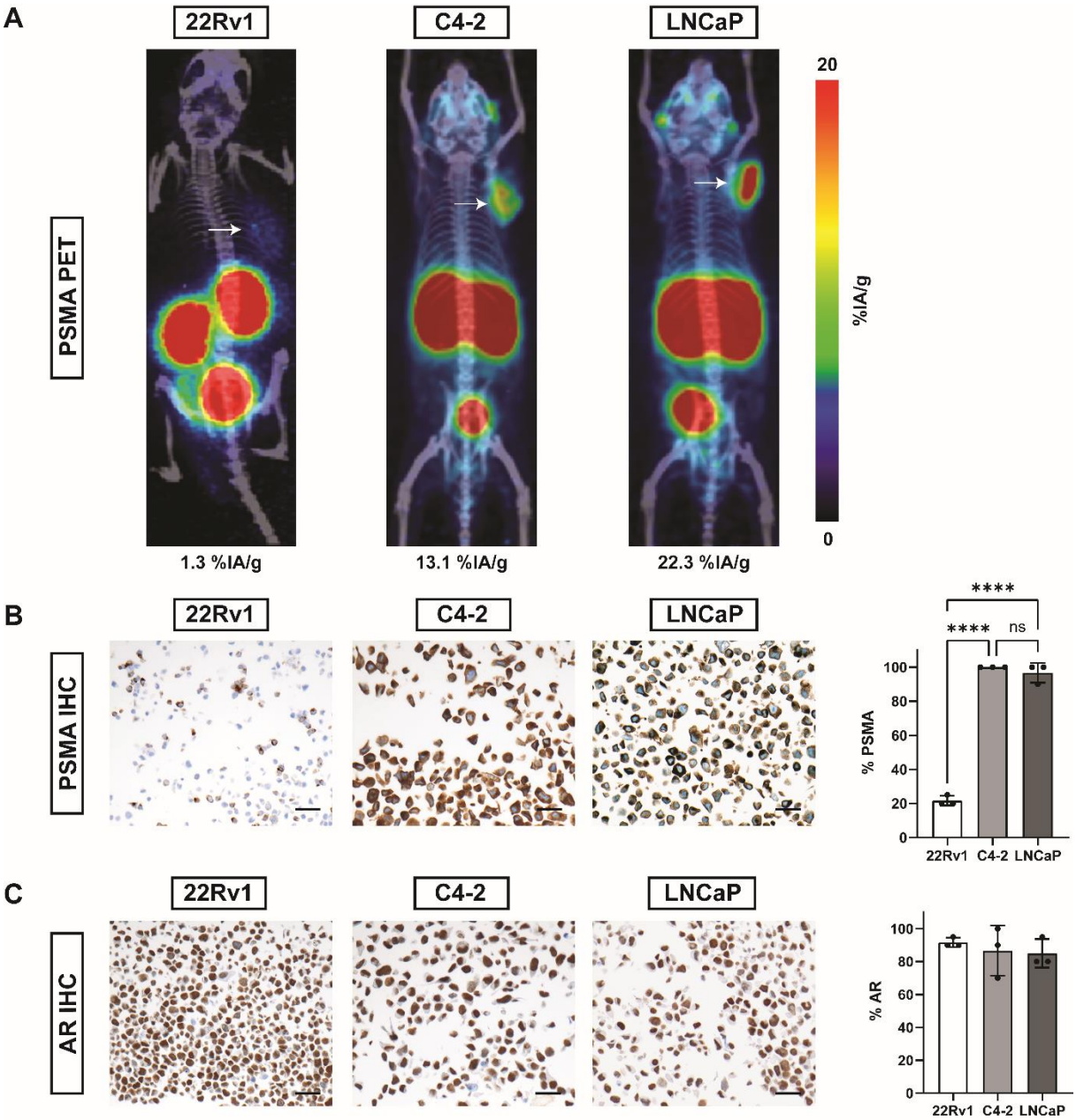

Figure 12 PSMA and AR in 22Rv1, C4-2, and LNCaP PCa cell lines by PET and IHC. (A) Exemplary ^{68}Ga-PSMA-11-PET/CT maximum intensity projection (MIP) images of NOD/Scid mice bearing 22Rv1, C4-2, or LNCaP tumors (white arrows). Average tumor uptake (%IA/g) is stated below the image. (B) Representative images of PSMA IHC on cultured cells and bar plots for % positivity (mean ± SD, n = 3). (C) Representative images of AR IHC on cultured cells and bar plots for % positivity (mean ± SD, n = 3). Scale = 20 µm. Statistics: ordinary one-way ANOVA with Sidak's multiple comparisons test; **** $p \leq 0.0001$; ns = non-significant.

3.1.2 Enzalutamide increases PSMA expression in three different PCa cell lines

Enzalutamide significantly increased PSMA expression levels after one week of treatment in all cell lines compared to vehicle-treated controls (DMSO vs. enzalutamide, fold change, mean ± SD: 22Rv1 8.0 ± 2.3 vs. 16.3 ± 5.7, p = 0.01; C4-2 67.6 ± 37.3 vs. 155.0 ± 74.6, p = 0.03; LNCaP 46.0 ± 31.8 vs. 159.1 ± 114.7, p =

0.045, all n = 5). PSMA levels remained elevated at two weeks (DMSO vs. enzalutamide, fold change, mean ± SD: 22Rv1 6.5 ± 5.3 vs. 14.75 ± 13.0, p = 0.15; C4-2 60.6 ± 47.1 vs. 166.2 ± 65.0, p = 0.02; LNCaP 44.7 ± 24.7 vs. 170.8 ± 52.9, p = 0.005, all n = 4) and three weeks (DMSO vs. enzalutamide, fold change, mean ± SD: 22Rv1 14.2 ± 4.6 vs. 24.0 ± 6.5, p = 0.054; C4-2 129.4 ± 142.6 vs. 421.0 ± 382.8, p = 0.16; LNCaP 30.0 ± 10.9 vs. 221.5 ± 180.5, p = 0.10, all n = 3) after treatment start (**Fig. 13 A and B**).

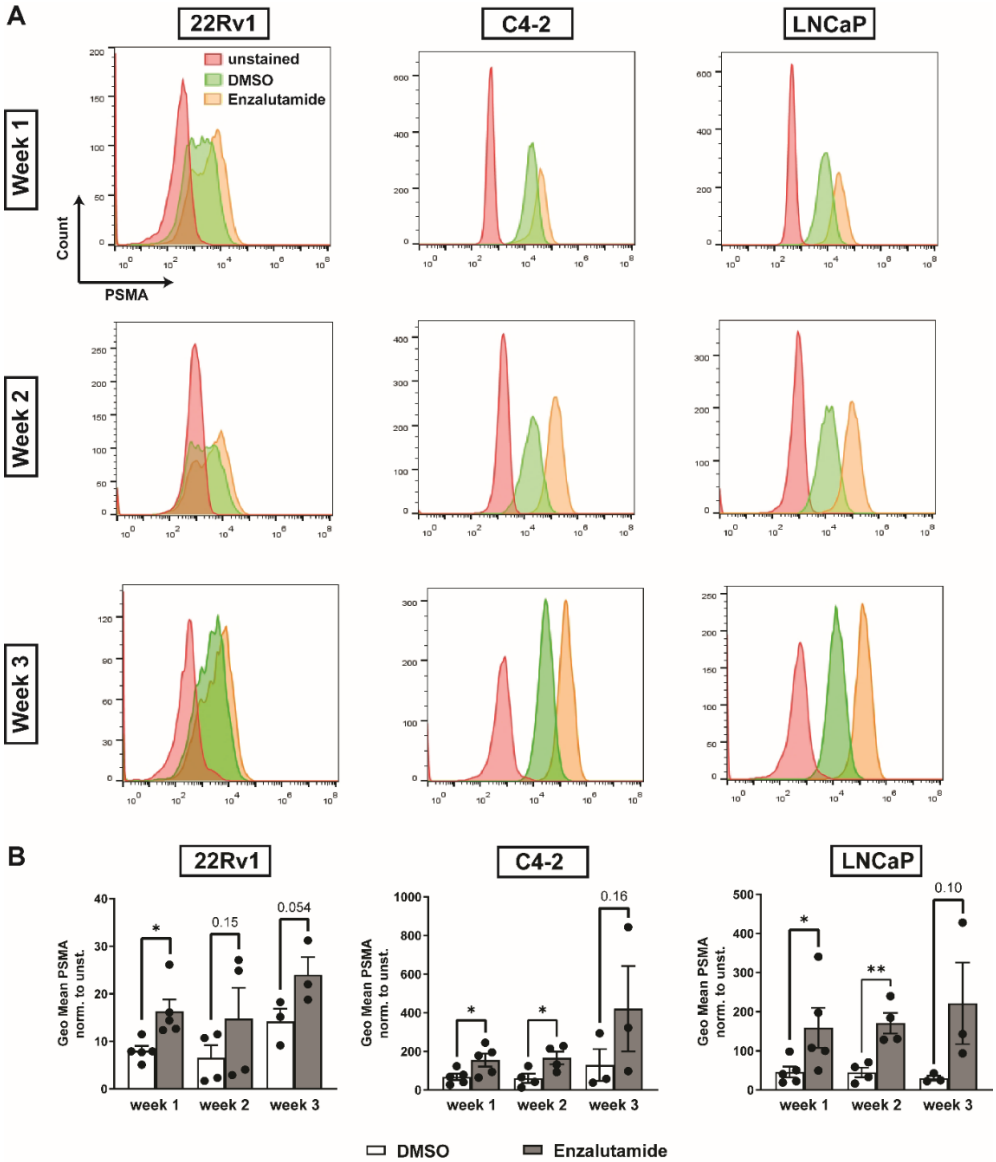

Figure 13 *In vitro* PSMA expression after enzalutamide treatment over time measured by flow cytometry.
(A) Representative histograms of unstained and PSMA-stained DMSO-treated or enzalutamide-treated 22Rv1, C4-2 and LNCaP cells. Cells were treated for one, two, or three weeks. (B) Enzalutamide treatment significantly increased PSMA levels in 22Rv1, C4-2, and LNCaP cells after one week compared to DMSO-treated controls as assessed by flow cytometry; PSMA levels remained increased in all three cell lines two and three weeks after treatment initiation. Data are shown as geometric mean normalized to unstained control. Statistics: unpaired t test with Welch's correction; *p ≤ 0.05; **p ≤ 0.01.

3.1.3 Monitoring enzalutamide-induced changes in PSMA expression using ^{68}Ga-PSMA

To validate *in vivo* that enzalutamide increases PSMA levels in PSMA-low PCa, mice bearing 22Rv1 tumors were imaged before and after 14 days enzalutamide treatment (**Fig. 14**). ^{68}Ga-PSMA-11 PET/CT confirmed ARB-induced enhancement of PSMA expression (mean ± SD %IA/g: baseline: 1.0 ± 0.3, follow-up: 1.9 ± 0.7; p = 0.004; n = 9; **Fig. 14 A**). Measurements of bloodpool (mean ± SD: baseline: 0.4 ± 0.2 %IA/g, follow-up: 0.5 ± 0.2; p = 0.65; n = 9; **Fig.14 C**), salivary glands (mean ± SD: baseline: 0.6 ± 0.2 %IA/g, follow-up: 0.6 ± 0.2; p = 0.49; n = 9; **Fig. 14 D**), kidneys (mean ± SD: baseline: 73.9 ± 19.3 %IA/g, follow-up: 91.2 ± 23.0; p = 0.10; n = 9; **Fig. 14 E**), and liver (mean ± SD: baseline: 0.5 ± 0.2 %IA/g, follow-up: 0.7 ± 0.3; p = 0.16; n = 9; **Fig. 14 F**) served as controls and did not show a significant increase in ^{68}Ga-PSMA-11 uptake. The mean tumor size at the beginning of enzalutamide treatment was 0.14 ± 0.16 cm^3 and 1.08 ± 0.47 cm^3 (n = 9) at the last day of therapy. Small VOI measured in PET (such as small tumors) can lead to an over- or underestimation of the signal measured within the VOI. Because of this so-called partial volume effect (PVE), it is difficult to determine whether the increased PSMA signal after enzalutamide is due to the treatment or due to tumor growth. Therefore, ^{68}Ga-PSMA-11 uptake in tumors was additionally assessed with a partial volume coefficient which confirmed a significant increase in PSMA levels after two weeks of enzalutamide treatment (mean ± SD: baseline: 2.2 ± 0.8 %IA/g, follow-up: 3.3 ± 1.3 %IA/g; p = 0.02; n = 9; **Fig. 14 B, G**).

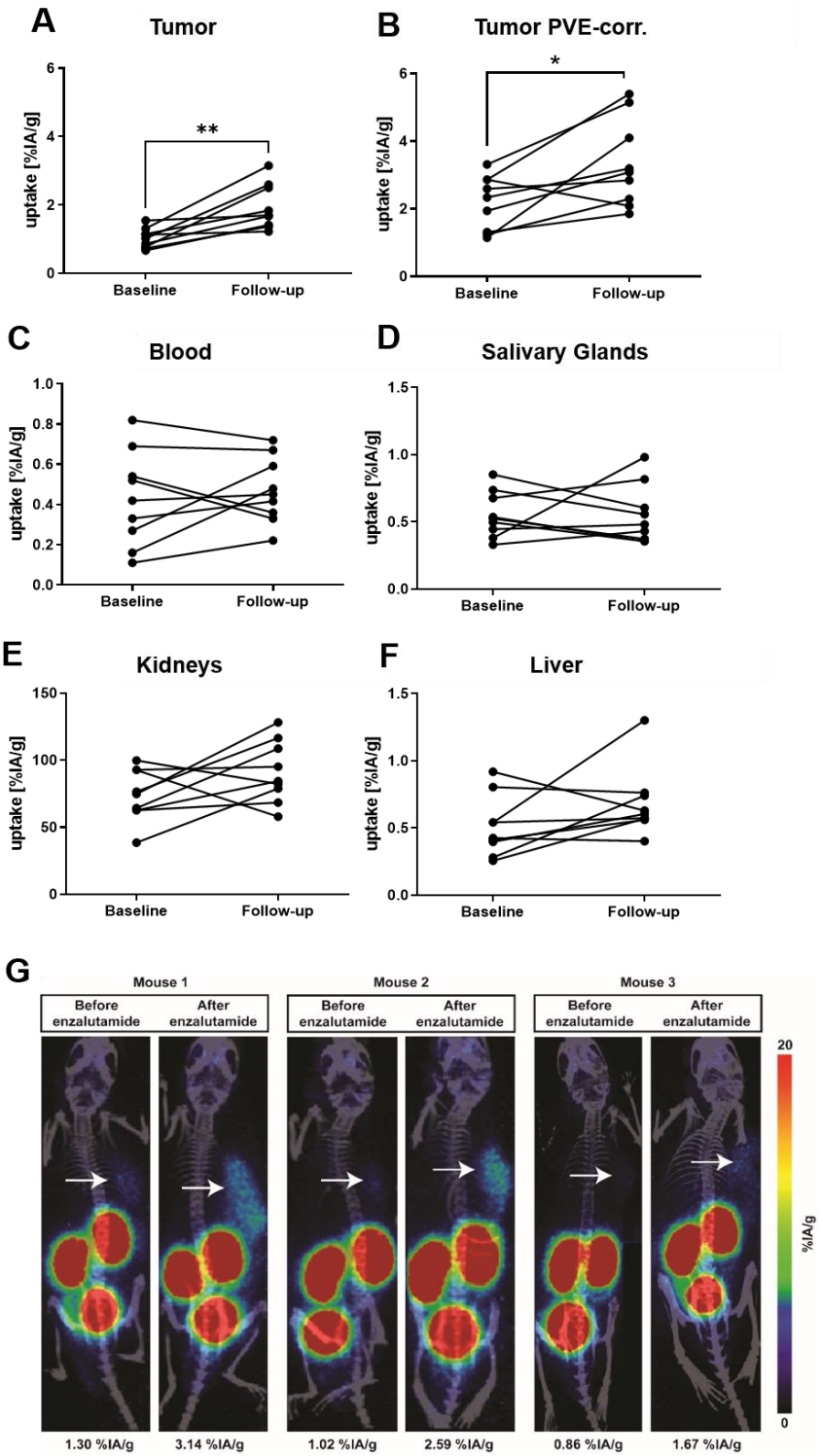

Figure 14 Enzalutamide-induced changes in PSMA expression using ^{68}Ga-PSMA-11. (A) ^{68}Ga-PSMA-11 uptake (%IA/g) in 22Rv1 tumors increased significantly after two weeks of treatment with enzalutamide (B) PVE-corrected tumor size before and after enzalutamide (C) Measurements of bloodpool (D) salivary glands (E) kidneys and (F) liver served as controls and did not show a significant change in ^{68}Ga-PSMA-11 uptake. Statistics: Wilcoxon matched-pairs signed-rank test. * $p \leq 0.05$, ** $p \leq 0.01$. (G) ^{68}Ga-PSMA-11 PET/CT before and after enzalutamide. Representative maximum intensity projections (MIP) of three different mice bearing 22Rv1 tumors (arrow) before (baseline) and after a two-week treatment with enzalutamide are shown (n = 9). Average ^{68}Ga-PSMA-11 tumor uptake is given below the image.

Part 2

3.2 Inhibition of DDR to improve the efficacy of RLT

RLT induces DNA damage leading to activation of DDR signaling[54]. DDR activation might mitigate RLT-induced cytotoxicity and, vice versa, inhibition of DDR signaling using inhibitors, e.g., of ATR or PARP might sensitize tumors to RLT. Here, efficacy of a regimen combining RLT (*in vitro* surrogate: IR), ATRi and/or PARPi in PCa models was investigated with the goal to establish more effective, translatable RLT-approaches. *In vitro*, treatment with ATRi ± PARPi ± IR was assessed in different human PCa cell lines representing different PCa stages: LNCaP (androgen-sensitive), C4-2 (castration-resistant), and 22Rv1 (castration-resistant). To challenge this approach *in vivo*, we selected the PSMA-low 22Rv1 PCa model.

3.2.1 DDR inhibitors impair cell proliferation in a concentration-dependent manner

IC50 is the concentration of a drug which inhibits cell proliferation by 50 %. IC50 values for ceralasertib and olaparib in 22Rv1, C4-2 and LNCaP cells were evaluated using the CellTiter-Glo assay 72 h after adding the inhibitors (0.0045-10 µM). Luminescence was decreased in a concentration-dependent manner in all three cell lines, with an IC50 of 1 µM for both drugs (**Fig. 15**) confirming cytostatic effects of both inhibitors.

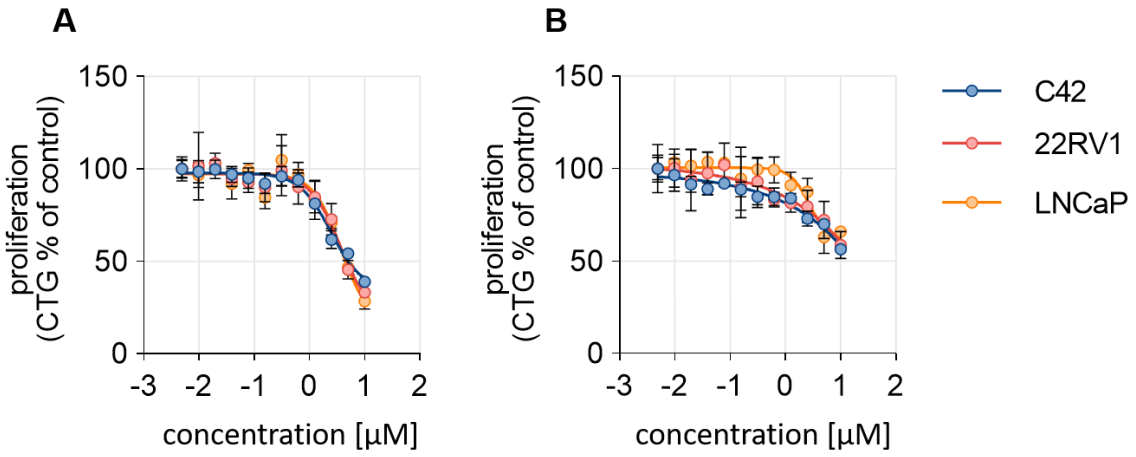

Figure 15 DDR inhibitors impair cell proliferation in a concentration-dependent manner. To assess IC50 concentrations of (A) ceralasertib (B) and olaparib 22Rv1, C4-2 and LNCaP cells were exposed to ceralasertib and olaparib, respectively at different concentrations (range: 0.0045-10 µM). Luminescence was measured after 72 h. Values represent the mean ± S.D. of four replicates for each concentration.

3.2.2 Combined IR/ATRi/PARPi impairs cell growth

To investigate if the anti-cancer effects of IR could be enhanced by combination with an ATRi and/or PARPi inhibitor, cell growth inhibition upon treatment was investigated using a modified days-to-confluence assay as an *in vitro* surrogate of *in vivo* tumor growth inhibition (**Fig.16 A**). Low dose IR (2 Gy) impaired cell growth, indicating inherent radiosensitivity of all three cell lines. Ionizing radiation combined with either ceralasertib or olaparib led to enhanced inhibition of cell growth as compared to IR alone. However, combined IR/ATRi/PARPi resulted in most profound tumor cell growth inhibition. To further investigate cytotoxic effects of combined the IR-DDRi combinations, cell cycle profile and DNA content were analyzed by flow cytometry (PI staining) (**Fig. 16 B**). Cells were treated with ceralasertib (1 µM), olaparib (1 µM) and IR (8 Gy) and analyzed after 72 h. Shown is the % sub-G1 fraction that represents dead cells. In agreement with crystal violet data, all cell lines were shown to be radiosensitive. For 22Rv1, the addition of ATRi or PARPi to IR increased the sub-G1 fraction as compared to IR alone. Addition of IR to ATRi/PARPi did not result in enhanced cell death. In C4-2, ATRi and PARPi monotherapies showed only slight increase in the fraction of sub-G1 cells compared to IR alone; addition of IR to ATRi or PARPi did not result in increased sub-G1 fractions as compared to IR alone. However, the triple combination enhanced cell death (vs. IR). In LNCaP, PARPi resulted in a higher fraction of sub-G1 cells compared to ATRi. Addition of IR to ATRi did not further increase cells death as compared to IR alone; addition of IR to PARPi, however, led to an enhanced sub-G1 fraction as compared to IR alone and was comparable with the triple combination.

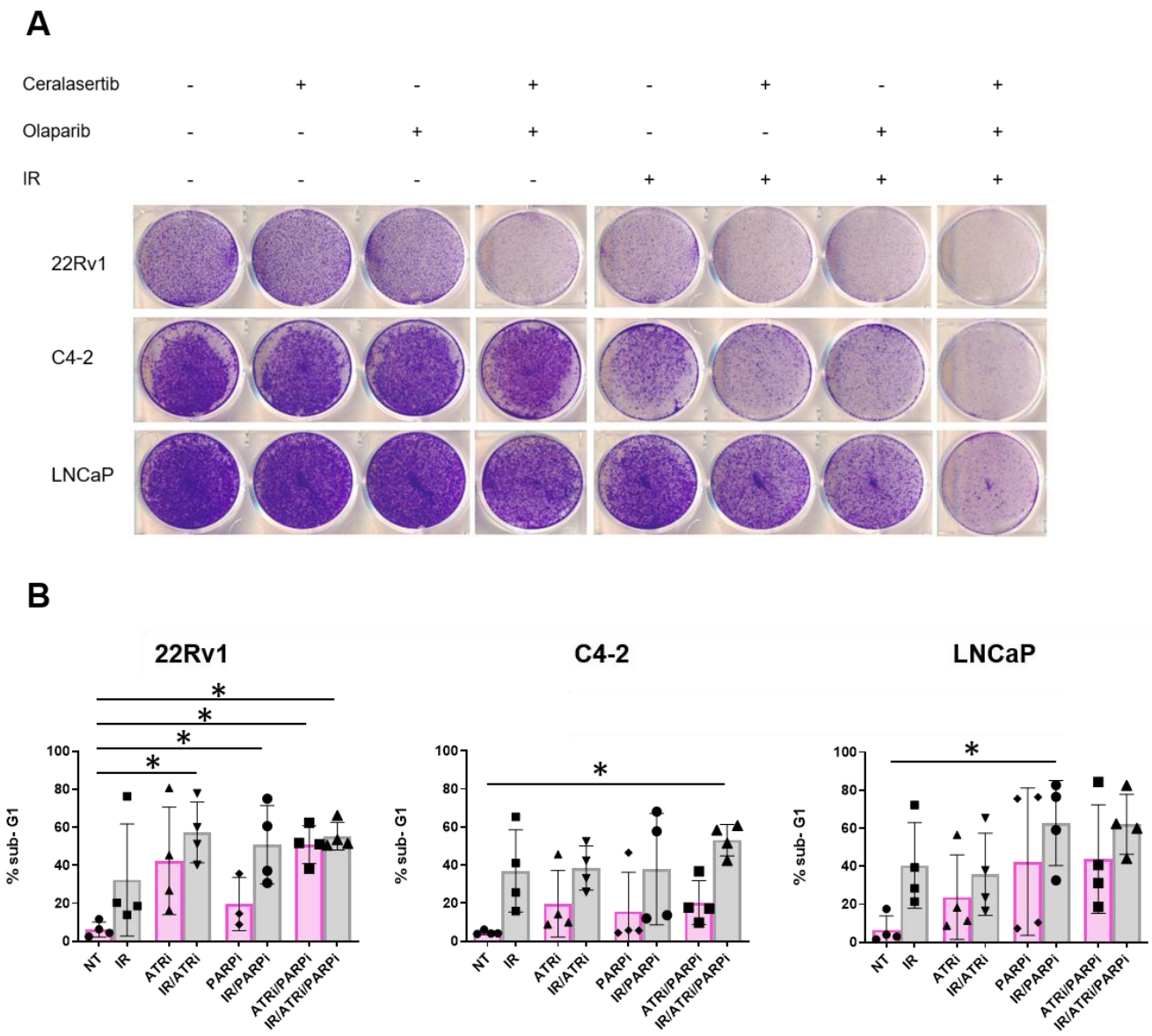

Figure 16 Combined IR/ATRi/PARPi impairs cell growth.
(A) Cells were treated with ceralasertib (1 µM), olaparib (1 µM) and irradiated with 2 Gy as indicated. When untreated controls were confluent (~1 week), cells were fixed with 4 % PFA and stained with Crystal violet. One representative experiment out of three is shown. (B) Flow cytometric analysis of the sub-G1 fraction in 22Rv1, C4-2 and LNCaP cells. Cells were treated with ceralasertib (1 µM), olaparib (1 µM) and irradiated with 8 Gy. Cells were analyzed 72 h after IR. Statistics: one-way ANOVA; *p ≤ 0.05; n = 4.

3.2.3 Combined RLT/ATRi/PARPi to inhibit tumor growth in PSMA-low xenograft model

The *in vitro* results in PCa cell lines support the combination of PSMA-RLT with DDR inhibition. Therefore, we tested if ^{177}Lu-PSMA-617 could be enhanced by concomitant inhibition of ATR and/or PARP in the 22Rv1 PCa model. Because we showed that ARB

upregulated PSMA in 22Rv1 PSMA-low model, mice were pretreated with enzalutamide before combination therapy (**Fig. 10**).

^{68}Ga-PSMA-11 PET/CT confirmed enhanced PSMA expression after one week of enzalutamide treatment (mean ± SD %IA/g: baseline: 1.968 ± 0.5400, follow-up: 5.080 ± 3.283; p = 0.0156; n = 8, **Fig. 17**).

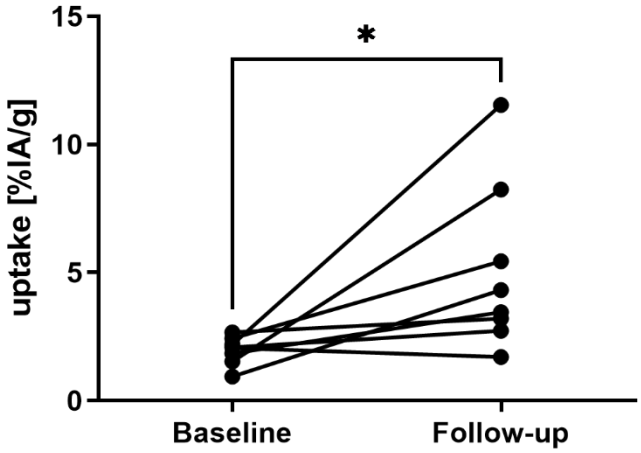

Figure 17 ^{68}Ga-PSMA-11 uptake (%IA/g) in 22Rv1 tumors after one week treatment with enzalutamide.
^{68}Ga-PSMA-11 uptake (%IA/g) in 22Rv1 tumors increased significantly after one week treatment with enzalutamide. Statistics: Wilcoxon matched-pairs signed-rank test. * p ≤ 0.05, ** p ≤ 0.01.

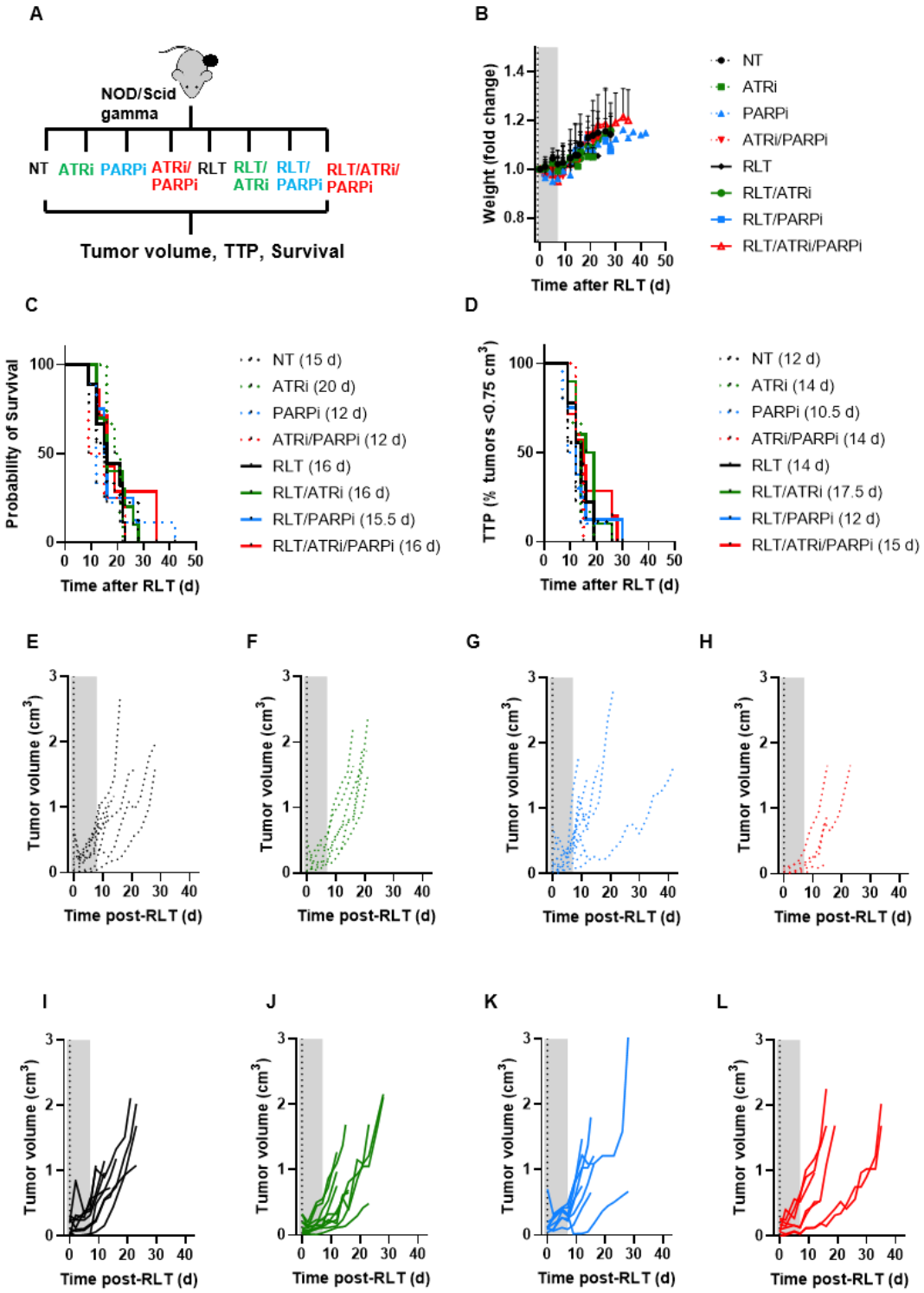

Figure 18 Combined RLT/ATRi/PARPi to inhibit tumor growth in PSMA-low xenograft model.

(A) Study outline. (B) Survival control: NT (15 d), ATRi (20 d), PARPi (12 d), ATRi/PARPi (12 d), RLT (16 d), RLT/ATRi (16 d), RLT/PARPi (15.5 d) and IR/ATRi/PARPi (16 d). (C) TTP: RLT/ATRi/PARPi (15 d), RLT (14 d), ATRi/PARPi (14 d), ATRi (14 d), PARPi (10.5 d), RLT/ATRi (17.5 d) and RLT/PARPi (12 d). (D) Body weights (mean ± SD). Dasher line indicate start of RLT Shaded area indicate treatment duration. (E-L) Tumor volumes for individual mice. All p = ns.

None of the monotherapies exhibited significant anti-tumor efficacy; median TTP was: NT 12 d, RLT 14 d, ATRi 14 d, PARPi 10.5 d. Double treatments did not show significantly prolonged TTP: ATRi/PARPi 14 d, RLT/PARPi 12 d. The RLT/ATRi combination (17.5 d) resulted in a slightly prolonged TTP that, however, did not reach statistical significance. TTP for combined RLT/ATRi/PARPi was 15 d (**Fig. 18 D**). Survival was 15 d for NT, 20 d for ATRi, 12 d for PARPi,12 d for ATRi/PARPi, 16 d for RLT, 16 d for RLT/ATRi, 15.5 d for RLT/PARPi and 16 d for IR/ATRi/PARPi (**Fig. 18 C**, all p = ns. P- value summary in Appendix, **Table 10 and 11**). Treatments were well tolerated as indicated by stable body weight (**Fig. 18 B**). No histopathological changes were detected in organs or blood upon necropsy (data shown in Appendix, **Fig. 22**). Together, this underlines safety of the mono- and combination therapies.

As an alternative measure of treatment efficacy, ^{18}F-FDG uptake one day prior to and and 7 days post RLT was evaluated to assess metabolic response. Increased glucose uptake and glycolytic activity are the hallmarks of cancer.

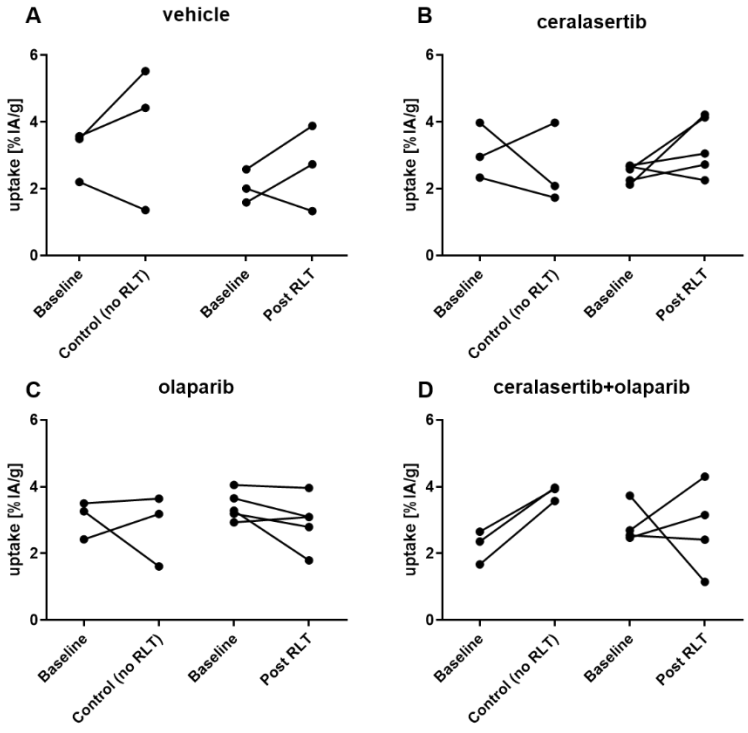

Figure 19 ^{18}F-FDG uptake in 22Rv1 tumor before and after RLT.
^{18}F-FDG uptake per gram tissue was evaluated 1 day prior to RLT and 7 days after RLT in 22Rv1 tumors in vehicle- treated animals (A), ceralasertib treated animals (B), olaparib treated animals (C) and ceralasertib+olaparib treated animals (D). Data are not PVE-corrected. Abbreviations: %IA/g, % injected activity per gram tissue. Statistics: Wilcoxon matched-pairs signed-rank test. * $p \leq 0.05$, ** $p \leq 0.01$.

No significant changes in ^{18}F-FDG uptake were detected in any treatment group: (mean ± SD %IA/g): NT: baseline: 2.63 ± 1.073, NT follow-up: 2.798 ± 1.975; p = 0.8438, RLT: baseline: 3.252 ± 1.261, RLT follow-up: 2.949 ± 1.448; p > 0.9999; ATRi: baseline: 3.083 ± 0.8281, ATRi: 2.593 ± 1.205; p = 0.7500, RLT/ATRi baseline: 2.460 ± 0.2584, RLT/ATRi follow-up: 3.274 ± 0.8708; p = 0.1875; PARPi: baseline: 3.060 ± 0.5671, PARPi follow-up: 2.810 ± 1.064; p > 0,9999, RLT/PARPi: baseline: 3.420 ± 0.4366, RLT/PARPi follow-up: 2.944 ± 0.7795; p = 0.1875; ATRi/PARPi: baseline: 2.227 ± 0.5034, ATRi/PARPi follow-up: 3.823 ± 0.2203; p = 0.2500, RLT/ATRi/PARPi: baseline: 2.858 ± 0.5889, RLT/ATRi/PARPi follow-up: 2.753 ± 1.321; p > 0.9999 (**Fig. 19).**

Part 3

3.3 PD-1 immune checkpoint blockade enhances PSMA-RLT efficacy

In the third part of the thesis, we hypothesized that RLT induces immunogenic cell death leading to activation of the cancer-immunity cycle and thus, activation of anti-cancer immune responses. To test this hypothesis and further investigate potential improvement of RLT by its combination with PD-1 ICB, responsiveness of the murine cell line RM1-PGLS, which was engineered to express human PSMA, to IFN-γ was tested *in vitro*. IFN- γ is an important modulator of immune responses and is released by activated T cells; however, it can also induce tumors to activate immunosuppressive mechanisms, e.g., PD-L1 expression.

Exposure of RM1-PGLS cells to IFN-γ induced phosphorylation of STAT1 (**Fig. 20 A**), leading to expression of the interferon-stimulated genes PD-L1 and MHC class I on tumor cells, indicating a functional IFN-γ -response in these cells (PD-L1: IFN-γ 10.98 ± 2.87, $p \leq 0.0001$; MHC class I: IFN-γ 6.32 ± 3.53, $p \leq 0.05$; values normalized to NT; **Fig. 20 B**). Upregulation of PD-L1 and MHC class I has also been reported following radiation[129,130]. Treating RM1-PGLS cells with IR (10 Gy) significantly increased both, PD-L1 and MHC class I levels, although at a lower magnitude and with slower kinetics than IFN-γ (**Fig. 20 C and D**).

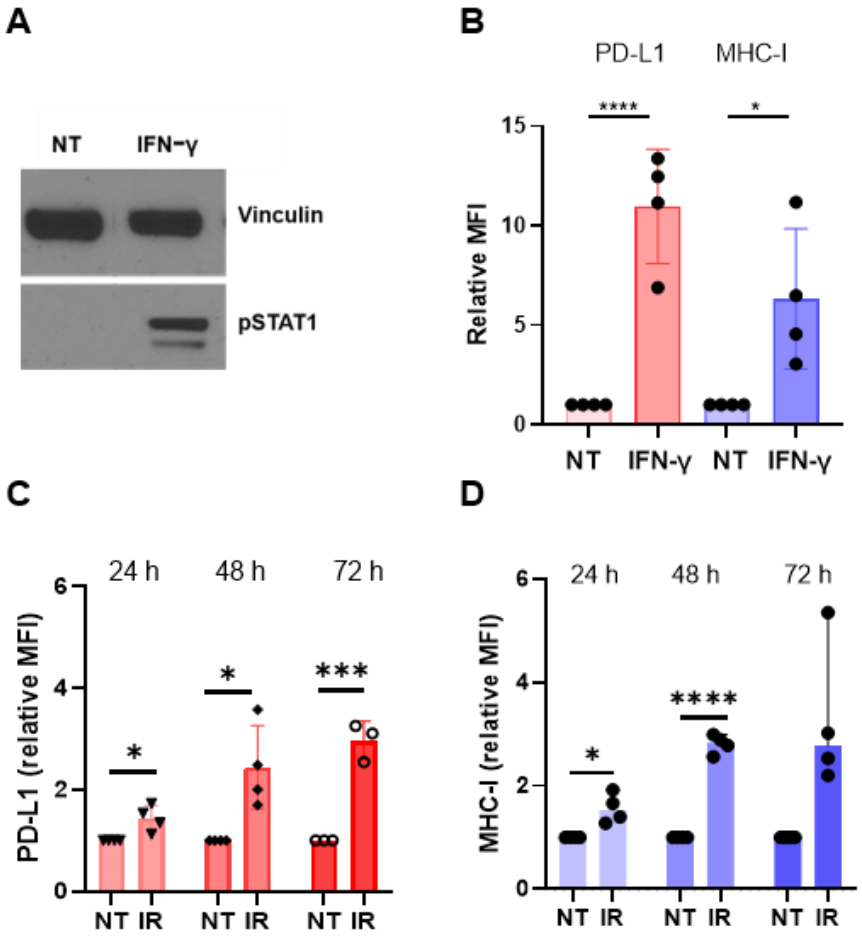

Figure 20 IFN-γ and IR induced expression of PD-L1 and MHC-I in RM1-PGLS cells. (A) Immunoblot analysis of IFN-γ- treated RM1-PGLS cells. RM1-PGLS cells were exposed to IFN-γ (10 ng/mL) for 24 h and analyzed by immunoblot using antibodies against pSTAT1 (clone Y701; 84 and 91 kDa) and Vinculin (clone E1EV; 116 kDa) (B) Flow cytometric analysis of RM1-PGLS cells exposed to IFN-γ. RM1-PGLS cells were exposed to IFN-γ (10 ng/mL) for 24 h. Levels of PD-L1 and MHC-I were analyzed by flow cytometry. Data are shown as mean ± SD. Statistics: one-way ANOVA: *p ≤ 0.05, ****p ≤ 0.0001. (C-D) RM1-PGLS cells were irradiated with 10 Gy and analyzed for PD-L1 and MHC-I expression levels by flow cytometry 24 h, 48 h and 72 h post IR. PD-L1: 24 h: IR 1.43 ± 0.26, p = 0.0157, n = 4; 48 h: IR 2.44 ± 0.94, p = 0.0128, n = 4, 72 h: IR 2.97 ± 0.38, p = 0.0008, n =3. MHC class I: 24 h: IR 1.53 ± 0.29, p = 0.0298, n = 4; 48 h: IR 2.84 ± 0.18, p < 0.0001, n = 4, 72 h: IR 2.78 ± 0.41, p = 0.0729, n = 4. Data is shown as mean ± SD. Statistics: Mann Whitney and unpaired t test. *p ≤ 0.05, ****p ≤ 0.0001.

Upregulated PDL-1 expression after IFN-γ and IR provided the rationale for testing ^{177}Lu-PSMA-617 RLT in combination with PD-1 ICB *in vivo* (**Fig. 21 A**). Combined PD-1 ICB and PSMA-targeted alpha-RLT ^{225}Actinium (Ac)-PSMA was previously reported to synergistically improve therapeutic outcomes in PCa model[131]. Alpha particles have a much shorter range and greater linear energy transfer (LET) compared to beta particles which might result in induction of more severe DNA damage. In contrast to ^{225}Ac-PSMA-617, ^{177}Lu-PSMA-617 is the clinically used version of PSMA-RLT and we

aimed at investigating the potential of combined ^{177}Lu-PSMA-617/ anti-PD-1 in a syngenic PCa model.

While RLT and anti-PD-1 alone moderately improved median TTP half max tumor volume RLT (19 d, $p < 0.0001$; vs. NT, 11 d) and anti-PD-1 (19 d, $p < 0.0001$), combined RLT/anti-PD-1 significantly increased median TTP compared to NT (25 d, $p < 0.0001$ vs NT and $p < 0.2273$ vs. monotherapies) (**Fig. 21 C**).

Survival was 14 d for NT, 20.5 d for anti-PD-1 ($p = 0.0001$ vs. NT), 18.5 d for RLT ($p < 0.0001$ vs NT), 23.5 d for RLT/anti-PD-1 ($p < 0.0001$ vs. NT and $p < 0.0431$ vs. monotherapies) (**Fig. 21 B**). None of the mice lost weight during the treatment, indicating that the treatment was well tolerated (**Fig. 21 D**).

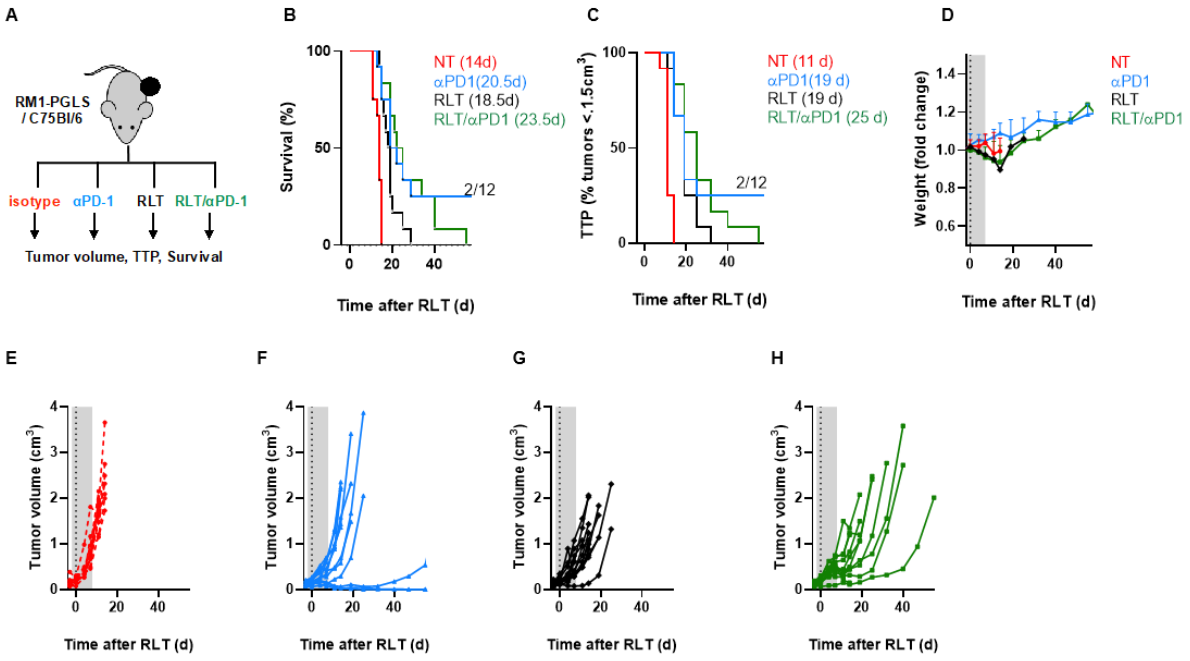

Figure 21 anti-PD1 enhances PSMA-RLT efficacy in RM1-PGLS allograft model.
(A) Study outline (B) Survival control: NT, 14 d, anti-PD1, 20.5 d ($p = 0.0001$ vs NT), RLT, 18.5 d ($p < 0.0001$ vs NT) and RLT/anti-PD1, 23.5 d,($p < 0.0001$ vs NT and $p < 0.0431$ vs. monotherapies) (C) TTP to half maximal tumor volume NT, 11 d, RLT, 19 d ($p < 0.0001$), anti-PD1, 19 d ($p < 0.0001$), RLT/anti-PD1, 25 d ($p < 0.0001$ vs NT and $p < 0.2273$ vs. monotherapies) (D). Body weights (mean ± SD). (E-H) Tumor volumes for individual mice. Dasher line indicate start of RLT. Shaded area indicates treatment duration.

4. Discussion

Metastatic castration-resistant prostate cancer remains incurable despite several improvements in the therapeutic landscape. Recently approved therapies provide only life-prolonging treatment but are not curative. Thus, there is still a high demand for developing more effective approaches which will further improve clinical outcomes. The concept of combination therapy gained attention in recent years when it became obvious that monotherapies might be insufficient to reach durable responses and patients will eventually relapse. To address this issue, this work focused on establishing rational and well-balanced combination therapies for PCa. The main focus was on PSMA-targeted RLT which is a novel therapeutic option for mCRPC patients showing promising effects in clinical trials, including the recent phase 3 VISION trial. However, approx. 50 % of patients will not respond to RLT. In the current study, three approaches to improve the efficacy of ^{177}Lu-PSMA-617 RLT in PCa were investigated: 1. To improve tumor targeting by using ARB to enhance PSMA expression levels; 2. To exploit tumor vulnerabilities induced by ^{177}Lu-PSMA (combination ^{177}Lu-PSMA-617 with DDR inhibition); and 3. To use ^{177}Lu-PSMA-617 as an *in situ* vaccine to enhance PCa immunogenicity (combination ^{177}Lu-PSMA-617 and ICB).

1. To improve tumor targeting by using ARB to enhance PSMA expression levels. PSMA expression is a prerequisite for RLT eligibility and low or heterogeneous PSMA-expression represent a resistance mechanism to RLT[126,127]. Current et al. demonstrated that the degree of PSMA expression and the fraction of PSMA$^-$positive cells correlate with ^{177}Lu-/^{225}Ac-PSMA617 tumor uptake and DNA damage, and thus, RLT efficacy[132]. The VISION trial demonstrated that about 10 % of mCRPC patients will not be eligible for RLT due to insufficient tumoral PSMA expression. Moreover, more than half of patients will not present with radiographic response after ^{177}Lu-PSMA-617 RLT. High-intensity tumour uptake on PSMA-PET was reported to correlate with tumor radiation dose, as well as PSA response at 12 weeks in ^{177}Lu-PSMA-617 RLT treated patients[127]. PSMA expression level has also been classified as a clinical predictor of non-response in a recent multi-center analysis[133]. Therefore, enhancing PSMA expression levels might improve the efficacy of ^{177}Lu-PSMA-617 RLT and might render patients with initially low PSMA expression eligible for RLT. In the first part of this thesis, the effect of ARB on PSMA expression in the PSMA-low human prostate

cancer cell line 22Rv1 and the PSMA-high human prostate cancer cell lines C4-2 and LNCaP was investigated *in vitro* and *in vivo* (22Rv1 only). Enzalutamide (ARB) significantly increased PSMA expression in all three cell lines already after one week of treatment. 22Rv1 was shown by IHC and flow cytometry to express low levels of PSMA, thus closely representing the challenging patient cohorts who will eventually not be eligible for or responsive to RLT. This finding provided the rationale for investigating the effect of ARB with enzalutamide on PSMA expression *in vivo*. In accordance with the *in vitro* results, ^{68}Ga-PSMA-11 uptake significantly increased after two weeks of enzalutamide treatment in the 22Rv1 xenograft model. Notably, PSMA expression remained significantly increased after correcting ^{68}Ga-PSMA-11 uptake for PVE on PET images related to tumor size; however, tumor growth may have contributed to an overestimation of changes in PSMA expression using PET. Moreover, the study has been evaluated in intact male mice which did not undergo surgical or chemical castration. The modulation of PSMA expression might differ in an androgen depleted setting. Androgens were previously reported to inhibit PSMA expression[134,135], therefore, ARB might lead to elevated PSMA expression. The exact mechanism which controls PSMA expression is still not completely understood; however, it is known, that it is regulated by a PSMA promoter and a PSMA enhancer, located within the third intron of PSMA[136]. After binding of androgens to AR, the androgen/AR complex translocates to the nucleus and binds to the PSMA enhancer region of the PSMA gene leading to its inactivation. Conversely, androgen binding to AR is inhibited by ADT/ARB which can result in activation of the PSMA enhancer region. Thus, androgen/AR complex might mediate downregulation of PSMA gene transcription. Several studies reported on enhanced PSMA expression in PSMA-high LNCaP and C4-2 xenografts upon ADT/ARB[137-139]. Lückerath et al. demonstrated that pre-treatment with enzalutamide before RLT led to more substantial DNA damage (phospho-γH2A.X) compared to RLT monotherapy but did not result in additional tumor growth retardation. However, due to already high basal PSMA levels in C4-2, ARB-induced elevation of PSMA might not translate in further improved RLT efficacy. Taken together, various PCa cell line models demonstrated enhanced PSMA expression after ARB which might translate into improved RLT radiation delivery. On the clinical site, enhanced PSMA expression levels in mCRPC patient with low-PSMA nodal metastases after enzalutamide treatment has been reported[124]. In accordance with this

finding, Hope et al. reported increased PSMA uptake after the initiation of ADT in a castration-sensitive PCa patient[139]. Emmett et al. demonstrated an increased intensity of ^{68}Ga-PSMA-11 PET in men with mCRPC receiving ARB demonstrated on day 9 of treatment compared with baseline levels[140]. In contrast, 86 % of men with castrate-sensitive PCa showed significant reduction in ^{68}Ga-PSMA-11 intensity as early as day 9 after ADT start.

These findings suggest that the effect of ARB on PSMA expression might depend on PCa stage. Treatment with enzalutamide in hormone-naïve cancer might lead to more effective tumor shrinkage resulting in an overall decrease in cells expressing PSMA as detected by ^{68}Ga-PSMA-11 PET/CT. In contrast, ARB in advanced PC might result in PSMA increase with weaker anti-tumor effects. A possible explanation might center on AR signaling driving PCa development; in case of androgen-independent disease, the initiation of cell death via AR-signaling might be impaired. However, it has to be taken into account that ARB in CRPC has been reported to have anti-tumor effects[141] which might suggest that the ability of enzalutamide to increase PSMA levels is independent of its ability to induce tumor shrinkage.

Thus, the effect of ARB on PSMA is still not fully understood mainly because the exact role and regulation of PSMA in the pathogenesis of PCa remains elusive. Due to its high expression levels in PCa, PSMA emerged as an atrractive theranostic target. Its expression has been reported to increase with tumor grade and to inversely correlate with survival[42,43]. Additionally, PSMA has been reported to be involved in cell survival and cell proliferation signaling pathways such as phosphatidylinositol-3-kinase (PI3K)[142] and mitogen-activated protein kinase (MAPK)[143]. The PI3K/Akt/mammalian target of rapamycin (mTOR, PI3K-Akt-mTOR) pathway was reported to play an important role in facilitating tumor formation, disease progression and therapeutic resistance in PCa. Recently, Kaitannis et al. demonstrated that PSMA releases glutamate from folic acid; the glutamate, in turn, activates metabotropic glutamate receptors leading to PTEN-independent activation of p110β isoform of PI3K and concomitantly negatively regulate the AR pathway[40]. Inhibition of PSMA decreased tumor growth in animals with PSMA-positive xenografts which was enhanced by concomitant inhibition of the AR pathway. Previously it was shown that PI3K signaling in PCa depends mainly on the p110β isoform[144]. These results indicate a novel oncogenic signaling role of PSMA and its involvement in establishing the PI3K-AR

regulatory loop. Thus, this might have a significant clinical implication: it has been reported, that combination therapy with PI3K and AR inhibitors suppresses the reciprocal negative feedback loop between PI3K and AR-signaling in PCa[145]. Moreover, due to its folate hydrolase activity, PSMA was shown to contribute to PCa in environments with low or physiological folate levels[146].

In summary, ARB is a promising approach to enhance PSMA levels in PSMA-low cancer. Nevertheless, it has to be investigated if pharmacologically-enhanced PSMA expression will translate into increased radiation delivery and enhanced RLT efficacy. Notably, a positive association for ^{68}Ga-PSMA-11 and ^{177}Lu-PSMA-617 uptake in animal models has already been reported[147,148].

The effect of ARB on PSMA expression is now assessed in clinical trials (NCT04279561) which highlights high interest in that topic.

2. Combined ^{177}Lu-PSMA and DDR inhibition

The approval of olaparib for BRCA1/2-deficient ovarian cancer and its successful application in disease management has driven the interest towards DDR inhibition. Since then, several other targets for different tumor entities are under investigation. The identification of DDR defects in mCRPC (although at a relatively small rate) provided the rationale to further evaluate DDR inhibitors providing opportunities for generation of synthetic lethality. Due to its potency to generate DNA damage, IR might synergize with DDR inhibition. Synthetic lethality between HR mutations and a radioligand therapeutic have already been shown by a retrospective single-institution study where germline or somatic HR-deficient patients showed improved response to ^{223}Ra, a bone-seeking alpha-particle emitter, compared to wild-type patients (80 % vs 39 %; based on alkaline phosphatase levels)[149]. Van der Doelen et al. also reported improved response to ^{223}Ra in mCRPC patients harbouring DDR aberrations[150]. Targeted ^{227}Thorium conjugates have been reported to synergize with ATRi and PARPi *in vivo*[151]. Moreover, Kratochwil et al. have shown that PCa patients resistant to alpha-targeted PSMA-RLT (despite sufficient tumor uptake in PSMA PET/CT) may harbor mutations in DDR associated genes[152].

Data presented in this thesis confirmed, that IR induces activation of the ATR/CHK1 signaling pathway in 22Rv1, C4-2 and LNCaP cell lines (data not shown). As hypothesized, Crystal violet staining, which was used as a *in vitro* equivalent for *in vivo*

tumor growth inhibition, demonstrated synergy of combined IR and ATRi or PARPi, whereas the triple combination proved most effective. In agreement with cell growth inhibition data, cell cycle analysis confirmed radiosensivity of all cell lines to IR as shown by increases in the sub-G1 fraction. In 22Rv1, combined IR and ATRi and/or PARPi and the triple combination IR/ATRi/PARPi led to increases in the sub-G1 fraction as compared to monotherapies. In C4-2, only the triple combination increased the sub-G1 fraction compared to IR and double treatments. In LNCaP, combined IR/PARPi and the triple combination seemed to have the stongest effect. These *in vitro* data indicating enhanced cytotoxicity after combining IR with ATRi and/or PARPi encouraged further evaluation of combined DDRi and RLT *in vivo*.

Combined PARP and ATR inhibition has been shown to potentiate genome instability and cell death in ATM-deficient cancer cells[153]. In an ovarian cancer model, PARPi-resistance was shown to be accompanied by increased ATR-CHK1 activity and sensitivity to ATR inhibition[154]. These findings indicate that there might be a cross-talk between PARP and ATR signaling pathways and inhibition of one of those pathways may induce an escape mechanism through upregulation of alternative DDR pathway. Supporting this hypothesis, olaparib treatment has been shown to activate the G2-M checkpoint which, in turn, was abrogated by ATR inhibition[155,156]. Investigating the potential of ATR and PARPi inhibition to enhance the efficacy of ^{177}Lu-PSMA-617 RLT in the 22Rv1 xenograft model in immunodeficient mice, we found that neither RLT alone nor any combination treatment showed any significant anti-tumor effects. Additionally, no significant metabolic changes were monitored by FDG-PET. A likely explanation for the lack of RLT efficacy might be insufficient PSMA expression. 22Rv1 has low basal PSMA levels. The animals were treated with ARB for one week prior to RLT and significant increase in PSMA expression levels were detected; however, PSMA levels might still have been too low to achieve RLT-mediated anti-tumor effects. 22Rv1 tumors are rapidly-growing tumors which become necrotic very fast as observed in tumors resected post-mortem. Early tumor necrosis might have contributed to lack of responsiveness to therapies. Moreover, beta-emitters such as ^{177}Lu might not be able to generate sufficient levels of DNA damage in such challenging model as 22Rv1, allowing the tumor cells to repair of the damaged DNA strands. Therefore, alpha-emitters such as ^{225}Ac should be investigated as an alternative due

to their high LET and high density of ionizations along the path length of emitted particles, which may result in more profound and difficult to repair DNA damage[157].
Neither PARPi nor ATRi (whether monotherapy or combined with RLT) treatment showed anti-tumor effect except for RLT/ATRi for which a non-significant tendency for prolonged TTP was observed. Given that PSMA expression in the 22Rv1 model was too low to achieve sufficient RLT-delivery to tumors and thus DNA damage, a possible synergy with DDR inhibition could probably not be achieved. Possibly, activation of other compensatory mechanisms could have contributed to lack of effect. Also, tumor necrosis might prevented drug delivery. Efficient drug delivery to tumors is essential to achieve anti-tumor effects. Therefore, in the next steps ATR and PARP expression should be investigated *in vivo* using ATR and PARP radiotracers to assess if: 1. PARP/ATR are expressed in tumors, 2. inhibitors reach the tumor, 3. PARP/ATR levels change under RLT. Synergistic cytotoxicity of the ATR inhibitor ceralasertib with olaparib has already been reported in ATM-deficient lung carcinoma cells, but not in ATM-proficient cells[153]. Moreover, ATM loss has been shown to confer greater sensitivity to ATRi than to PARPi in PCa[158]. Therefore, ATM status might have an impact on therapy response which needs to be taken into account for patients stratification. Genome analysis of 22Rv1 cells by next generation sequencing did not reveal any ATM aberration (data not shown) which might have contributed to lack of effect of ATRi based combination therapies. Additionally, PARPi efficacy was reported to depend on intratumoral cyclic GMP-AMP synthase (cGAS)–stimulator of interferon genes (STING) signaling pathway[159]. A dysfunctional DDR machinery (e.g., through PARPi) can result in accumulation of DNA damage such as cytosolic double stranded DNA (dsDNA) and mincronuclei which are recognized by the immune system inducing the immune response via cGAS-STING pathway[160-162]. PARPi prevents repair of damaged DNA which may not be sufficient to achieve anti-tumor effects without proficient cGAS-STING signaling. Thus, achieving of PARPi-mediated anti-tumor effetcs might by impeded in an immunodeficient model. Moreover, cytosolic dsDNA accumulation coupled with STING signaling in PCa was reported to increase from hyperplasia to stage II and then to decrease in stage III [163]. In accordance with that, gene-level transcript expression data for STING in PCa (TCGA) reveal lower espression levels as compared to healthy tissue. Despite the missing evidence in this *in vivo* study, DDR inhibition to enhance the efficacy of RLT still is a promising strategy.

However, the interplay between different DDR pathways needs to be better understood as well as the mechanisms of induction of specific DDR pathways by different therapeutic isotopes.

Noteworthy, the therapy was well tolerated and no signs of toxicitiy were observed. In contrast, another ATR inhibitor, VE-822, led to toxicity resulting in weight loss (data not shown) which led to study-discontinuation and substitution with ceralasertib. Combining PARP inhibitors with other inhibitors of DDR and/or RLT may broaden its application beyond HR-deficient malignancies. Olaparib is already sucessfuly applied in the treatment of advanced HR-deficient PCa and is currently evaluated in combination with ^{177}Lu-PSMA-617 (NCT03874884; phase I) and ceralasertib (NCT03787680; phase II) in advanced PCa.

3. Combined ^{177}Lu-PSMA-617 and ICB

In the third part of the thesis, potential enhancement of the efficacy of RLT by ICB was investigated. The immunological consequences of RLT are still poorly documented; however, emerging evidence suggests that dying irradiated cancer cells can release immunostimulatory molecules to induce ICD[164]. The immunostimulatory molecules, called damage-associated molecular patterns (DAMPs), lead to recruitment of APC and inititation of an immune response. Based on the hypothesis that RLT induces ICD, the responsiveness of murine RM1-PGLS cells to IFN-γ was investigated *in vitro*. IFN-γ is released by activated T cells in the course of an immune response and can induce tumors to activate immunosuppressive mechanisms, e.g., upregulation of PD-L1 and MHC class I expression. In this scenario, PD-L1 expression would inhibit cytotoxic T cell activation and thus, function, but at the same time would present a therapeutic target; antigen presentation by MHC I in the absence of co-stimulation would lead to T cell anergy. Exposure to IFN-γ increased expression of both, PD-L1 and MHC class I on the cell surface. PD-1 and MHC I expression was also upregulated following IR. These data provided the rationale for treating RM1-PGLS tumors with PD-1 ICB. RLT alone and PD1 blockade alone moderately improved TTP and survival. However, the treatment combination significantly prolonged TTP and survival compared to either monotherapy. The UCLA group previously evaluated combined alpha-emitting PSMA RLT with PD-1 ICB in the RM1-PGLS model[131]. Given the differences in LET for beta and alpha-emitters which might result in different complexity of DNA damage, the

current study aimed to compare alpha vs. beta PSMA RLT to investigate, if beta-emitting RLT may suffice to create durable responses when combined with ICB. Data of this study confirmed that ^{177}Lu-PSMA-617 RLT synergized with ICB resulting in prolonged TTP and survival. However, animals from the ^{225}Ac-RLT study showed longer survival time when compared to ^{177}Lu-PSMA-617 RLT study suggesting that the choice of the isotope might contribute to stronger anti-tumor effects. Mechanisms of RLT-mediated immunomodulation are still under investigation and its outcome may vary in response to dose, temporal dynamics or effects of tumor-micronenvironment (TME). Reportedly, RLT-induced immune responses are T cell-dependent and might lead to anti-tumor memory; mice which were classifyied as complete responders to RLT were immune to tumor re-challenge[131,165,166] and co-culturing of splenocytes from these mice with tumor cells increased IFN-γ production[167]. Also, modulation of the TME by RLT was demonstrated with increases in tumor infiltrating $CD8^+$ lymphocytes and decreased abundance of regulatory T cells (T_{reg}) suggesting the development of an immune susceptible TME following treatment[165]. In contrast, recruitment of T_{reg} after RLT was also reported[166,168], probably due to experimental differences which highlight the importance of investigating the temporal dynamics of immunomodulation. Additionally, RLT has been shown to induce more profound tumor-specific T cell responses and prolonged survival of mice when given at higher doses[165]. In contrast, low-dose RLT has not or only moderately increased T cell recruitment in mice[166,169]. However, combining low dose RLT with ICB was sufficient to reach durable tumor cell-specific $CD8^+$ T cell responses. The mechanistic basis whereby RLT elicits immune responses might center around cGAS-STING pathway and IFN type 1. Investigating the role of functional STING signaling in tumor cells, RLT-treated tumor cells were found to induce IFN-γ production by $CD8^+$ T cells independent of tumoral STING expression. However, comparison of therapeutic efficacy in STING wildtype vs. STING knockout tumors showed that tumoral STING signaling seems to be required for optimal RLT efficacy and synergy of RLT with CTLA-4 ICB, presumably due to significantly higher CTLA-4 levels on T cells exposed to STING-deficient (vs. STING-wildtype) tumor cells following RLT[170]. Hence, more detailed analysis on mechanisms of RLT-induced anti-tumor immune responses needs to be conducted. For instance, presence of specific DAMPs like calreticulin or high mobility group box 1 (HMGB1) should be investigated to verify if RLT can induce ICD. Moreover, other immune

escape mechanism beyond PD-1/PDL-1 should be taken into account; recently, immunological ignorance (low expression levels of the genes involved in antigen processing and presentation, immune cell recruitment, and immune activation), CTLA-4, and DcR3 overexpression were identified as major evasion mechanisms in PCa[171]. Combining RLT and dual ICB (PD-1, CTLA-4) might address both, RLT-induced upregulation of PD-L1 on tumor cells and CTLA-4 on immune cells; this regimen might also counteract CTLA-4 ICB mediated T cell exhaustion[168,170] and RLT-induced $CD8^+$ T cell loss[172]. However, this approach would have to be designed carefully as dual ICB resulted in increased toxicities in patients in clinical trials[173,174]. The high interest of combined RLT and ICB is reflected in various clinical trials (e.g., ^{177}Lu-PSMA-617 + PD-1 ICB: NCT03658447, NCT03805594; ^{177}Lu-DOTATATE + PD-1 ICB: NCT03457948, + PD-L1 ICB: NCT04261855). ICB has been proven effective in tumors with inflammatory phenotypes; although a large fraction of PCa is characterized by immune-desert or immune-excluded phenotype, RLT might change the immune phenotype of PCa to an inflammatory one rendering it sensitive to ICB. In order to achieve that, important insights need to be gained to fully exploit RLT-induced immunomodulation, including better understanding of spatio-temporal dynamics of RLT-induced immunomodulation, physical properties of RLT, other signaling pathways involved, the role of tumor stroma, metabolic and oxygen status and translatability from rodents to humans.

Outlook

The presented studies provide a basis for establishing translatable combination therapies to improve the efficacy of ^{177}Lu-PSMA-617 RLT and thus the outcome for mCRPC patients. Elucidating the exact relationship of PSMA and ARB, esp. in the context of androgen-dependency, would help to exploit the potential of ARB to enhance PSMA expression to levels enabling targeting with PSMA-RLT. Modulation of PSMA expression with ARB is extensively investigated and the results of clinical studies are eagerly awaited.

For combined RLT and DDRi, the lack of efficacy after combined RLT and DDRi has to be evaluated. Notably, several studies report synergy of conventional radiotherapy and first data on RLT and DDRi emerge. Significant RLT-induced upregulation of DDR pathways and ATR and ATM activity has been reported in PCa xenografts[54]. Thus, combined RLT and DDRi should be investigated in models more sensitive to RLT, incl. with higher target expression, than 22Rv1 to ensure that sufficient DNA damage is being induced. The complex interplay between different DDR pathways, allowing for compensation when one pathway is inhibited, needs to be elucidated and might necessitate patient stratification. To this end, future studies will investigate the versatility of radioligands targeting ATR, ATM or PARP to monitor expression of the respective proteins, successfull drug-to-tumor-delivery, and response to treatment. Synthesis of DDRi radioligands is currently being established at the Clinic for Nuclear Medicine in Essen. Cancer cell lines often exhibit high baseline replication stress (RS) levels which might act as predictive biomarker for RLT responsiveness. Thus, baseline RS-levels and RS-response proficiency should be assessed as pCHK1/2 levels and fraction of cells capable of completing cell cycle after hydroxyurea-induced RS[175], respectively. Given that ATM-status might play an important role for successful ATRi/PARPi, ATRi and PARPi should be invesigated in (isogenic) ATM-deficient models such as cells with ATM knockdown. Moreover, application of immunocompetent models has to be considered as optimal ATRi and PARPi efficacy might depend on the ability to activate cGas/STING signaling (in tumor cells and/or immune cells) and thus, immune responses[159,176,177]. In this context, the combination of RLT with a DDRi and IT might be promising (see below).

For combined RLT and ICB, future studies will aim at extending the findings to more translationally-relevant PCa mouse models (e.g., models of systemic disease;

immunologically cold models), and at the in depth analysis of the molecular and cellular outcome of RLT. The spatio-temporal dynamics of directly cytotoxic and indirectly anti-tumorigenic effects of RLT will be assessed in tumor cells, cancer-associated fibroblasts/stroma and immune cells; this will include analysis of radiobiological paramters (e.g., DNA damage, senescence, [immunogenic] cell death), immune cell and fibroblast sub-populations, and transcriptional profiles to identify mechanisms that may mitigate, or enhance, the cytotoxic effects of RLT. Insights gained on reactive mechanisms elicited by RLT will help to develop rational RLT/IT combination regimens to improve the outcome of PCa. Recently, ceralasertib has been reported to potentiate $CD8^+$ T cell dependent anti-tumor activity following radiation[177] and inhibition of ATR was shown to downregulate PD-L1 and sensitize tumor cells to T cell-mediated killing[178]. Shen et al. demonstrated that PARPi triggered a STING-dependent immune response and enhanced the therapeutic efficacy of ICB[179]. PARPi was also reported to attenuate T cell killing through PD-L1 induction[180]. PARPi/ICB[181-184] and ATRi/ICB[185] combinations have already been and ^{177}Lu-PSMA-617/ICB (NCT03658447, NCT03805594) is being tested in clinical trials. Notably, due to unique toxicity characteristics of IT[186], these combination regimens should have non-overlaping toxicities, potentially avoiding adverse events observed when combining different IT. Hence, combined RLT/IT/DDRi may be a safer candidate regimen to improve the outcome of PCa.

Lastly, data obtained in cell and mouse models need to be validated in patients. We recently launched a study that allows us to investigate biopsies from metastatic, PSMA-avid lesions in mCRPC patients undergoing ^{177}Lu-PSMA-617 therapy, and thus, to compare mouse and human data and to identifying predictors and determinants of RLT efficacy in mCRPC patients.

Abstract

Radioligand therapy (RLT) with a ligand binding the prostate specific antigen (PSMA; ^{177}Lu-PSMA-617) is a promising therapeutic option for patients with metastatic castration-resistant prostate cancer (mCRPC). However, approx. 50 % of patients do not respond to RLT. Thus, there is an urgent need to improve RLT efficacy through rationally designed combination therapies. In this work three approaches to enhance the efficacy of RLT were explored: 1. To improve tumor targeting by using ARB to enhance PSMA expression levels; 2. To exploit tumor vulnerabilities induced by ^{177}Lu-PSMA-617 (combination ^{177}Lu-PSMA-617 with DDR inhibition); and 3. To use ^{177}Lu-PSMA-617 as an *in situ* vaccine to enhance PCa immunogenicity (combination ^{177}Lu-PSMA-617 and ICB).

1. Effect of ARB on PSMA expression was assessed in human PCa cell lines 22Rv1, C4-2, and LNCaP. Immunohistochemistry and flow cytometry revealed low (22Rv1) and high (C4-2 and LNCaP) basal PSMA expression. ARB increased PSMA levels in 22Rv1, C4-2, and LNCaP (2.2/2.3/2.6-fold, p = 0.0005/0.03/0.046) after one week. 22Rv1 xenografts were treated with ARB for two weeks. Positron emission tomography /computed tomography (PET/CT) demonstrated higher tumor uptake of ^{68}Ga-PSMA-11 after ARB (p = 0.004). Thus, ARB enhances PSMA expression which might allow for improved targeting with RLT.

2. RLT induces DNA damage leading to activation of DDR signaling. DDR activation might mitigate RLT-induced cytotoxicity and, vice versa, inhibition of DDR signaling might sensitize tumors to RLT. Here, a combination regimen of Ataxia telangiectasia and Rad3 related (ATR) and/or Poly(ADP-ribose)-Polymerase (PARP) inhibitors and ionizing radiation (IR/RLT) was investigated in 22Rv1, C4-2, and LNCaP *in vitro* and in the 22Rv1 xenograft model. Combined IR and DDRi impaired cell growth and enhanced cell death as demonstrated by a modified colony formation assay and flow cytometry. *In vivo*, RLT/DDRi combinations did not enhance anti-tumor efficacy; the RLT/ATRi combination resulted in a slightly but non-significantly prolonged time to progression. Future studies will focus on evaluating the lack of efficacy of combined RLT and DDRi *in vivo* and how to overcome it.

3. Hypothesizing that RLT may enhance anti-prostate cancer immunity by inducing immunogenic cell death, synergy of RLT with PD-1 immune checkpoint blockade (ICB) was investigated. *In vitro*, stimulation of murine RM1-PGLS cells with IFN-γ

phosphorylated STAT1 leading to upregulation of PD-L1 and MHC class I; additionally, IR enhanced PD-L1 and MHC class I expression. This provided the rationale for testing the RLT/ICB combination *in vivo*. While monotherapies did not improve outcome significantly, the RLT/ICB regiment significantly increased median time-to-progression compared to NT ($p < 0.0001$ vs NT). Future studies, using PCa mouse models and patient samples, will explore the mechanistic basis for these observation with the goal to identify the most promising RLT/immunotherapy combination(s) for inducing durable responses in PCa

Together, PSMA-RLT has become a game-changer in the management of PCa. To exploit its full potential the field needs to understand what constitutes an optimal radiotherapeutic strategy, and which tumor cell-intrinsic resistance mechanisms and protective tumor-microenvironment interactions need to be targeted, in order to develop more effective RLT-combination therapies. The design of and treatment with combination therapies is very complex and challenging. Data presented in this work shed light on this complexity and first encouraging results show that RLT efficacy can be enhanced by rational combinatorial approaches.

Zusammenfassung

Die Radioligandentherapie (RLT) die das prostataspezifische Antigen (PSMA; ^{177}Lu-PSMA-617) bindet, ist eine vielversprechende Therapiealternative für Patienten mit metastasiertem kastrationsresistentem Prostatakarzinom (mCRPC). Allerdings sprechen ca. 50 % der Patienten nicht auf die RLT an. Daher muss die Wirksamkeit der PSMA-RLT verbessert werden, z.B. durch rational konzipierte Kombinationstherapien. In dieser Arbeit wurden drei Ansätze zur Verbesserung der RLT-Wirksamkeit untersucht: 1. Verbesserung des Tumor-Targetings durch Androgen Rezeptor Blokade (ARB)-vermittelte Erhöhung der PSMA Expression; 2. Hemmung der Reparatur von DNA Schäden (DDR), die durch ^{177}Lu-PSMA-617 induziert wurden, durch Kombination mit Ataxia Telangiectasia and Rad3-related (ATR) und Poly(ADP-ribose)-Polymerase (PARP)-Hemmern (ATRi/PARPi); 3. Verwendung von ^{177}Lu-PSMA-617 als *in situ* Impfstoff zur Erhöhung der Immunogenität des Prostatakarzinoms (PCa) (Kombination RLT und Immuncheckpoint-Inhibitor, ICB).

1. Der Effekt von ARB auf die PSMA-Expression wurde in humanen PCa Zelllinien (22Rv1, C4-2 und LNCaP) untersucht. Mittels Immunhistochemie und Durschluss-zytometrie konnte gezeigt werden, dass 22Rv1 eine niedrige und C4-2 und LNCaP eine hohe basale PSMA-Expression aufweisen. ARB erhöhte das PSMA-Level in 22Rv1, C4-2 und LNCaP nach einer Woche (2,2/2,3/2,6-fach, p = 0,0005/0,03/0,046). Mäuse mit 22Rv1 Xenotransplantaten wurden über zwei Wochen mit ARB behandelt. Positronen-Emissions-Tomographie/Computertomographie (PET/CT) zeigte eine höhere Anreicherung von ^{68}Ga-PSMA-11 im Tumor nach ARB (p = 0,004). Somit konnte gezeigt werden, dass ARB zur Erhöhung der PSMA-Expression führt, was ein verbessertes Tumor-targeting mit RLT ermöglichen könnte.

2. RLT induziert DNA-Schäden, die zur Aktivierung der DDR-Signalwege führen. Die DDR-Aktivierung könnte die RLT-induzierte Zytotoxizität abschwächen; umgekehrt könnte die Hemmung der DDR eine Sensibilisierung der Tumore für RLT erzielen. In dieser Arbeit wurde eine Kombinationstherapie bestehend aus ionisierender Strahlung (IR/RLT) und ATRi und/oder PARPi in 22Rv1, C4-2 und LNCaP *in vitro* und 22Rv1 *in vivo* untersucht. IR/ATRi/PARPi führte zu einer Beeinträchtigung des Zellwachstums *in vitro*, wie durch einen modifizierten Koloniebildungsassay und Durchflusszytometrie gezeigt wurde. *In vivo* konnte keine Anti-Tumor Wirksamkeit der RLT/DDRi Kombinationen nachgewiesen werden; die RLT/ATRi Behandlung verlängerte tendentiell die Zeit bis zur Progression , allerdings ohne statistische Signifikanz zu

erreichen. In Zukunft soll untersucht werden, wie die Effektivität von kombinierten RLT/DDRi Therapien *in vivo* verbessert werden kann.

3. Unter der Annahme, dass RLT die Anti-Tumor Immunität durch Induktion eines immunogenen Zelltods verstärken kann, wurde eine mögliche Synergie von RLT mit PD-1-ICB untersucht. *In vitro* Stimulation muriner RM1-PGLS-Zellen mit IFN-γ induzierte die Phosphorylierung von STAT1 was zu einer Hochregulierung von PD-L1 und MHC Klasse I führte; ausserdem erhöhte IR die PD-L-1 und MHC Klasse I Expression. Auf Basis dieser Beobachtungen wurden Mäuse mit RM1-PGLS Tumoren mit RLT und ICB behandelt. Während die Monotherapien das Ergebnis nicht signifikant verbesserten, verlängerte die RLT/ICB Kombination die progressions-freie Zeit im Vergleich zu unbehandleten Tieren signifikant ($p < 0,0001$ vs. NT). Zukünftige Studien mit PCa-Mausmodellen und Patientenproben werden die mechanistischen Grundlagen der RLT-vermittelten Immunmodulation untersuchen, um die vielversprechendsten RLT/Immuntherapie-Kombinationen zur Induktion dauerhafter Therapieantworten im Prostatakarzinom zu identifizieren.

Die PSMA-RLT hat eine Wende in der Behandlung des PCa erbracht. Um das volle Potenzial der RLT auszuschöpfen, muss verstanden werden, was eine optimale strahlentherapeutische Strategie ausmacht und welche tumorzellintrinsichen Resistenzmechanismen und schützenden Tumor-Mikroumgebungs-Wechselwirkungen addressiert werden müssen, um effektivere RLT-Kombinationstherapien zu entwickeln. Das Design von und die Behandlung mit Kombinationstherapien ist sehr komplex und herausfordernd. Die in dieser Arbeit vorgestellten Daten beleuchten diese Komplexität und erste Ergebnisse zeigen, dass die RLT-Wirksamkeit durch rationale kombinatorische Ansätze verbessert werden kann.

References

1 Sung, H. *et al.* Global Cancer Statistics 2020: GLOBOCAN Estimates of Incidence and Mortality Worldwide for 36 Cancers in 185 Countries. *CA: A Cancer Journal for Clinicians* **71**, 209-249, doi:https://doi.org/10.3322/caac.21660 (2021).

2 Hanahan, D. & Weinberg, Robert A. Hallmarks of Cancer: The Next Generation. *Cell* **144**, 646-674, doi:https://doi.org/10.1016/j.cell.2011.02.013 (2011).

3 Kalluri, R. The biology and function of fibroblasts in cancer. *Nature Reviews Cancer* **16**, 582-598 (2016).

4 Henry, G. H. *et al.* A Cellular Anatomy of the Normal Adult Human Prostate and Prostatic Urethra. *Cell reports* **25**, 3530-3542.e3535, doi:10.1016/j.celrep.2018.11.086 (2018).

5 Shen, M. M. & Abate-Shen, C. Molecular genetics of prostate cancer: new prospects for old challenges. *Genes & development* **24**, 1967-2000 (2010).

6 Beltran, H. *et al.* Aggressive variants of castration-resistant prostate cancer. *Clinical cancer research : an official journal of the American Association for Cancer Research* **20**, 2846-2850, doi:10.1158/1078-0432.ccr-13-3309 (2014).

7 Timms, B. G. Prostate development: a historical perspective. *Differentiation; research in biological diversity* **76**, 565-577, doi:10.1111/j.1432-0436.2008.00278.x (2008).

8 Gann, P. H. Risk factors for prostate cancer. *Reviews in urology* **4 Suppl 5**, S3-s10 (2002).

9 de Bono, J. S. *et al.* Prostate carcinogenesis: inflammatory storms. *Nature Reviews Cancer* **20**, 455-469, doi:10.1038/s41568-020-0267-9 (2020).

10 Parnham, A. & Serefoglu, E. C. Retrograde ejaculation, painful ejaculation and hematospermia. *Translational andrology and urology* **5**, 592-601, doi:10.21037/tau.2016.06.05 (2016).

11 Mellinger, G. T., Gleason, D. & Bailar, J., 3rd. The histology and prognosis of prostatic cancer. *The Journal of urology* **97**, 331-337, doi:10.1016/s0022-5347(17)63039-8 (1967).

12 Ohori, M., Wheeler, T. M. & Scardino, P. T. The New American Joint Committee on Cancer and International Union Against Cancer TNM classification of prostate cancer. Clinicopathologic correlations. *Cancer* **74**, 104-114, doi:10.1002/1097-0142(19940701)74:1<104::aid-cncr2820740119>3.0.co;2-5 (1994).

13 Bostwick, D. G. *et al.* Independent origin of multiple foci of prostatic intraepithelial neoplasia: comparison with matched foci of prostate carcinoma. *Cancer* **83**, 1995-2002, doi:10.1002/(sici)1097-0142(19981101)83:9<1995::aid-cncr16>3.0.co;2-2 (1998).

14 De Marzo, A. M. *et al.* Human prostate cancer precursors and pathobiology. *Urology* **62**, 55-62, doi:10.1016/j.urology.2003.09.053 (2003).

15 He, L. *et al.* Metastatic castration-resistant prostate cancer: Academic insights and perspectives through bibliometric analysis. *Medicine* **99** (2020).

16 Kirby, M., Hirst, C. & Crawford, E. Characterising the castration-resistant prostate cancer population: a systematic review. *International journal of clinical practice* **65**, 1180-1192 (2011).

17 Aihara, M., Wheeler, T. M., Ohori, M. & Scardino, P. T. Heterogeneity of prostate cancer in radical prostatectomy specimens. *Urology* **43**, 60-66; discussion 66-67, doi:10.1016/s0090-4295(94)80264-5 (1994).

18 Macintosh, C. A., Stower, M., Reid, N. & Maitland, N. J. Precise microdissection of human prostate cancers reveals genotypic heterogeneity. *Cancer research* **58**, 23-28 (1998).

19 Liu, W. *et al.* Copy number analysis indicates monoclonal origin of lethal metastatic prostate cancer. *Nature medicine* **15**, 559-565, doi:10.1038/nm.1944 (2009).

20 Aggarwal, R. R. & Small, E. J. Small-cell/neuroendocrine prostate cancer: a growing threat? *Oncology* **28**, 838-838 (2014).

21 Aggarwal, R. *et al.* Clinical and genomic characterization of treatment-emergent small-cell neuroendocrine prostate cancer: a multi-institutional prospective study. *Journal of Clinical Oncology* **36**, 2492 (2018).

22 Berger, M. F. *et al.* The genomic complexity of primary human prostate cancer. *Nature* **470**, 214-220, doi:10.1038/nature09744 (2011).

23 Genomics,c.f.C. <https://www.cbioportal.org/results/oncoprint?cancer_study_list=prad_mich%2Cprad_su2c_2019%2Cprad_su2c_2015%2Cprad_mpcproject_2018&Z_SRE_THRESHOLD=2.0&RPPA_SCORE_THRESHOLD=2.0&data_priority=0&profileFilter=0&case_set_id=all&gene_list=ATM%250AATR%250ABRCA1%250ABRCA2%250ATP53&geneset_list=%20&tab_index=tab_visualize&Action=Submit. >

24 Rosner, W., Hryb, D. J., Khan, M. S., Nakhla, A. M. & Romas, N. A. Sex hormone-binding globulin: anatomy and physiology of a new regulatory system. *The Journal of steroid biochemistry and molecular biology* **40**, 813-820, doi:10.1016/0960-0760(91)90307-q (1991).

25 Baker, M. E. Albumin, steroid hormones and the origin of vertebrates. *The Journal of endocrinology* **175**, 121-127, doi:10.1677/joe.0.1750121 (2002).

26 Tan, M. H. E., Li, J., Xu, H. E., Melcher, K. & Yong, E.-l. Androgen receptor: structure, role in prostate cancer and drug discovery. *Acta Pharmacologica Sinica* **36**, 3-23, doi:10.1038/aps.2014.18 (2015).

27 Huggins, C. & Hodges, C. V. Studies on prostatic cancer: I. The effect of castration, of estrogen and of androgen injection on serum phosphatases in metastatic carcinoma of the prostate. 1941. *The Journal of urology* **168**, 9-12, doi:10.1016/s0022-5347(05)64820-3 (2002).

28 Beer, T. M. *et al.* Enzalutamide in Men with Chemotherapy-naïve Metastatic Castration-resistant Prostate Cancer: Extended Analysis of the Phase 3 PREVAIL Study. *Eur Urol* **71**, 151-154, doi:10.1016/j.eururo.2016.07.032 (2017).

29 Davis, I. D. *et al.* Enzalutamide with Standard First-Line Therapy in Metastatic Prostate Cancer. *The New England journal of medicine* **381**, 121-131, doi:10.1056/NEJMoa1903835 (2019).

30 Beltran, H. *et al.* New therapies for castration-resistant prostate cancer: efficacy and safety. *Eur Urol* **60**, 279-290, doi:10.1016/j.eururo.2011.04.038 (2011).

31 Knudsen, K. E. & Scher, H. I. Starving the addiction: new opportunities for durable suppression of AR signaling in prostate cancer. *Clinical cancer research : an official journal of the American Association for Cancer Research* **15**, 4792-4798, doi:10.1158/1078-0432.ccr-08-2660 (2009).

32 Israeli, R. S., Powell, C. T., Corr, J. G., Fair, W. R. & Heston, W. D. Expression of the prostate-specific membrane antigen. *Cancer research* **54**, 1807-1811 (1994).

33 Silver, D. A., Pellicer, I., Fair, W. R., Heston, W. D. & Cordon-Cardo, C. Prostate-specific membrane antigen expression in normal and malignant human tissues. *Clinical cancer research : an official journal of the American Association for Cancer Research* **3**, 81-85 (1997).

34 O'Keefe, D. S. *et al.* Mapping, genomic organization and promoter analysis of the human prostate-specific membrane antigen gene. *Biochimica et Biophysica Acta (BBA)-Gene Structure and Expression* **1443**, 113-127 (1998).

35 Leek, J. *et al.* Prostate-specific membrane antigen: evidence for the existence of a second related human gene. *British journal of cancer* **72**, 583-588 (1995).

36 Davis, M. I., Bennett, M. J., Thomas, L. M. & Bjorkman, P. J. Crystal structure of prostate-specific membrane antigen, a tumor marker and peptidase. *Proceedings of the National Academy of Sciences of the United States of America* **102**, 5981-5986, doi:10.1073/pnas.0502101102 (2005).

37 Rajasekaran, S. A. *et al.* A novel cytoplasmic tail MXXXL motif mediates the internalization of prostate-specific membrane antigen. *Molecular biology of the cell* **14**, 4835-4845, doi:10.1091/mbc.e02-11-0731 (2003).

38 Matthias, J. *et al.* Cytoplasmic Localization of Prostate-Specific Membrane Antigen Inhibitors May Confer Advantages for Targeted Cancer Therapies. *Cancer research* **81**, 2234-2245, doi:10.1158/0008-5472.can-20-1624 (2021).

39 Pinto, J. T. *et al.* Prostate-specific membrane antigen: a novel folate hydrolase in human prostatic carcinoma cells. *Clinical Cancer Research* **2**, 1445-1451 (1996).

40 Kaittanis, C. *et al.* Prostate-specific membrane antigen cleavage of vitamin B9 stimulates oncogenic signaling through metabotropic glutamate receptors. *Journal of experimental medicine* **215**, 159-175 (2018).

41 Fendler, W. P. *et al.* Preliminary experience with dosimetry, response and patient reported outcome after 177Lu-PSMA-617 therapy for metastatic castration-resistant prostate cancer. *Oncotarget* **8**, 3581 (2017).

42 Herlemann, A. *et al.* 68Ga-PSMA positron emission tomography/computed tomography provides accurate staging of lymph node regions prior to lymph node dissection in patients with prostate cancer. *European urology* **70**, 553-557 (2016).

43 Rahbar, K. *et al.* German multicenter study investigating 177Lu-PSMA-617 radioligand therapy in advanced prostate cancer patients. *Journal of Nuclear Medicine* **58**, 85-90 (2017).

44 Phelps, M. E. Positron emission tomography provides molecular imaging of biological processes. *Proceedings of the National Academy of Sciences* **97**, 9226-9233, doi:10.1073/pnas.97.16.9226 (2000).

45 Horoszewicz, J. S., Kawinski, E. & Murphy, G. P. Monoclonal antibodies to a new antigenic marker in epithelial prostatic cells and serum of prostatic cancer patients. *Anticancer research* **7**, 927-935 (1987).

46 Liu, H. *et al.* Monoclonal antibodies to the extracellular domain of prostate-specific membrane antigen also react with tumor vascular endothelium. *Cancer research* **57**, 3629-3634 (1997).

47 Bander, N. H. *et al.* Phase I trial of 177lutetium-labeled J591, a monoclonal antibody to prostate-specific membrane antigen, in patients with androgen-independent prostate cancer. *Journal of Clinical Oncology* **23**, 4591-4601 (2005).

48 Niaz, M. J. *et al.* Pilot Study of Hyperfractionated Dosing of Lutetium-177-Labeled Antiprostate-Specific Membrane Antigen Monoclonal Antibody J591 ((177) Lu-J591) for Metastatic Castration-Resistant Prostate Cancer. *The oncologist* **25**, 477-e895, doi:10.1634/theoncologist.2020-0028 (2020).
49 Fendler, W. P. *et al.* Assessment of 68Ga-PSMA-11 PET Accuracy in Localizing Recurrent Prostate Cancer: A Prospective Single-Arm Clinical Trial. *JAMA Oncol* **5**, 856-863, doi:10.1001/jamaoncol.2019.0096 (2019).
50 Afshar-Oromieh, A., Haberkorn, U., Eder, M., Eisenhut, M. & Zechmann, C. M. [68Ga]Gallium-labelled PSMA ligand as superior PET tracer for the diagnosis of prostate cancer: comparison with 18F-FECH. *European journal of nuclear medicine and molecular imaging* **39**, 1085-1086, doi:10.1007/s00259-012-2069-0 (2012).
51 Hofman, M. S. *et al.* [(177)Lu]-PSMA-617 radionuclide treatment in patients with metastatic castration-resistant prostate cancer (LuPSMA trial): a single-centre, single-arm, phase 2 study. *The Lancet. Oncology* **19**, 825-833, doi:10.1016/s1470-2045(18)30198-0 (2018).
52 Sartor, O. *et al.* Lutetium-177–PSMA-617 for Metastatic Castration-Resistant Prostate Cancer. *New England Journal of Medicine* (2021).
53 Hofman, M. S. *et al.* [177Lu] Lu-PSMA-617 versus cabazitaxel in patients with metastatic castration-resistant prostate cancer (TheraP): a randomised, open-label, phase 2 trial. *The Lancet* (2021).
54 Stuparu, A. D. *et al.* Mechanisms of Resistance to Prostate-Specific Membrane Antigen-Targeted Radioligand Therapy in a Mouse Model of Prostate Cancer. *Journal of Nuclear Medicine*, jnumed.120.256263, doi:10.2967/jnumed.120.256263 (2020).
55 Lee, Y. *et al.* Therapeutic effects of ablative radiation on local tumor require CD8+ T cells: changing strategies for cancer treatment. *Blood, The Journal of the American Society of Hematology* **114**, 589-595 (2009).
56 Staniszewska, M. *et al.* Drug and molecular radiotherapy combinations for metastatic castration resistant prostate cancer. *Nucl Med Biol* **96-97**, 101-111, doi:10.1016/j.nucmedbio.2021.03.009 (2021).
57 Barnes, D. E. & Lindahl, T. Repair and genetic consequences of endogenous DNA base damage in mammalian cells. *Annual review of genetics* **38**, 445-476, doi:10.1146/annurev.genet.38.072902.092448 (2004).
58 Schipler, A. & Iliakis, G. DNA double-strand-break complexity levels and their possible contributions to the probability for error-prone processing and repair pathway choice. *Nucleic acids research* **41**, 7589-7605, doi:10.1093/nar/gkt556 (2013).
59 Mladenov, E., Magin, S., Soni, A. & Iliakis, G. DNA double-strand break repair as determinant of cellular radiosensitivity to killing and target in radiation therapy. *Frontiers in oncology* **3**, 113, doi:10.3389/fonc.2013.00113 (2013).
60 Resnick, M. A. The repair of double-strand breaks in DNA: a model involving recombination. *Journal of Theoretical Biology* **59**, 97-106 (1976).
61 Ceccaldi, R., Rondinelli, B. & D'Andrea, A. D. Repair pathway choices and consequences at the double-strand break. *Trends in cell biology* **26**, 52-64 (2016).
62 Grindedal, E. M. *et al.* Germ-line mutations in mismatch repair genes associated with prostate cancer. *Cancer Epidemiology and Prevention Biomarkers* **18**, 2460-2467 (2009).
63 Leongamornlert, D. *et al.* Germline BRCA1 mutations increase prostate cancer risk. *British journal of cancer* **106**, 1697-1701 (2012).

64 Grasso, C. S. *et al.* The mutational landscape of lethal castration-resistant prostate cancer. *Nature* **487**, 239-243 (2012).
65 Na, R. *et al.* Germline Mutations in ATM and BRCA1/2 Distinguish Risk for Lethal and Indolent Prostate Cancer and are Associated with Early Age at Death. *Eur Urol* **71**, 740-747, doi:10.1016/j.eururo.2016.11.033 (2017).
66 de Bono, J. *et al.* Olaparib for metastatic castration-resistant prostate cancer. *New England Journal of Medicine* **382**, 2091-2102 (2020).
67 Rancati, G., Moffat, J., Typas, A. & Pavelka, N. Emerging and evolving concepts in gene essentiality. *Nature Reviews Genetics* **19**, 34 (2018).
68 Ashworth, A. & Lord, C. J. Synthetic lethal therapies for cancer: what's next after PARP inhibitors? *Nature Reviews Clinical Oncology* **15**, 564-576, doi:10.1038/s41571-018-0055-6 (2018).
69 de Bono, J. *et al.* Olaparib for Metastatic Castration-Resistant Prostate Cancer. *The New England journal of medicine* **382**, 2091-2102, doi:10.1056/NEJMoa1911440 (2020).
70 Murai, J. *et al.* Trapping of PARP1 and PARP2 by Clinical PARP Inhibitors. *Cancer research* **72**, 5588-5599, doi:10.1158/0008-5472.can-12-2753 (2012).
71 Rass, E., Chandramouly, G., Zha, S., Alt, F. W. & Xie, A. Ataxia telangiectasia mutated (ATM) is dispensable for endonuclease I-SceI-induced homologous recombination in mouse embryonic stem cells. *The Journal of biological chemistry* **288**, 7086-7095, doi:10.1074/jbc.M112.445825 (2013).
72 Kim, D., Liu, Y., Oberly, S., Freire, R. & Smolka, M. B. ATR-mediated proteome remodeling is a major determinant of homologous recombination capacity in cancer cells. *Nucleic acids research* **46**, 8311-8325, doi:10.1093/nar/gky625 (2018).
73 Gralewska, P. *et al.* PARP Inhibition Increases the Reliance on ATR/CHK1 Checkpoint Signaling Leading to Synthetic Lethality-An Alternative Treatment Strategy for Epithelial Ovarian Cancer Cells Independent from HR Effectiveness. *International journal of molecular sciences* **21**, doi:10.3390/ijms21249715 (2020).
74 Qiu, Z., Oleinick, N. L. & Zhang, J. ATR/CHK1 inhibitors and cancer therapy. *Radiotherapy and oncology : journal of the European Society for Therapeutic Radiology and Oncology* **126**, 450-464, doi:10.1016/j.radonc.2017.09.043 (2018).
75 Abida, W. *et al.* Preliminary results from the TRITON2 study of rucaparib in patients (pts) with DNA damage repair (DDR)-deficient metastatic castration-resistant prostate cancer (mCRPC): Updated analyses. *Annals of Oncology* **30**, v327-v328 (2019).
76 Smith, M. R. *et al.* (American Society of Clinical Oncology, 2019).
77 Shen, Y. *et al.* BMN 673, a novel and highly potent PARP1/2 inhibitor for the treatment of human cancers with DNA repair deficiency. *Clinical Cancer Research* **19**, 5003-5015 (2013).
78 Boussios, S. *et al.* Poly (ADP-Ribose) Polymerase Inhibitors: Talazoparib in Ovarian Cancer and Beyond. *Drugs in R&D* **20**, 55-73, doi:10.1007/s40268-020-00301-8 (2020).
79 Bono, J. S. D. *et al.* TALAPRO-1: A phase II study of talazoparib (TALA) in men with DNA damage repair mutations (DDRmut) and metastatic castration-resistant prostate cancer (mCRPC)—First interim analysis (IA). *Journal of Clinical Oncology* **38**, 119-119, doi:10.1200/JCO.2020.38.6_suppl.119 (2020).
80 de Bono, J. S. *et al.* Talazoparib monotherapy in metastatic castration-resistant prostate cancer with DNA repair alterations (TALAPRO-1): an open-label,

phase 2 trial. *The Lancet. Oncology* **22**, 1250-1264, doi:10.1016/s1470-2045(21)00376-4 (2021).

81 Smith, M. R. *et al.* Niraparib in patients with metastatic castration-resistant prostate cancer and DNA repair gene defects (GALAHAD): a multicentre, open-label, phase 2 trial. *The Lancet. Oncology*, doi:10.1016/s1470-2045(21)00757-9 (2022).

82 Kunkel, T. A. & Erie, D. A. DNA mismatch repair. *Annual review of biochemistry* **74**, 681-710, doi:10.1146/annurev.biochem.74.082803.133243 (2005).

83 Alexandrov, L. B. *et al.* Signatures of mutational processes in human cancer. *Nature* **500**, 415-421, doi:10.1038/nature12477 (2013).

84 Le, D. T. *et al.* PD-1 Blockade in Tumors with Mismatch-Repair Deficiency. *The New England journal of medicine* **372**, 2509-2520, doi:10.1056/NEJMoa1500596 (2015).

85 Abida, W. *et al.* Analysis of the prevalence of microsatellite instability in prostate cancer and response to immune checkpoint blockade. *JAMA oncology* **5**, 471-478 (2019).

86 Yarchoan, M., Hopkins, A. & Jaffee, E. M. Tumor Mutational Burden and Response Rate to PD-1 Inhibition. *The New England journal of medicine* **377**, 2500-2501, doi:10.1056/NEJMc1713444 (2017).

87 Hodi, F. S. *et al.* Improved survival with ipilimumab in patients with metastatic melanoma. *New England Journal of Medicine* **363**, 711-723 (2010).

88 Topalian, S. L. *et al.* Safety, activity, and immune correlates of anti–PD-1 antibody in cancer. *New England Journal of Medicine* **366**, 2443-2454 (2012).

89 Gandhi, L. *et al.* Pembrolizumab plus chemotherapy in metastatic non–small-cell lung cancer. *New England Journal of Medicine* **378**, 2078-2092 (2018).

90 Lopez-Bujanda, Z. & Drake, C. G. Myeloid-derived cells in prostate cancer progression: phenotype and prospective therapies. *Journal of Leukocyte Biology* **102**, 393-406 (2017).

91 Venturini, N. J. & Drake, C. G. Immunotherapy for prostate cancer. *Cold Spring Harbor perspectives in medicine* **9**, a030627 (2019).

92 Hegde, P. S. & Chen, D. S. Top 10 Challenges in Cancer Immunotherapy. *Immunity* **52**, 17-35, doi:10.1016/j.immuni.2019.12.011 (2020).

93 Joyce, J. A. & Fearon, D. T. T cell exclusion, immune privilege, and the tumor microenvironment. *Science (New York, N.Y.)* **348**, 74-80, doi:10.1126/science.aaa6204 (2015).

94 Kantoff, P. W. *et al.* Sipuleucel-T immunotherapy for castration-resistant prostate cancer. *New England Journal of Medicine* **363**, 411-422 (2010).

95 Gulley, J. L. *et al.* Phase III Trial of PROSTVAC in Asymptomatic or Minimally Symptomatic Metastatic Castration-Resistant Prostate Cancer. *J Clin Oncol* **37**, 1051-1061, doi:10.1200/jco.18.02031 (2019).

96 Bilusic, M. *et al.* Phase I study of a multitargeted recombinant Ad5 PSA/MUC-1/brachyury-based immunotherapy vaccine in patients with metastatic castration-resistant prostate cancer (mCRPC). *J Immunother Cancer* **9**, doi:10.1136/jitc-2021-002374 (2021).

97 Ahmadzadeh, M. *et al.* Tumor antigen-specific CD8 T cells infiltrating the tumor express high levels of PD-1 and are functionally impaired. *Blood* **114**, 1537-1544, doi:10.1182/blood-2008-12-195792 (2009).

98 Sharpe, A. H., Wherry, E. J., Ahmed, R. & Freeman, G. J. The function of programmed cell death 1 and its ligands in regulating autoimmunity and infection. *Nature immunology* **8**, 239-245, doi:10.1038/ni1443 (2007).

99 Dong, P., Xiong, Y., Yue, J., Hanley, S. J. B. & Watari, H. Tumor-Intrinsic PD-L1 Signaling in Cancer Initiation, Development and Treatment: Beyond Immune Evasion. *Frontiers in oncology* **8**, 386, doi:10.3389/fonc.2018.00386 (2018).

100 Jiang, Y., Chen, M., Nie, H. & Yuan, Y. PD-1 and PD-L1 in cancer immunotherapy: clinical implications and future considerations. *Human vaccines & immunotherapeutics* **15**, 1111-1122, doi:10.1080/21645515.2019.1571892 (2019).

101 Antonarakis, E. S. *et al.* Pembrolizumab for Treatment-Refractory Metastatic Castration-Resistant Prostate Cancer: Multicohort, Open-Label Phase II KEYNOTE-199 Study. *J Clin Oncol* **38**, 395-405, doi:10.1200/jco.19.01638 (2020).

102 Schwartz, J.-C. D., Zhang, X., Fedorov, A. A., Nathenson, S. G. & Almo, S. C. Structural basis for co-stimulation by the human CTLA-4/B7-2 complex. *Nature* **410**, 604-608 (2001).

103 Seidel, J. A., Otsuka, A. & Kabashima, K. Anti-PD-1 and Anti-CTLA-4 Therapies in Cancer: Mechanisms of Action, Efficacy, and Limitations. *Frontiers in oncology* **8**, 86, doi:10.3389/fonc.2018.00086 (2018).

104 Beer, T. M. *et al.* Randomized, double-blind, phase III trial of ipilimumab versus placebo in asymptomatic or minimally symptomatic patients with metastatic chemotherapy-naive castration-resistant prostate cancer. *J Clin Oncol* **35**, 40-47 (2017).

105 Kwon, E. D. *et al.* Ipilimumab versus placebo after radiotherapy in patients with metastatic castration-resistant prostate cancer that had progressed after docetaxel chemotherapy (CA184-043): a multicentre, randomised, double-blind, phase 3 trial. *The lancet oncology* **15**, 700-712 (2014).

106 Fizazi, K. *et al.* Final Analysis of the Ipilimumab Versus Placebo Following Radiotherapy Phase III Trial in Postdocetaxel Metastatic Castration-resistant Prostate Cancer Identifies an Excess of Long-term Survivors. *Eur Urol* **78**, 822-830, doi:10.1016/j.eururo.2020.07.032 (2020).

107 Deegen, P. *et al.* The PSMA-targeting Half-life Extended BiTE Therapy AMG 160 has Potent Antitumor Activity in Preclinical Models of Metastatic Castration-resistant Prostate Cancer. *Clinical cancer research : an official journal of the American Association for Cancer Research* **27**, 2928-2937, doi:10.1158/1078-0432.ccr-20-3725 (2021).

108 Hernandez-Hoyos, G. *et al.* MOR209/ES414, a Novel Bispecific Antibody Targeting PSMA for the Treatment of Metastatic Castration-Resistant Prostate Cancer. *Molecular cancer therapeutics* **15**, 2155-2165, doi:10.1158/1535-7163.mct-15-0242 (2016).

109 June, C. H. & Sadelain, M. Chimeric Antigen Receptor Therapy. *The New England journal of medicine* **379**, 64-73, doi:10.1056/NEJMra1706169 (2018).

110 Altenschmidt, U. *et al.* Cytolysis of tumor cells expressing the Neu/erbB-2, erbB-3, and erbB-4 receptors by genetically targeted naive T lymphocytes. *Clinical cancer research : an official journal of the American Association for Cancer Research* **2**, 1001-1008 (1996).

111 Kahlon, K. S. *et al.* Specific recognition and killing of glioblastoma multiforme by interleukin 13-zetakine redirected cytolytic T cells. *Cancer research* **64**, 9160-9166, doi:10.1158/0008-5472.can-04-0454 (2004).

112 Zhong, X. S., Matsushita, M., Plotkin, J., Riviere, I. & Sadelain, M. Chimeric antigen receptors combining 4-1BB and CD28 signaling domains augment PI3kinase/AKT/Bcl-XL activation and CD8+ T cell-mediated tumor eradication.

Molecular therapy : the journal of the American Society of Gene Therapy **18**, 413-420, doi:10.1038/mt.2009.210 (2010).

113 Ma, Q., Gomes, E. M., Lo, A. S. & Junghans, R. P. Advanced generation anti-prostate specific membrane antigen designer T cells for prostate cancer immunotherapy. *The Prostate* **74**, 286-296, doi:10.1002/pros.22749 (2014).

114 Slovin, S. F. *et al.* Chimeric antigen receptor (CAR+) modified T cells targeting prostate-specific membrane antigen (PSMA) in patients (pts) with castrate metastatic prostate cancer (CMPC). *Journal of Clinical Oncology* **31**, 72-72, doi:10.1200/jco.2013.31.6_suppl.72 (2013).

115 Narayan, V. *et al.* A phase I clinical trial of PSMA-directed/TGFβ-insensitive CAR-T cells in metastatic castration-resistant prostate cancer. *Journal of Clinical Oncology* **37**, TPS347-TPS347, doi:10.1200/JCO.2019.37.7_suppl.TPS347 (2019).

116 Junghans, R. P. *et al.* Phase I Trial of Anti-PSMA Designer CAR-T Cells in Prostate Cancer: Possible Role for Interacting Interleukin 2-T Cell Pharmacodynamics as a Determinant of Clinical Response. *The Prostate* **76**, 1257-1270, doi:10.1002/pros.23214 (2016).

117 Petrylak, D. P. *et al.* Docetaxel and estramustine compared with mitoxantrone and prednisone for advanced refractory prostate cancer. *New England Journal of Medicine* **351**, 1513-1520 (2004).

118 Tannock, I. F. *et al.* Docetaxel plus prednisone or mitoxantrone plus prednisone for advanced prostate cancer. *New England Journal of Medicine* **351**, 1502-1512 (2004).

119 De Bono, J. S. *et al.* Prednisone plus cabazitaxel or mitoxantrone for metastatic castration-resistant prostate cancer progressing after docetaxel treatment: a randomised open-label trial. *The Lancet* **376**, 1147-1154 (2010).

120 Parker, C. *et al.* Alpha emitter radium-223 and survival in metastatic prostate cancer. *The New England journal of medicine* **369**, 213-223, doi:10.1056/NEJMoa1213755 (2013).

121 Frei, E., 3rd *et al.* The effectiveness of combinations of antileukemic agents in inducing and maintaining remission in children with acute leukemia. *Blood* **26**, 642-656 (1965).

122 Lugade, A. A. *et al.* Local radiation therapy of B16 melanoma tumors increases the generation of tumor antigen-specific effector cells that traffic to the tumor. *The Journal of Immunology* **174**, 7516-7523 (2005).

123 Chen, D. S. & Mellman, I. Oncology meets immunology: the cancer-immunity cycle. *Immunity* **39**, 1-10, doi:10.1016/j.immuni.2013.07.012 (2013).

124 Staniszewska, M. *et al.* Enzalutamide Enhances PSMA Expression of PSMA-Low Prostate Cancer. *International journal of molecular sciences* **22**, doi:10.3390/ijms22147431 (2021).

125 Klose, J. M. *et al.* Administration routes for SSTR- / PSMA- and FAP-directed theranostic radioligands in mice. *J Nucl Med*, doi:10.2967/jnumed.121.263453 (2022).

126 Ferdinandus, J. *et al.* Prognostic biomarkers in men with metastatic castration-resistant prostate cancer receiving [177Lu]-PSMA-617. *European journal of nuclear medicine and molecular imaging* **47**, 2322-2327, doi:10.1007/s00259-020-04723-z (2020).

127 Violet, J. *et al.* Long-Term Follow-up and Outcomes of Retreatment in an Expanded 50-Patient Single-Center Phase II Prospective Trial of ¹⁷⁷Lu-PSMA-617 Theranostics in Metastatic Castration-Resistant

Prostate Cancer. *Journal of Nuclear Medicine* **61**, 857-865, doi:10.2967/jnumed.119.236414 (2020).

128 Thang, S. P. *et al.* Poor Outcomes for Patients with Metastatic Castration-resistant Prostate Cancer with Low Prostate-specific Membrane Antigen (PSMA) Expression Deemed Ineligible for (177)Lu-labelled PSMA Radioligand Therapy. *Eur Urol Oncol* **2**, 670-676, doi:10.1016/j.euo.2018.11.007 (2019).

129 Reits, E. A. *et al.* Radiation modulates the peptide repertoire, enhances MHC class I expression, and induces successful antitumor immunotherapy. *The Journal of experimental medicine* **203**, 1259-1271 (2006).

130 Dovedi, S. J. *et al.* Acquired resistance to fractionated radiotherapy can be overcome by concurrent PD-L1 blockade. *Cancer research* **74**, 5458-5468 (2014).

131 Czernin, J. *et al.* Immune-Checkpoint Blockade Enhances ²²⁵Ac-PSMA617 Efficacy in a Mouse Model of Prostate Cancer. *Journal of Nuclear Medicine* **62**, 228-231, doi:10.2967/jnumed.120.246041 (2021).

132 Current, K. *et al.* Investigating PSMA-Targeted Radioligand Therapy Efficacy as a Function of Cellular PSMA Levels and Intratumoral PSMA Heterogeneity. *Clinical cancer research : an official journal of the American Association for Cancer Research* **26**, 2946-2955, doi:10.1158/1078-0432.ccr-19-1485 (2020).

133 Gafita, A. *et al.* Nomograms to predict outcome after LuPSMA radionuclide therapy in men with metastatic castration-resistant prostate cancer: an international multicenter retrospective study. *The Lancet. Oncology* **in press** (2021).

134 Meller, B. *et al.* Alterations in androgen deprivation enhanced prostate-specific membrane antigen (PSMA) expression in prostate cancer cells as a target for diagnostics and therapy. *EJNMMI research* **5**, 66, doi:10.1186/s13550-015-0145-8 (2015).

135 Wright, G. L., Jr. *et al.* Upregulation of prostate-specific membrane antigen after androgen-deprivation therapy. *Urology* **48**, 326-334, doi:10.1016/s0090-4295(96)00184-7 (1996).

136 O'Keefe, D. S. *et al.* Mapping, genomic organization and promoter analysis of the human prostate-specific membrane antigen gene. *Biochimica et biophysica acta* **1443**, 113-127, doi:10.1016/s0167-4781(98)00200-0 (1998).

137 Lückerath, K. *et al.* Preclinical evaluation of PSMA expression in response to androgen receptor blockade for theranostics in prostate cancer. *EJNMMI research* **8**, 96, doi:10.1186/s13550-018-0451-z (2018).

138 Evans, M. J. *et al.* Noninvasive measurement of androgen receptor signaling with a positron-emitting radiopharmaceutical that targets prostate-specific membrane antigen. *Proceedings of the National Academy of Sciences of the United States of America* **108**, 9578-9582, doi:10.1073/pnas.1106383108 (2011).

139 Hope, T. A. *et al.* ⁶⁸Ga-PSMA-11 PET Imaging of Response to Androgen Receptor Inhibition: First Human Experience. *Journal of Nuclear Medicine* **58**, 81-84, doi:10.2967/jnumed.116.181800 (2017).

140 Emmett, L. *et al.* Rapid Modulation of PSMA Expression by Androgen Deprivation: Serial (68)Ga-PSMA-11 PET in Men with Hormone-Sensitive and Castrate-Resistant Prostate Cancer Commencing Androgen Blockade. *J Nucl Med* **60**, 950-954, doi:10.2967/jnumed.118.223099 (2019).

141 Sternberg, C. N. *et al.* Enzalutamide and Survival in Nonmetastatic, Castration-Resistant Prostate Cancer. *The New England journal of medicine* **382**, 2197-2206, doi:10.1056/NEJMoa2003892 (2020).

142 Caromile, L. A. & Shapiro, L. H. PSMA redirects MAPK to PI3K-AKT signaling to promote prostate cancer progression. *Molecular & cellular oncology* **4**, e1321168, doi:10.1080/23723556.2017.1321168 (2017).
143 Colombatti, M. *et al.* The prostate specific membrane antigen regulates the expression of IL-6 and CCL5 in prostate tumour cells by activating the MAPK pathways. *PloS one* **4**, e4608, doi:10.1371/journal.pone.0004608 (2009).
144 Jia, S. *et al.* Essential roles of PI(3)K-p110beta in cell growth, metabolism and tumorigenesis. *Nature* **454**, 776-779, doi:10.1038/nature07091 (2008).
145 Carver, B. S. *et al.* Reciprocal feedback regulation of PI3K and androgen receptor signaling in PTEN-deficient prostate cancer. *Cancer cell* **19**, 575-586 (2011).
146 Yao, V. & Bacich, D. J. Prostate specific membrane antigen (PSMA) expression gives prostate cancer cells a growth advantage in a physiologically relevant folate environment in vitro. *The Prostate* **66**, 867-875, doi:10.1002/pros.20361 (2006).
147 Weineisen, M. *et al.* ⁶⁸Ga- and ¹⁷⁷Lu-Labeled PSMA I&T: Optimization of a PSMA-Targeted Theranostic Concept and First Proof-of-Concept Human Studies. *Journal of Nuclear Medicine* **56**, 1169-1176, doi:10.2967/jnumed.115.158550 (2015).
148 Umbricht, C. A. *et al.* (44)Sc-PSMA-617 for radiotheragnostics in tandem with (177)Lu-PSMA-617-preclinical investigations in comparison with (68)Ga-PSMA-11 and (68)Ga-PSMA-617. *EJNMMI research* **7**, 9, doi:10.1186/s13550-017-0257-4 (2017).
149 Isaacsson Velho, P. *et al.* Efficacy of Radium-223 in Bone-metastatic Castration-resistant Prostate Cancer with and Without Homologous Repair Gene Defects. *Eur Urol* **76**, 170-176, doi:10.1016/j.eururo.2018.09.040 (2019).
150 van der Doelen, M. J. *et al.* Impact of DNA damage repair defects on response to radium-223 and overall survival in metastatic castration-resistant prostate cancer. *European journal of cancer (Oxford, England : 1990)* **136**, 16-24, doi:10.1016/j.ejca.2020.05.001 (2020).
151 Wickstroem, K. *et al.* Synergistic Effect of a Mesothelin-Targeted (227)Th Conjugate in Combination with DNA Damage Response Inhibitors in Ovarian Cancer Xenograft Models. *J Nucl Med* **60**, 1293-1300, doi:10.2967/jnumed.118.223701 (2019).
152 Kratochwil, C. *et al.* Patients Resistant Against PSMA-Targeting α-Radiation Therapy Often Harbor Mutations in DNA Damage-Repair-Associated Genes. *J Nucl Med* **61**, 683-688, doi:10.2967/jnumed.119.234559 (2020).
153 Lloyd, R. L. *et al.* Combined PARP and ATR inhibition potentiates genome instability and cell death in ATM-deficient cancer cells. *Oncogene* **39**, 4869-4883, doi:10.1038/s41388-020-1328-y (2020).
154 Kim, H. *et al.* Combining PARP with ATR inhibition overcomes PARP inhibitor and platinum resistance in ovarian cancer models. *Nature communications* **11**, 3726, doi:10.1038/s41467-020-17127-2 (2020).
155 Jette, N. R. *et al.* Combined poly-ADP ribose polymerase and ataxia-telangiectasia mutated/Rad3-related inhibition targets ataxia-telangiectasia mutated-deficient lung cancer cells. *Br J Cancer* **121**, 600-610, doi:10.1038/s41416-019-0565-8 (2019).
156 Kim, H. *et al.* Targeting the ATR/CHK1 Axis with PARP Inhibition Results in Tumor Regression in BRCA-Mutant Ovarian Cancer Models. *Clinical cancer research : an official journal of the American Association for Cancer Research* **23**, 3097-3108, doi:10.1158/1078-0432.ccr-16-2273 (2017).

157 Graf, F. *et al.* DNA double strand breaks as predictor of efficacy of the alpha-particle emitter Ac-225 and the electron emitter Lu-177 for somatostatin receptor targeted radiotherapy. *PloS one* **9**, e88239, doi:10.1371/journal.pone.0088239 (2014).
158 Rafiei, S. *et al.* ATM Loss Confers Greater Sensitivity to ATR Inhibition Than PARP Inhibition in Prostate Cancer. *Cancer research* **80**, 2094-2100, doi:10.1158/0008-5472.can-19-3126 (2020).
159 Pantelidou, C. *et al.* PARP Inhibitor Efficacy Depends on CD8(+) T-cell Recruitment via Intratumoral STING Pathway Activation in BRCA-Deficient Models of Triple-Negative Breast Cancer. *Cancer discovery* **9**, 722-737, doi:10.1158/2159-8290.cd-18-1218 (2019).
160 Stewart, R. A., Pilié, P. G. & Yap, T. A. Development of PARP and Immune-Checkpoint Inhibitor Combinations. *Cancer research* **78**, 6717-6725, doi:10.1158/0008-5472.can-18-2652 (2018).
161 Pham, M. M., Ngoi, N. Y. L., Peng, G., Tan, D. S. P. & Yap, T. A. Development of poly(ADP-ribose) polymerase inhibitor and immunotherapy combinations: progress, pitfalls, and promises. *Trends in cancer* **7**, 958-970, doi:10.1016/j.trecan.2021.05.004 (2021).
162 Peyraud, F. & Italiano, A. Combined PARP Inhibition and Immune Checkpoint Therapy in Solid Tumors. *Cancers* **12**, doi:10.3390/cancers12061502 (2020).
163 Ho, Samantha S. W. *et al.* The DNA Structure-Specific Endonuclease MUS81 Mediates DNA Sensor STING-Dependent Host Rejection of Prostate Cancer Cells. *Immunity* **44**, 1177-1189, doi:https://doi.org/10.1016/j.immuni.2016.04.010 (2016).
164 Green, D. R., Ferguson, T., Zitvogel, L. & Kroemer, G. Immunogenic and tolerogenic cell death. *Nature Reviews Immunology* **9**, 353-363, doi:10.1038/nri2545 (2009).
165 Hernandez, R. *et al.* (90)Y-NM600 targeted radionuclide therapy induces immunologic memory in syngeneic models of T-cell Non-Hodgkin's Lymphoma. *Communications biology* **2**, 79, doi:10.1038/s42003-019-0327-4 (2019).
166 Patel, R. B. *et al.* Low-dose targeted radionuclide therapy renders immunologically cold tumors responsive to immune checkpoint blockade. *Science translational medicine* **13**, doi:10.1126/scitranslmed.abb3631 (2021).
167 Hernandez, R. *et al.* Y-NM600 targeted radionuclide therapy induces immunologic memory in syngeneic models of T-cell Non-Hodgkin's Lymphoma. *Commun Biol* **2**, 79, doi:10.1038/s42003-019-0327-4 (2019).
168 Rouanet, J. *et al.* Immune checkpoint inhibitors reverse tolerogenic mechanisms induced by melanoma targeted radionuclide therapy. *Cancer immunology, immunotherapy : CII* **69**, 2075-2088, doi:10.1007/s00262-020-02606-8 (2020).
169 Clark, P. A. *et al.* Low-Dose Radiation Potentiates the Propagation of Anti-Tumor Immunity against Melanoma Tumor in the Brain after In Situ Vaccination at a Tumor outside the Brain. *Radiation research* **195**, 522-540, doi:10.1667/rade-20-00237.1 (2021).
170 Jagodinsky, J. C. *et al.* Temporal analysis of type 1 interferon activation in tumor cells following external beam radiotherapy or targeted radionuclide therapy. *Theranostics* **11**, 6120-6137, doi:10.7150/thno.54881 (2021).
171 Bou-Dargham, M. J., Sha, L., Sang, Q.-X. A. & Zhang, J. Immune landscape of human prostate cancer: immune evasion mechanisms and biomarkers for personalized immunotherapy. *BMC Cancer* **20**, 572, doi:10.1186/s12885-020-07058-y (2020).

172 Vito, A. *et al.* Combined Radionuclide Therapy and Immunotherapy for Treatment of Triple Negative Breast Cancer. *International journal of molecular sciences* **22**, doi:10.3390/ijms22094843 (2021).
173 Villadolid, J. & Amin, A. Immune checkpoint inhibitors in clinical practice: update on management of immune-related toxicities. *Translational lung cancer research* **4**, 560-575, doi:10.3978/j.issn.2218-6751.2015.06.06 (2015).
174 Johnson, D. B. *et al.* Immune checkpoint inhibitor toxicities: systems-based approaches to improve patient care and research. *The Lancet. Oncology* **21**, e398-e404, doi:10.1016/s1470-2045(20)30107-8 (2020).
175 McGrail, D. J. *et al.* Replication stress response defects are associated with response to immune checkpoint blockade in nonhypermutated cancers. *Science translational medicine* **13**, eabe6201, doi:10.1126/scitranslmed.abe6201 (2021).
176 Feng, X. *et al.* ATR inhibition potentiates ionizing radiation-induced interferon response via cytosolic nucleic acid-sensing pathways. *The EMBO journal* **39**, e104036, doi:10.15252/embj.2019104036 (2020).
177 Vendetti, F. P. *et al.* ATR kinase inhibitor AZD6738 potentiates CD8+ T cell-dependent antitumor activity following radiation. *J Clin Invest* **128**, 3926-3940, doi:10.1172/jci96519 (2018).
178 Sun, L. L. *et al.* Inhibition of ATR downregulates PD-L1 and sensitizes tumor cells to T cell-mediated killing. *American journal of cancer research* **8**, 1307-1316 (2018).
179 Shen, J. *et al.* PARPi Triggers the STING-Dependent Immune Response and Enhances the Therapeutic Efficacy of Immune Checkpoint Blockade Independent of BRCAness. *Cancer research* **79**, 311-319, doi:10.1158/0008-5472.can-18-1003 (2019).
180 Jiao, S. *et al.* PARP Inhibitor Upregulates PD-L1 Expression and Enhances Cancer-Associated Immunosuppression. *Clinical cancer research : an official journal of the American Association for Cancer Research* **23**, 3711-3720, doi:10.1158/1078-0432.ccr-16-3215 (2017).
181 Konstantinopoulos, P. A. *et al.* Single-Arm Phases 1 and 2 Trial of Niraparib in Combination With Pembrolizumab in Patients With Recurrent Platinum-Resistant Ovarian Carcinoma. *JAMA Oncol* **5**, 1141-1149, doi:10.1001/jamaoncol.2019.1048 (2019).
182 Vinayak, S. *et al.* Open-label Clinical Trial of Niraparib Combined With Pembrolizumab for Treatment of Advanced or Metastatic Triple-Negative Breast Cancer. *JAMA Oncol* **5**, 1132-1140, doi:10.1001/jamaoncol.2019.1029 (2019).
183 Domchek, S. M. *et al.* Olaparib and durvalumab in patients with germline BRCA-mutated metastatic breast cancer (MEDIOLA): an open-label, multicentre, phase 1/2, basket study. *The Lancet. Oncology* **21**, 1155-1164, doi:10.1016/s1470-2045(20)30324-7 (2020).
184 Lampert, E. J. *et al.* Combination of PARP Inhibitor Olaparib, and PD-L1 Inhibitor Durvalumab, in Recurrent Ovarian Cancer: a Proof-of-Concept Phase II Study. *Clinical cancer research : an official journal of the American Association for Cancer Research* **26**, 4268-4279, doi:10.1158/1078-0432.ccr-20-0056 (2020).
185 Kim, R. *et al.* Phase II study of ceralasertib (AZD6738) in combination with durvalumab in patients with advanced/metastatic melanoma who have failed prior anti-PD-1 therapy. *Annals of oncology : official journal of the European Society for Medical Oncology* **33**, 193-203, doi:10.1016/j.annonc.2021.10.009 (2022).

186 Kennedy, L. B. & Salama, A. K. S. A review of cancer immunotherapy toxicity. *CA Cancer J Clin* **70**, 86-104, doi:10.3322/caac.21596 (2020).

Appendix

Table 10 P-values for statistical analysis of survival of combined ^{177}Lu-PSMA-617 – DDRi combination therapies

Treatment group	Significant	p-value
NT vs ATRi	ns	0.7703
NT vs PARPi	ns	0.7596
NT vs ATRi/PARPi	ns	0.4759
NT vs RLT	ns	0.7884
NT vs RLT/ATRi	ns	0.8702
NT vs RLT/PARPi	ns	0.9478
NT vs RLT/ATRi/PARPi	ns	0.249
ATRi vs PARPi	ns/*	0.2474
ATRi vs ATRi/PARPi	ns	0.9028
ATRi vs RLT	ns	0.5332
ATRi vs RLT/ATRi	ns	0.6771
ATRi vs RLT/PARPi	ns	0.7656
ATRi vs RLT/ATRi/PARPi	ns	0.9028
PARPi vs ATRi/PARPi	ns	0.8574
PARPi vs RLT/ATRi	ns	0.4002
PARPi vs RLT/PARPi	ns	0.5244
PARPi vs RLT/ATRi/PARPi	ns	0.3389
ATRi/PARPi vs RLT	ns	0.8112
RLT vs RLT/ATRi	ns	0.3356
RLT vs RLT/PARPi	ns	0.5255
RLT vs RLT/ATRi/PARPi	ns	0.3813
RLT/ATRi vs RLT/PARPi	ns	0.9724
RLT/ATRi vs RLT/ATRi/PARPi	ns	0.3463
RLT/PARPi vs RLT/ATRi/PARPi	ns	0.2708

Table 11 P-values for statistical analysis of TTP < 0.75 cm^3 of combined ^{177}Lu-PSMA-617 – DDRi combination therapies

Treatment group	Significant	p-value
NT vs ATRi	ns	0.7827
NT vs PARPi	ns	0.7129
NT vs ATRi/PARPi	ns	0.7068
NT vs RLT	ns	0.7849
NT vs RLT/ATRi	ns	0.2372
NT vs RLT/PARPi	ns	0.5335
NT vs RLT/ATRi/PARPi	ns	0.2834
ATRi vs PARPi	ns	0.4599
ATRi vs ATRi/PARPi	ns	0.9571
ATRi vs RLT	ns	0.8866
ATRi vs RLT/ATRi	ns	0.205
ATRi vs RLT/PARPi	ns	0.9824
ATRi vs RLT/ATRi/PARPi	ns	0.3248
PARPi vs ATRi/PARPi	ns	0.28
PARPi vs RLT	ns	0.3875
PARPi vs RLT/ATRi	ns	0.0777
PARPi vs RLT/PARPi	ns	0.3071
PARPi vs RLT/ATRi/PARPi	ns	0.1154
ATRi/PARPi vs RLT	ns	0.623
ATRi/PARPi vs RLT/ATRi	ns	0.1012
ATRi/PARPi vs RLT/PARPi	ns	0.9758
ATRi/PARPi vs RLT/ATRi/PARPi	ns	0.3381
RLT vs RLT/ATRi	ns	0.193
RLT vs RLT/PARPi	ns	0.8948
RLT vs RLT/ATRi/PARPi	ns	0.3823
RLT/ATRi vs RLT/PARPi	ns	0.4317
RLT/ATRi vs RLT/ATRi/PARPi	ns	0.898
RLT/PARPi vs RLT/ATRi/PARPi	ns	0.862

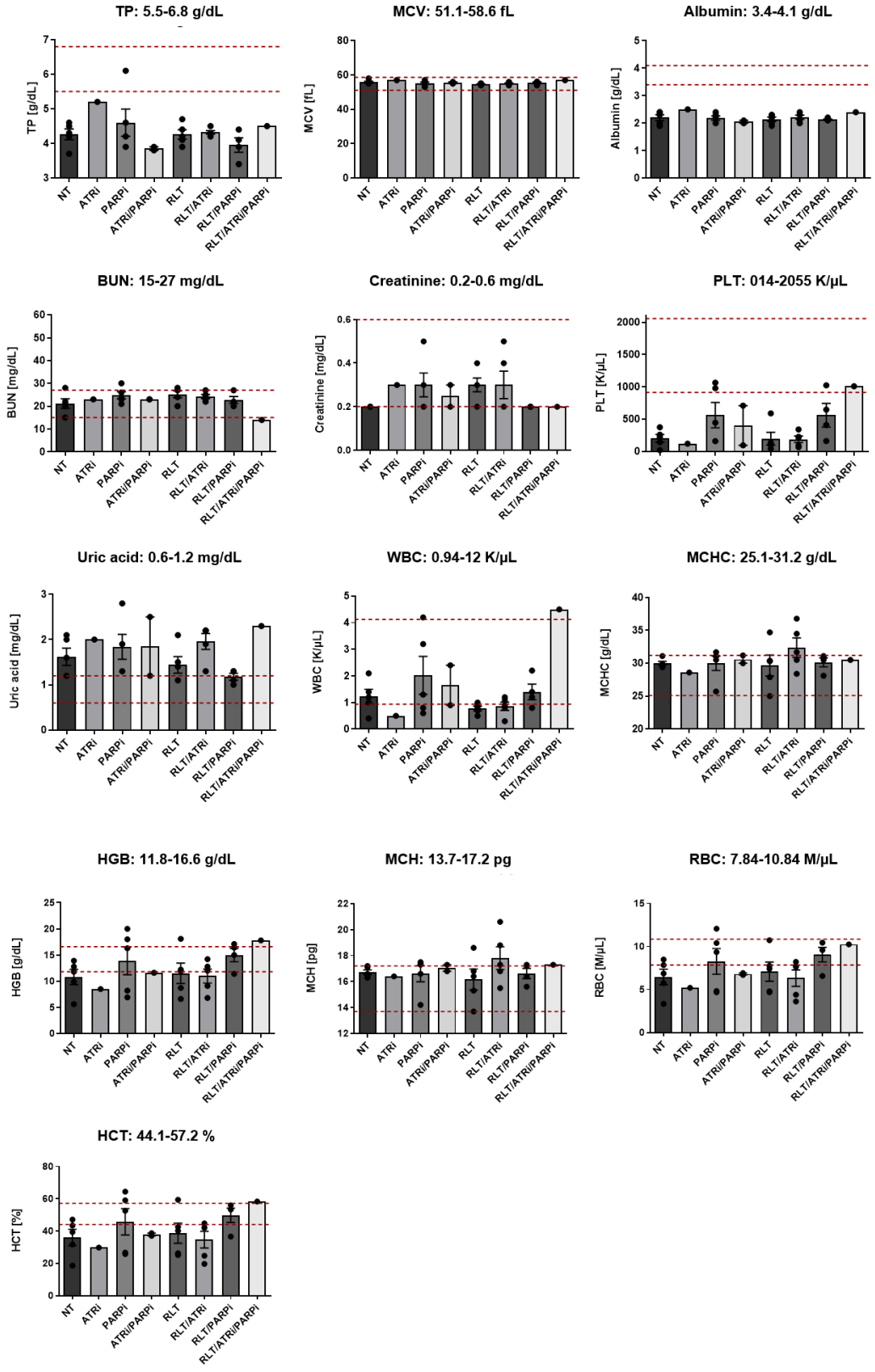

Figure 22 Blood parameter analysis for ^{177}Lu-PSMA-617 – DDRi combination therapies. To measure drug toxicity, blood was analyzed when animals reached termination critieria including total protein (TP), mean corpuscular volume (MCV), albumine, blood urea nitrogen (BUN), creatinine, platelet count (PLT), uric acid, white blood cell (WBC) count, mean corpuscular hemoglobin concentration (MCHC), hemoglobin (HGB), mean corpuscular hemoglobin (MCH), red blood cell (RBC) count and hematocrit (HCT). Red dashed lines represent reference range. Data are shown as mean ± SD.

Acknowledgments

There have been many people, both during and prior to my graduate research education, who played an important role in my journey and helped me to reach my objectives. I will not be able to thank them all individually, but I want to extend a warm thank to those who supported me.

First and foremost, I would like to thank my supervisors, Prof. Dr. Ken Herrmann and Prof. Dr. Wolfgang Fendler, for providing me the opportunity to carry out my PhD thesis in this unique and exciting field of nuclear medicine and for giving me the privilege to contribute to establishing their new research group. Additionally, I would like to thank you for making possible my research exchange at UCLA.

Special thank goes to my mentor Prof. Dr. Katharina Lückerath for her constant support and guidance. Your dedicated mentorship and immense knowledge were invaluable. Furthermore, I would like to thank you for your tireless proofreading of this manuscript. This PhD thesis would not be as accomplished without your stimulative input and helpful ideas.

Additionally, I would like to give many thanks to my graduate program GRK 1739 that provided the frame for my research training at UK Essen and that helped further my graduate training by financing my research exchange at UCLA. Thank you for providing me such a unique experience.

I would also like to thank every past and present lab member: Jasmin K., Janette, Anna and especially Jasmin W. for your excellent technical assistance, support and always positive attitude. Many thanks to the medical physicists: Pedro, Sandra, Alex, Patrick and Dietmar- it is always a pleasure to work with you! Further, I would like to thank the Urology team: Tibor, Alina, Csilla and Jacqueline for hosting me in your lab and for the great work atmosphere.

My sincere thanks go to the UCLA team: Christine, Marco, Elie and Johannes for giving me a warm welcome in LA and taking care of me in and outside the lab. Thank you for the great team spirit and fun time in Cali.

While I am truly lucky and grateful to have been mentored and supported professionally, I would have never had the opportunity were it not for my family, especially my parents, and my partner Simon. I would like to give them a heartfelt and heartful thank for always standing by my side and supporting me, no matter what. I love you!

Curriculum vitae

The curriculum vitae is not included in the online version for data protection reasons.

Awards

October 2018 Wiedenfeld-Stiftung Award 2018 of the Westdeutsches Tumorzentrum, Stiftung Krebsforschung Duisburg (15.000 €) for highly qualified PhD projects to fund innovative oncological research

Publications

Klose JM, Wosniack J, Iking J, **Staniszewska M**, Zarrad F, Trajkovic-Arsic M, Herrmann K, Fragoso Costa P, Lueckerath K, Fendler WP. Administration routes for SSTR- / PSMA- and FAP-directed theranostic radioligands in mice. J Nucl Med. 2022 Jan 6:jnumed.121.263453. doi: 10.2967/jnumed.121.263453. Epub ahead of print. PMID: 34992151.

IF: 10.06

Staniszewska M, Fragoso Costa P, Eiber M, Klose JM, Wosniack J, Reis H, Szarvas T, Hadaschik B, Lückerath K, Herrmann K, Fendler WP, Iking J. Enzalutamide Enhances PSMA Expression of PSMA-Low Prostate Cancer. Int J Mol Sci. 2021 Jul 11;22(14):7431. doi: 10.3390/ijms22147431. PMID: 34299051; PMCID: PMC8304389

IF: 5.923

Staniszewska M, Iking J, Lückerath K, Hadaschik B, Herrmann K, Ferdinandus J, Fendler WP. Drug and molecular radiotherapy combinations for metastatic castration resistant prostate cancer. Nucl Med Biol. 2021 May-Jun;96-97:101-111. doi: 10.1016/j.nucmedbio.2021.03.009. Epub 2021 Apr 9. PMID: 33866131

IF: 2.408

Sahm A, Platzer M, Koch P, Henning Y, Bens M, Groth M, Burda H, Begall S, Ting S, Goetz M, Van Daele P, **Staniszewska M**, Klose JM, Costa PF, Hoffmann S, Szafranski K, Dammann P. Increased longevity due to sexual activity in mole-rats is associated with transcriptional changes in the HPA stress axis. Elife. 2021 Mar 16;10:e57843. doi: 10.7554/eLife.57843. PMID: 33724179, PMCID: PMC8012063

IF: 8.14

Iking J, **Staniszewska M**, Kessler L, Klose JM, Lückerath K, Fendler WP, Herrmann K, Rischpler C. Imaging Inflammation with Positron Emission Tomography. Biomedicines. 2021 Feb 19;9(2):212. doi: 10.3390/biomedicines9020212. PMID:33669804; PMCID: PMC7922638

IF: 5.612

Kollenda SA, Klose JM, Knuschke T, Sokolova V, Schmitz J, **Staniszewska M**, Costa PF, Herrmann K, Westendorf AM, Fendler WP, Epple M. *In vivo* biodistribution of calcium phosphate nanoparticles after intravascular, intramuscular, intratumoral, and soft tissue administration in mice investigated by small animal PET/CT. Acta Biomater. 2020 Jun;109:244-253. doi: 10.1016/j.actbio.2020.03.031. Epub 2020 Apr 4. PMID: 32251787.

IF: 8.947

Iking J, Klose JM, **Staniszewska M**, Fendler WP, Herrmann K, Rischpler C Imaging inflammation after myocardial infarction: implications for prognosis and therapeutic guidance. Q J Nucl Med Mol Imaging. 2020 Mar;64(1):35-50. doi: 10.23736/S1824-4785.20.03232-X. Epub 2020 Feb 18

IF: 2.346

Koelsch B, Theurer S, **Staniszewska M**, Heupel J, Koch A, Mergener S, Walk F, Fischer C, Kutritz A, Schmid KW, Kindler-Röhrborn A. An Animal Model Further Uncovers the Role of Mutant BrafV600E during Papillary Thyroid Cancer Development. Am J Pathol. 2020 Mar;190(3):702-710.doi: 10.1016/j.ajpath.2019.11.006. Epub 2020 Jan. PMID: 31953036.

IF: 4.307

Congress Contributions

February 2022 — **Staniszewska M**, Taddio MF, Current K, Wei L, Czernin J, Mona CE, Lückerath K. PSMA-RLT Enhances Efficacy of Immune Checkpoint Blockade in a Mouse Model of Prostate Cancer, Essen Translational Oncology Symposium, virtual
Oral presentation

October 2021 — Costa PF, Puellen L, Klose JM, Iking J, Sandach P, **Staniszewska M**, Herrmann K, Radtke JP, Tschirdewahn S, Hadaschik B, Fendler WP. Ga-68-versus F18-PSMA for Cerenkov Luminescence and autoradiography in a prostate cancer mouse model, European Association of Nuclear Medicine, virtual
Oral presentation

September 2021 — Darr C, Püllen L, Iking J, Klose JM, Sandach P, **Staniszewska M**, Herrmann K, Radtke JP, Tschirdewahn S, Hadaschik B, Fendler WP, Costa PF. Cerenkov Luminescence (CLI) and autoradiography imaging (ARI) in a prostate cancer mouse model using 18-Fluorine and to 68-Gallium-PSMA small ligands, Deutsche Gesellschaft für Urologie, Stuttgart
Oral presentation

Settelmeier S, Reyes F, Iking J, Zarrad F, **Staniszewska M**, Rischpler C, Fendler WP, Herrmann K, Rassaf T , Hendgen-Cotta UB. A [^{68}Ga] peptide conjugate PET tracer enables *in vivo* tracing of BNIP3 antagonistic peptide, Deutsche Gesellschaft für Kardiologie, Herztage, Bonn
Poster presentation

August 2021 — **Staniszewska M**, Iking J, Klose JM, Wosniack J, Szarvas T, Hadaschik B, Lückerath K, Herrmann K, Fendler WP. Combined Androgen Receptor and DNA damage response inhibition to enhance prostate-specific membrane antigen (PSMA)-directed

radioligand therapy of PSMA-low prostate cancer, European Molecular Imaging Meeting, Göttingen
Poster presentation

Staniszewska M, Klose JM, Wosniack J, Costa PF, Nader M, Hadaschik B, Lückerath K, Herrmann K, Fendler WP, Iking J. Enzalutamide to enhance PSMA expression in three prostate cancer cell lines: implications for Lu-177-PSMA617 radioligand therapy, European Molecular Imaging Meeting, Göttingen,
Poster presentation

Klose JM, **Staniszewska M**, Wosniack J, Zarrad F, Lückerath K, Iking J, Herrmann K, Costa PF, Fendler WP. Alternative application routes for small animal theranostics, European Molecular Imaging Meeting, Göttingen
Oral presentation

July 2021

Staniszewska M, Iking J, Klose JM, Wosniack J, Szarvas T, Hadaschik B, Lückerath K, Herrmann K, Fendler WP. Combined Androgen Receptor and DNA damage response inhibition to enhance prostate-specific membrane antigen (PSMA)-directed radioligand therapy of PSMA-low prostate cancer, GyMIC Molecular Imaging Symposium, virtual
Oral presentation

Klose JM, Iking J, **Staniszewska M**, Wosniack J, Zarrad F, Lückerath K, Trajkovic-Arsic M, Herrmann K, Costa PF, Fendler WP. Alternative application routes for small animal theranostics, GyMIC Molecular Imaging Symposium, virtual
Poster presentation

April 2021

Staniszewska M, Klose JM, Wosniack J, Costa PF, Nader M, Hadaschik B, Lückerath K, Herrmann K, Fendler WP, Iking J. Enhanced PSMA expression in three prostate cancer cell lines after treatment with enzalutamide: implications for Lu-177-PSMA617 radioligand therapy, Deutsche Gesellschaft für Nuklearmedizin, virtual
Oral presentation

Klose JM, **Staniszewska M**, Wosniack J, Zarrad F, Lückerath K, Iking J, Herrmann K, Costa PF, Fendler WP. Alternative application routes for small animal theranostics, Deutsche Gesellschaft für Nuklearmedizin, virtual
Oral presentation

Himmen S, **Staniszewska M**, Wosniack J, Sandach P, Ferdinandus J, Schramm A, Hassiepen C, Iking J, Herrmann K, Klose JM, Fendler WP. Intraperitoneal contrast-enhanced small animal FDG PET/CT for improved abdominal delineation and

uptake quantification, Deutsche Gesellschaft für Nuklearmedizin, virtual
Poster presentation

February 2021 **Staniszewska M**, Klose JM, Wosniack J, Costa PF, Nader M, Hadaschik B, Lückerath K, Herrmann K, Fendler WP, Iking J. Enhanced PSMA expression in three prostate cancer cell lines after treatment with enzalutamide: implications for Lu-177-PSMA617 radioligand therapy, Essen Translational Oncology Symposium, virtual
Poster presentation

Klose JM, **Staniszewska M**, Wosniack J, Zarrad F, Lückerath K, Iking J, Herrmann K, Costa PF, Fendler WP. Alternative application routes for small animal theranostics, Essen Translational Oncology Symposium, virtual
Poster presentation

Himmen S, **Staniszewska M**, Wosniack J, Sandach P, Ferdinandus J, Schramm A, Hassiepen C, Iking J, Herrmann K, Klose J, Fendler WP. Intraperitoneal contrast-enhanced small animal FDG PET/CT for improved abdominal delineation and uptake quantification (Abdominal small-animal PET/CT i.p. Contrast), Essen Translational Oncology Symposium, virtual
Oral presentation

May 2020 Kollenda SA, Sokolova V, Schmitz J, Klose JM, **Staniszewska M**, Fendler WP, Wosniack J, Liebig C, Costa PF, Knuschke T, Buer J, Herrmann K, Westendorf A, Epple M, *In vivo* Biodistribution of Immunostimulatory Calcium Phosphate Nanoparticles using Small Animal PET/CT, World Biomaterials Congress, virtual
Oral presentation

October 2019 **Staniszewska M**, Lückerath K, Wei L, Radu CG, Eiber M, Czernin J, Klose JM, Herrmann K, Fendler WP. Combined Androgen Receptor and DNA damage response inhibition to enhance prostate-specific membrane antigen-directed radioligand therapy of prostate cancer, GRK 1739 DNA damage and beyond, Essen
Poster presentation

September 2019 **Staniszewska M**, Iking J, Klose JM, Wosniack J, Szarvas T, Hadaschik B, Lückerath K, Herrmann K, Fendler WP. Combined Androgen Receptor and DNA damage response inhibition to enhance prostate-specific membrane antigen (PSMA)-directed radioligand therapy of PSMA-low prostate cancer, GyMIC Molecular Imaging Symposium, Münster,
Poster Presentation

December 2018 **Staniszewska M**, Lückerath K, Wei L, Radu CG, Eiber M, Czernin J, Klose JM, Herrmann K, Fendler WP. Combined Androgen Receptor and DNA damage response inhibition to enhance prostate-specific membrane antigen-directed radioligand therapy of prostate cancer**.** Tag der Forschung der Medizinischen Fakultät, Essen
Poster presentation

Declarations

Declaration:

In accordance with § 6 (para. 2, clause g) of the Regulations Governing the Doctoral Proceedings of the Faculty of Biology for awarding the doctoral degree Dr. rer. nat., I hereby declare that I represent the field to which the topic “Combination therapies to enhance the efficacy of PSMA-targeted radioligand therapy in prostate cancer” is assigned in research and teaching and that I support the application of **Magdalena Staniszewska**.

Essen, date _____ _____

Prof. Dr. Ken Herrmann

Declaration:

In accordance with § 7 (para. 2, clause d and f) of the Regulations Governing the Doctoral Proceedings of the Faculty of Biology for awarding the doctoral degree Dr. rer. nat., I hereby declare that I have written the herewith submitted dissertation independently using only the materials listed, and have cited all sources taken over verbatim or in content as such.

Essen, date _____ _____

Magdalena Staniszewska

Declaration:

In accordance with § 7 (para. 2, clause e and g) of the Regulations Governing the Doctoral Proceedings of the Faculty of Biology for awarding the doctoral degree Dr. rer. nat., I hereby declare that I have undertaken no previous attempts to attain a doctoral degree, that the current work has not been rejected by any other faculty, and that I am submitting the dissertation only in this procedure.

Essen, date _____ _____

Magdalena Staniszewska